

**SLIDING-MODE CONTROL FOR HIGH-PRECISION MOTION CONTROL  
SYSTEMS**

by

**KHALID ABIDI**

Submitted to the Graduate School of Engineering and Natural Sciences  
in partial fulfillment of  
the requirements for the degree of  
Master of Science

Sabanci University

Spring 2004

SLIDING-MODE CONTROL FOR HIGH-PRECISION MOTION CONTROL  
SYSTEMS

APPROVED BY:

Prof. Dr. Asif Sabanovic .....

(Dissertation Supervisor)

Dr. Serhat Yesilyurt .....

Dr. Hasan Sait Olmez .....

DATE OF APPROVAL: .....

© Khalid Abidi 2004

All Rights Reserved

## ABSTRACT

In many of today's mechanical systems, high precision motion has become a necessity. As performance requirements become more stringent, classical industrial controllers such as PID can no longer provide satisfactory results. Although many control approaches have been proposed in the literature, control problems related to plant parameter uncertainties, disturbances and high-order dynamics remain as big challenges for control engineers.

Theory of Sliding Mode Control provides a systematic approach to controller design while allowing stability in the presence of parametric uncertainties and external disturbances. In this thesis a brief study of the concepts behind Sliding Mode Control will be shown. Description of Sliding Mode Control in discrete-time systems and the continuous Sliding Mode Control will be shown. The description will be supported with the design and robustness analysis of Sliding Mode Control for discrete-time systems.

In this thesis a simplified methodology based on discrete-time Sliding Mode Control will be presented. The main issues that this thesis aims to solve are friction and internal nonlinearities. The thesis can be outlined as follows:

- Implementation of discrete-time Sliding Mode Control to systems with nonlinearities and friction. Systems include; piezoelectric actuators that are known to suffer from nonlinear hysteresis behavior and ball-screw drives that suffer from high friction. Finally, the controller will be implemented on a 6-dof Stewart platform which is a system of higher complexity.
- It will also be shown that performance can be enhanced with the aid of disturbance compensation based on a nominal plant disturbance observer.

## ÖZET

Günümüzde kullanılan mekanik sistemlerde yüksek hassasiyetli hareket iletimi bir gereksinim haline gelmiştir. Performans gereksinimlerinin daha sıkılaşmasıyla birlikte, PID gibi klasik kontrol yöntemleri tatmin edici sonuçlar verememektedir. Literatürde birçok kontrol yaklaşımı önerilmesine rağmen sistem parametrelerindeki belirsizlikler, bozucu etkenler ve yüksek dereceli sistem dinamiği içeren kontrol problemleri, mühendisler için hala büyük bir sorun teşkil etmektedir.

Kayma Kipli Kontrol teorisi, parametrik belirsizliklere ve dışarıdan gelen bozucu etkenlere karşı kararlılık sağlayarak kontrolör tasarımında sistematik bir yaklaşım sunmaktadır. Bu tezde Kayma Kipli Kontrol'ün arkaplanındaki kavramlar kısaca gösterilecektir. Ayrık zamanlı Kayma Kipli Kontrol ve sürekli Kayma Kipli Kontrol tanımları gösterilecektir. Bu tanımlar ayrık zamanlı Kayma Kipli Kontrol tasarımı ve dayanıklılık analizi ile desteklenecektir.

Bu tezde ayrık zamanlı Kayma Kipli Kontrol üzerine kurulan basitleştirilmiş bir metodoloji sunulacaktır. Bu tezin çözümlemeyi amaçladığı ana noktalar sürtünme ve sisteme ait doğrusal olmayan özelliklerdir. Bu tezin ana hatları aşağıdaki gibi özetlenebilir:

- İçinde sürtünme ve doğrusal olmayan özellikler barındıran sistemlere ayrık zamanlı Kayma Kipli Kontrol'ün uygulanması. Bu sistemler şu bileşenleri içerir; doğrusal olmayan histerezis davranışı sergileyen kumanda aygıtları ve yüksek sürtünme kuvvetiyle karşı karşıya olan vida mekanizması. Son olarak kontrolör, yüksek oranda karmaşıklığa sahip olan altı serbestlik dereceli bir Stewart platformuna uygulanacaktır.
- Ayrıca, nominal sistem bozucu etken gözlemleyicisi üzerine kurulu bozucu etken kompanzasyonu yöntemi yardımı ile performansın iyileştirildiği gösterilecektir.

*To Peter Jackson for his everlasting inspiration...*

## ACKNOWLEDGEMENTS

I would like to convey my special thanks to Prof. Şabanoviç for his support and guidance regarding the theoretical work in the thesis and for his proposing this research to me. I would also like to give my thanks to Prof. Ahmet Onat for helping me with all the problems I had faced in the instrumentation and to Prof. Serhat Yeşilyurt for his recommendations. I should also convey my thanks to Prof. Mahmut Akşit for helping me with the mechanical design and Mehmet Guler for helping me with the actual manufacturing of the system.

I would also like to convey my thanks to the Mechatronics Graduate students especially Bahadır Kiliç, Yıldırım Yıldız, Kazim Çakır, Hakan Keskin, Ozan Ayhan, Yasser Elkahlout and Fazil Serincan for their everlasting support and for their having good discussions with me regarding the subject matter.

Finally I would like to give my thanks to my family and especially my mom and dad for giving me support throughout my education and to my brother Anas for always being there for me.

## TABLE OF CONTENTS

1. Introduction.....	1
1.1 Objective.....	1
1.2 Mechatronic Microsystems.....	2
1.2.1 Piezoelectric Actuator Driven Micromanipulators .....	3
1.2.2 Models of the Piezoelectric Actuator.....	4
1.2.2.1 Continuous Model.....	4
1.2.2.2 Preisach Model of Hysteresis .....	5
1.3 Control Techniques.....	7
1.3.1 $H_\infty$ Almost Disturbance Decoupling Controller .....	7
1.3.2 Neural Networks Based Controller.....	8
1.4 Motivation behind using Sliding-Mode Control.....	9
1.5 Stewart Platform for Flexible Six-dof Motion.....	10
2. Sliding-Mode Variable Structure Control.....	12
2.1 Introduction.....	12
2.2 Sliding-Mode in Variable Structure Systems .....	13
2.3 Sliding-Mode Controller Design and Realization of Discrete-time Control .....	14
2.4 Calculation of the Boundary Layer in Discrete-Time Sliding-Mode Control.....	18
2.5 Disturbance Observers based on Sliding-Mode Control .....	19
3. Model of the Piezoelectric Actuator .....	21
3.1 Introduction.....	21
3.2 Structure of the Piezoelectric Actuator.....	22
3.3 Model of the Piezoelectric Actuator .....	23
3.3.1 The Selected Model .....	23
3.3.2 Hysteresis Model .....	25
3.3.3 Simulation Results .....	27
3.4 Open-Loop Control of the Actuator.....	28

4. Implementation of SMC to a Piezoelectric Actuator.....	32
4.1 Introduction.....	32
4.2 Design of the Observers.....	33
4.2.1 Total Disturbance Estimation .....	33
4.2.2 Force Observer.....	38
4.3 Results of Closed-Loop Control Experiments.....	39
4.3.1 Position Control .....	40
4.3.2 Force Control .....	42
5. A Dual-Stage Servo System .....	45
5.1 Introduction.....	45
5.2 Structure of the System.....	46
5.3 Results with Single-Stage Servo.....	48
5.4 Proposed Controller .....	50
5.5 Results with Dual-Stage Servo .....	51
6. Analysis of the Kinematics of a 6-DOF Stewart-Gough Manipulator .....	54
6.1 Introduction.....	54
6.2 Description of the Stewart-Gough Manipulator .....	55
6.3 Geometry of the Stewart-Gough Manipulator .....	56
6.4 Direct Kinematics of the Stewart-Gough Manipulator.....	58
6.5 Inverse Kinematics of the Stewart-Gough Manipulator .....	60
6.5.1 Simulation Results for the Proposed Manipulator.....	61
7. Experiments on an Actual Stewart Platform.....	67
7.1 Introduction.....	67
7.2 Structure of the Experimental Stewart Platform.....	67
7.3 Experimental Results .....	69
CONCLUSION.....	74
REFERENCE.....	76

## LIST OF TABLES

Table 3.1. Parameters of the PZT model .....	27
Table 6.1. Manipulator joint coordinates.....	61

## LIST OF FIGURES

Figure 1.1. 3-Axis nanopositioning system, PI GmbH.....	4
Figure 1.2. Hysteresis operator $\gamma_{\alpha\beta}[u(t)]$ .....	6
Figure 1.3. Monotonically increasing input $u_1(t)$ .....	6
Figure 1.4. Closed-loop neural network controller.....	8
Figure 1.5. Six-dof Stewart platform, PI GmbH .....	10
Figure 1.6. Experimental Stewart platform .....	11
Figure 2.1. Geometric interpretation of two intersecting switching surfaces.....	15
Figure 2.2. Discrete-time system with discontinuous control .....	15
Figure 2.3. Discrete-time Sliding mode in sampled-data systems.....	17
Figure 2.4. Disturbance observer implementation.....	20
Figure 3.1. Stack actuators used in the experiments.....	22
Figure 3.2. Illustration of a PZT stack actuator .....	24
Figure 3.3. Electromechanical model of the PZT actuator, [1] .....	24
Figure 3.4. Block-Diagram representation of the electromechanical model .....	26
Figure 3.5. A hysteresis loop .....	26
Figure 3.6. Response to $u = 40 + 40\sin(t)$ and corresponding modeling error.....	28
Figure 3.7. Response to $u = 15 + 15\sin(t)$ and corresponding modeling error.....	29
Figure 3.8. Inverse model of the PZT actuator .....	29
Figure 3.9. Response to $x_r = 7.5 + 7.5\sin(t)$ .....	29
Figure 3.10. Open-loop tracking error and input voltage for $x_r = 7.5 + 7.5\sin(t)$ .....	30
Figure 3.11. Response to a varying amplitude sine reference .....	30
Figure 3.12. Input voltage for a varying amplitude sine reference (contd.).....	31
Figure 3.13. Response to a high frequency varying amplitude sine reference .....	31
Figure 4.1. Observer implementation .....	35
Figure 4.2. Response to $u_0 = 7.5\sin(10\pi t) + 7.5$ .....	36

Figure 4.3. Response to $u_0 = 7.5 \sin(100\pi t) + 7.5$ with disturbance compensation.....	36
Figure 4.4. Response to $u_0 = 30 \sin(10\pi t) + 30$ with disturbance compensation.....	37
Figure 4.5. Response to $u_0 = 30 \sin(100\pi t) + 30$ with disturbance compensation.....	37
Figure 4.6. Block-diagram for external force estimation.....	39
Figure 4.7. Results of the Force Observer Experiments .....	39
Figure 4.8. Sketch of the experimental setup.....	40
Figure 4.9. Structure of the experimental setup.....	40
Figure 4.10. Closed-loop control scheme .....	41
Figure 4.11. Closed-loop response to a 1Hz sinusoidal reference.....	41
Figure 4.12. 5nm step motion .....	42
Figure 4.13. 1nm step motion .....	42
Figure 4.14. Block-diagram of force control system .....	43
Figure 4.15. Sensor based force control .....	44
Figure 4.16. Observer based force control.....	44
Figure 5.1. CAD model of the dual-stage system.....	46
Figure 5.2. Anatomy of the dual-stage system .....	47
Figure 5.3. Model representation of the system.....	47
Figure 5.4. Single-stage controller scheme.....	48
Figure 5.5. Single-stage 0.5mm sigmoid reference tracking .....	49
Figure 5.6. Single-stage 1mm sigmoid reference tracking .....	49
Figure 5.7. Single-stage 1.5mm sigmoid reference tracking .....	50
Figure 5.8. Dual-stage Controller scheme .....	50
Figure 5.9. Dual-stage 0.5mm sigmoid reference tracking.....	51
Figure 5.10. Dual-stage 1mm sigmoid reference tracking.....	52
Figure 5.11. Dual-stage 1.5mm sigmoid reference tracking.....	52
Figure 5.12. Dual-stage 1.5mm sigmoid reference tracking (contd.).....	53
Figure 6.1. VARIAX <sup>®</sup> machining center, Giddings and Lewis machine tools .....	55
Figure 6.2. Spatial 6-dof, 6SPS parallel manipulator .....	57
Figure 6.3. MSC.ADAMS CAD model of the proposed manipulator .....	61
Figure 6.4. First set of reference trajectories for point $P$ .....	62
Figure 6.5. First set of reference trajectories for point $P$ .....	63
Figure 6.6. Required limb elongations for the first set of trajectories.....	63
Figure 6.7. CAD model response to the first set of trajectories.....	64

Figure 6.8. Second set of reference trajectories for point $P$ .....	65
Figure 6.9. Limb elongations for the second set of trajectories.....	65
Figure 6.10. Limb elongations for the second set of trajectories (contd.) .....	66
Figure 6.11. CAD model response to the second set of trajectories.....	66
Figure 7.1. Limb of the experimental system .....	68
Figure 7.2. Sketch of the system.....	68
Figure 7.3. Experimental Stewart platform .....	69
Figure 7.4. 0.2mm reference trajectory for $p_x$ and measured motion .....	69
Figure 7.5. Corresponding tracking error for the 0.2mm sigmoid.....	70
Figure 7.6. Reference limb trajectories for 0.2mm $p_x$ trajectory .....	70
Figure 7.7. 0.1mm reference trajectory for $p_x$ and measured motion .....	71
Figure 7.8. Reference limb trajectories for 0.1mm $p_x$ trajectory .....	71
Figure 7.9. Reference limb trajectories for 0.1mm $p_x$ trajectory (Contd.).....	72
Figure 7.10. 50 $\mu$ m reference trajectory for $p_x$ and measured motion .....	72
Figure 7.11. Reference limb trajectories for 50 $\mu$ m $p_x$ trajectory .....	73

## LIST OF SYMBOLS

<b>S</b>	:	Strain Tensor
$\mathbf{s}^E$	:	Elastic compliance matrix at constant electric field
<b>T</b>	:	Stress tensor
<b>d</b>	:	Piezoelectric material constants
<b>E</b>	:	Electric field vector
$\mathbf{D}^E$	:	Electric displacement vector
$\boldsymbol{\varepsilon}^T$	:	Permittivity at constant stress
$x$	:	Displacement
$v$	:	Velocity
$u_{in}$	:	Voltage input to the piezoelectric actuator
$t$	:	Time
$\gamma_{\alpha\beta}[\cdot]$	:	An operator
$\alpha$	:	Maximum value of input extrema
$\beta$	:	Minimum value of input extrema
$\mu(\alpha,\beta)$	:	Weighing function
<b>x</b>	:	State vector
<b>A</b>	:	System matrix
<b>B</b>	:	Input matrix
$\mathbf{x}_0$	:	Initial state matrix
<b>f</b>	:	Vector representing the dynamics of the system
$\boldsymbol{\sigma}(\mathbf{x})$	:	Vector of sliding functions
$S$	:	Sliding Surface
$V(\sigma)$	:	Lyapunov function
<b>D</b>	:	Positive definite matrix
<b>G</b>	:	A matrix

$\mathbf{u}_{eq}$	:	Equivalent control
$\hat{\mathbf{u}}_{eq}$	:	Estimate of the equivalent control
$\mathbf{K}$	:	Positive diagonal matrix
$T_s$	:	Sampling time
$\mathbf{x}^r$	:	Reference state vector
$\zeta(\cdot)$	:	Estimate of the boundary layer around the sliding surface
$\mathbf{A}_N$	:	Nominal system matrix
$\mathbf{B}_N$	:	Nominal input matrix
$\Delta\mathbf{A}$	:	Uncertainty in system matrix
$\Delta\mathbf{B}$	:	Uncertainty in input matrix
$\mathbf{u}_d$	:	Disturbance vector
$\hat{\mathbf{x}}$	:	Estimate of the state vector
$\mathbf{u}_c$	:	Vector of observer control input
$H$	:	Hysteresis operator
$u_h$	:	Voltage due to hysteresis effect
$T_{em}$	:	Electromechanical transformation ratio
$C_e$	:	Equivalent electrical capacitance of a piezoelectric actuator
$q$	:	Charge in a piezoelectric actuator
$q_p$	:	Charge due to mechanical strain
$u_p$	:	Voltage due to piezoelectric effect
$F_p$	:	Transduced force from the electrical side
$F_{ext}$	:	Externally applied force
$a_h, b_h, \alpha_h$	:	Constants used in the hysteresis model
$D, D_{est}, D_f, D_x$	:	Positive constants
$K_u, K_{est}, K_f, K_x$	:	Tuning constants
$\theta(t)$	:	Angular position
$i(t)$	:	Current input to the DC-motor
$q_1, q_2$	:	Linear position of macroactuator and microactuator
$z$	:	Deflection of the piezoelectric actuator relative to the DC-drive
$\bar{p}$	:	Position of the top plate w.r.t the base
${}^A R_B$	:	Transformation matrix from the top plate to bottom plate
$\bar{u}, \bar{v}, \bar{w}$	:	Unit vectors
$\bar{a}_i, \bar{b}_i$	:	Location of the $i^{th}$ joint w.r.t the base and the top plate

## **LIST OF ABBREVIATIONS**

VSS	:	Variable Structure System
VSC	:	Variable Structure Control
SMC	:	Sliding Mode Control
PID	:	Proportional Integral Derivative Control
PZT	:	Lead Zirconium Titanate

**SLIDING-MODE CONTROL FOR HIGH-PRECISION MOTION CONTROL  
SYSTEMS**

by

**KHALID ABIDI**

Submitted to the Graduate School of Engineering and Natural Sciences  
in partial fulfillment of  
the requirements for the degree of  
Master of Science

Sabanci University

Spring 2004

SLIDING-MODE CONTROL FOR HIGH-PRECISION MOTION CONTROL  
SYSTEMS

APPROVED BY:

Prof. Dr. Asif Sabanovic .....

(Dissertation Supervisor)

Dr. Serhat Yesilyurt .....

Dr. Hasan Sait Olmez .....

DATE OF APPROVAL: .....

© Khalid Abidi 2004

All Rights Reserved

## ABSTRACT

In many of today's mechanical systems, high precision motion has become a necessity. As performance requirements become more stringent, classical industrial controllers such as PID can no longer provide satisfactory results. Although many control approaches have been proposed in the literature, control problems related to plant parameter uncertainties, disturbances and high-order dynamics remain as big challenges for control engineers.

Theory of Sliding Mode Control provides a systematic approach to controller design while allowing stability in the presence of parametric uncertainties and external disturbances. In this thesis a brief study of the concepts behind Sliding Mode Control will be shown. Description of Sliding Mode Control in discrete-time systems and the continuous Sliding Mode Control will be shown. The description will be supported with the design and robustness analysis of Sliding Mode Control for discrete-time systems.

In this thesis a simplified methodology based on discrete-time Sliding Mode Control will be presented. The main issues that this thesis aims to solve are friction and internal nonlinearities. The thesis can be outlined as follows:

- Implementation of discrete-time Sliding Mode Control to systems with nonlinearities and friction. Systems include; piezoelectric actuators that are known to suffer from nonlinear hysteresis behavior and ball-screw drives that suffer from high friction. Finally, the controller will be implemented on a 6-dof Stewart platform which is a system of higher complexity.
- It will also be shown that performance can be enhanced with the aid of disturbance compensation based on a nominal plant disturbance observer.

## ÖZET

Günümüzde kullanılan mekanik sistemlerde yüksek hassasiyetli hareket iletimi bir gereksinim haline gelmiştir. Performans gereksinimlerinin daha sıkılaşmasıyla birlikte, PID gibi klasik kontrol yöntemleri tatmin edici sonuçlar verememektedir. Literatürde birçok kontrol yaklaşımı önerilmesine rağmen sistem parametrelerindeki belirsizlikler, bozucu etkenler ve yüksek dereceli sistem dinamiği içeren kontrol problemleri, mühendisler için hala büyük bir sorun teşkil etmektedir.

Kayma Kipli Kontrol teorisi, parametrik belirsizliklere ve dışarıdan gelen bozucu etkenlere karşı kararlılık sağlayarak kontrolör tasarımında sistematik bir yaklaşım sunmaktadır. Bu tezde Kayma Kipli Kontrol'ün arkaplanındaki kavramlar kısaca gösterilecektir. Ayrık zamanlı Kayma Kipli Kontrol ve sürekli Kayma Kipli Kontrol tanımları gösterilecektir. Bu tanımlar ayrık zamanlı Kayma Kipli Kontrol tasarımı ve dayanıklılık analizi ile desteklenecektir.

Bu tezde ayrık zamanlı Kayma Kipli Kontrol üzerine kurulan basitleştirilmiş bir metodoloji sunulacaktır. Bu tezin çözümlemeyi amaçladığı ana noktalar sürtünme ve sisteme ait doğrusal olmayan özelliklerdir. Bu tezin ana hatları aşağıdaki gibi özetlenebilir:

- İçinde sürtünme ve doğrusal olmayan özellikler barındıran sistemlere ayrık zamanlı Kayma Kipli Kontrol'ün uygulanması. Bu sistemler şu bileşenleri içerir; doğrusal olmayan histerezis davranışı sergileyen kumanda aygıtları ve yüksek sürtünme kuvvetiyle karşı karşıya olan vida mekanizması. Son olarak kontrolör, yüksek oranda karmaşıklığa sahip olan altı serbestlik dereceli bir Stewart platformuna uygulanacaktır.
- Ayrıca, nominal sistem bozucu etken gözlemleyicisi üzerine kurulu bozucu etken kompanzasyonu yöntemi yardımı ile performansın iyileştirildiği gösterilecektir.

*To Peter Jackson for his everlasting inspiration...*

## ACKNOWLEDGEMENTS

I would like to convey my special thanks to Prof. Şabanoviç for his support and guidance regarding the theoretical work in the thesis and for his proposing this research to me. I would also like to give my thanks to Prof. Ahmet Onat for helping me with all the problems I had faced in the instrumentation and to Prof. Serhat Yeşilyurt for his recommendations. I should also convey my thanks to Prof. Mahmut Akşit for helping me with the mechanical design and Mehmet Guler for helping me with the actual manufacturing of the system.

I would also like to convey my thanks to the Mechatronics Graduate students especially Bahadır Kiliç, Yıldırım Yıldız, Kazım Çakır, Hakan Keskin, Ozan Ayhan, Yasser Elkahlout and Fazıl Serincan for their everlasting support and for their having good discussions with me regarding the subject matter.

Finally I would like to give my thanks to my family and especially my mom and dad for giving me support throughout my education and to my brother Anas for always being there for me.

## TABLE OF CONTENTS

1. Introduction.....	1
1.1 Objective.....	1
1.2 Mechatronic Microsystems.....	2
1.2.1 Piezoelectric Actuator Driven Micromanipulators.....	3
1.2.2 Models of the Piezoelectric Actuator.....	4
1.2.2.1 Continuous Model.....	4
1.2.2.2 Preisach Model of Hysteresis.....	5
1.3 Control Techniques.....	7
1.3.1 $H_\infty$ Almost Disturbance Decoupling Controller.....	7
1.3.2 Neural Networks Based Controller.....	8
1.4 Motivation behind using Sliding-Mode Control.....	9
1.5 Stewart Platform for Flexible Six-dof Motion.....	10
2. Sliding-Mode Variable Structure Control.....	12
2.1 Introduction.....	12
2.2 Sliding-Mode in Variable Structure Systems.....	13
2.3 Sliding-Mode Controller Design and Realization of Discrete-time Control.....	14
2.4 Calculation of the Boundary Layer in Discrete-Time Sliding-Mode Control.....	18
2.5 Disturbance Observers based on Sliding-Mode Control.....	19
3. Model of the Piezoelectric Actuator.....	21
3.1 Introduction.....	21
3.2 Structure of the Piezoelectric Actuator.....	22
3.3 Model of the Piezoelectric Actuator.....	23
3.3.1 The Selected Model.....	23
3.3.2 Hysteresis Model.....	25
3.3.3 Simulation Results.....	27
3.4 Open-Loop Control of the Actuator.....	28

4. Implementation of SMC to a Piezoelectric Actuator.....	32
4.1 Introduction.....	32
4.2 Design of the Observers.....	33
4.2.1 Total Disturbance Estimation .....	33
4.2.2 Force Observer.....	38
4.3 Results of Closed-Loop Control Experiments.....	39
4.3.1 Position Control .....	40
4.3.2 Force Control .....	42
5. A Dual-Stage Servo System .....	45
5.1 Introduction.....	45
5.2 Structure of the System.....	46
5.3 Results with Single-Stage Servo.....	48
5.4 Proposed Controller .....	50
5.5 Results with Dual-Stage Servo .....	51
6. Analysis of the Kinematics of a 6-DOF Stewart-Gough Manipulator .....	54
6.1 Introduction.....	54
6.2 Description of the Stewart-Gough Manipulator .....	55
6.3 Geometry of the Stewart-Gough Manipulator .....	56
6.4 Direct Kinematics of the Stewart-Gough Manipulator.....	58
6.5 Inverse Kinematics of the Stewart-Gough Manipulator .....	60
6.5.1 Simulation Results for the Proposed Manipulator.....	61
7. Experiments on an Actual Stewart Platform.....	67
7.1 Introduction.....	67
7.2 Structure of the Experimental Stewart Platform.....	67
7.3 Experimental Results .....	69
CONCLUSION.....	74
REFERENCE.....	76

## LIST OF TABLES

Table 3.1. Parameters of the PZT model .....	27
Table 6.1. Manipulator joint coordinates.....	61

## LIST OF FIGURES

Figure 1.1. 3-Axis nanopositioning system, PI GmbH.....	4
Figure 1.2. Hysteresis operator $\gamma_{\alpha\beta}[u(t)]$ .....	6
Figure 1.3. Monotonically increasing input $u_1(t)$ .....	6
Figure 1.4. Closed-loop neural network controller.....	8
Figure 1.5. Six-dof Stewart platform, PI GmbH .....	10
Figure 1.6. Experimental Stewart platform .....	11
Figure 2.1. Geometric interpretation of two intersecting switching surfaces.....	15
Figure 2.2. Discrete-time system with discontinuous control .....	15
Figure 2.3. Discrete-time Sliding mode in sampled-data systems.....	17
Figure 2.4. Disturbance observer implementation.....	20
Figure 3.1. Stack actuators used in the experiments.....	22
Figure 3.2. Illustration of a PZT stack actuator .....	24
Figure 3.3. Electromechanical model of the PZT actuator, [1] .....	24
Figure 3.4. Block-Diagram representation of the electromechanical model .....	26
Figure 3.5. A hysteresis loop .....	26
Figure 3.6. Response to $u = 40 + 40\sin(t)$ and corresponding modeling error.....	28
Figure 3.7. Response to $u = 15 + 15\sin(t)$ and corresponding modeling error.....	29
Figure 3.8. Inverse model of the PZT actuator .....	29
Figure 3.9. Response to $x_r = 7.5 + 7.5\sin(t)$ .....	29
Figure 3.10. Open-loop tracking error and input voltage for $x_r = 7.5 + 7.5\sin(t)$ .....	30
Figure 3.11. Response to a varying amplitude sine reference .....	30
Figure 3.12. Input voltage for a varying amplitude sine reference (contd.).....	31
Figure 3.13. Response to a high frequency varying amplitude sine reference .....	31
Figure 4.1. Observer implementation .....	35
Figure 4.2. Response to $u_0 = 7.5\sin(10\pi t) + 7.5$ .....	36

Figure 4.3. Response to $u_0 = 7.5 \sin(100\pi) + 7.5$ with disturbance compensation.....	36
Figure 4.4. Response to $u_0 = 30 \sin(10\pi) + 30$ with disturbance compensation.....	37
Figure 4.5. Response to $u_0 = 30 \sin(100\pi) + 30$ with disturbance compensation.....	37
Figure 4.6. Block-diagram for external force estimation.....	39
Figure 4.7. Results of the Force Observer Experiments .....	39
Figure 4.8. Sketch of the experimental setup.....	40
Figure 4.9. Structure of the experimental setup.....	40
Figure 4.10. Closed-loop control scheme .....	41
Figure 4.11. Closed-loop response to a 1Hz sinusoidal reference.....	41
Figure 4.12. 5nm step motion .....	42
Figure 4.13. 1nm step motion .....	42
Figure 4.14. Block-diagram of force control system .....	43
Figure 4.15. Sensor based force control .....	44
Figure 4.16. Observer based force control.....	44
Figure 5.1. CAD model of the dual-stage system.....	46
Figure 5.2. Anatomy of the dual-stage system .....	47
Figure 5.3. Model representation of the system.....	47
Figure 5.4. Single-stage controller scheme.....	48
Figure 5.5. Single-stage 0.5mm sigmoid reference tracking .....	49
Figure 5.6. Single-stage 1mm sigmoid reference tracking .....	49
Figure 5.7. Single-stage 1.5mm sigmoid reference tracking .....	50
Figure 5.8. Dual-stage Controller scheme .....	50
Figure 5.9. Dual-stage 0.5mm sigmoid reference tracking.....	51
Figure 5.10. Dual-stage 1mm sigmoid reference tracking.....	52
Figure 5.11. Dual-stage 1.5mm sigmoid reference tracking.....	52
Figure 5.12. Dual-stage 1.5mm sigmoid reference tracking (contd.).....	53
Figure 6.1. VARIAX <sup>®</sup> machining center, Giddings and Lewis machine tools .....	55
Figure 6.2. Spatial 6-dof, 6SPS parallel manipulator .....	57
Figure 6.3. MSC.ADAMS CAD model of the proposed manipulator .....	61
Figure 6.4. First set of reference trajectories for point $P$ .....	62
Figure 6.5. First set of reference trajectories for point $P$ .....	63
Figure 6.6. Required limb elongations for the first set of trajectories.....	63
Figure 6.7. CAD model response to the first set of trajectories.....	64

Figure 6.8. Second set of reference trajectories for point $P$ .....	65
Figure 6.9. Limb elongations for the second set of trajectories.....	65
Figure 6.10. Limb elongations for the second set of trajectories (contd.) .....	66
Figure 6.11. CAD model response to the second set of trajectories.....	66
Figure 7.1. Limb of the experimental system .....	68
Figure 7.2. Sketch of the system.....	68
Figure 7.3. Experimental Stewart platform .....	69
Figure 7.4. 0.2mm reference trajectory for $p_x$ and measured motion .....	69
Figure 7.5. Corresponding tracking error for the 0.2mm sigmoid.....	70
Figure 7.6. Reference limb trajectories for 0.2mm $p_x$ trajectory .....	70
Figure 7.7. 0.1mm reference trajectory for $p_x$ and measured motion .....	71
Figure 7.8. Reference limb trajectories for 0.1mm $p_x$ trajectory .....	71
Figure 7.9. Reference limb trajectories for 0.1mm $p_x$ trajectory (Contd.).....	72
Figure 7.10. 50 $\mu$ m reference trajectory for $p_x$ and measured motion .....	72
Figure 7.11. Reference limb trajectories for 50 $\mu$ m $p_x$ trajectory .....	73

## LIST OF SYMBOLS

<b>S</b>	:	Strain Tensor
$\mathbf{s}^E$	:	Elastic compliance matrix at constant electric field
<b>T</b>	:	Stress tensor
<b>d</b>	:	Piezoelectric material constants
<b>E</b>	:	Electric field vector
$\mathbf{D}^E$	:	Electric displacement vector
$\boldsymbol{\varepsilon}^T$	:	Permittivity at constant stress
$x$	:	Displacement
$v$	:	Velocity
$u_{in}$	:	Voltage input to the piezoelectric actuator
$t$	:	Time
$\gamma_{\alpha\beta}[\cdot]$	:	An operator
$\alpha$	:	Maximum value of input extrema
$\beta$	:	Minimum value of input extrema
$\mu(\alpha,\beta)$	:	Weighing function
<b>x</b>	:	State vector
<b>A</b>	:	System matrix
<b>B</b>	:	Input matrix
$\mathbf{x}_0$	:	Initial state matrix
<b>f</b>	:	Vector representing the dynamics of the system
$\boldsymbol{\sigma}(\mathbf{x})$	:	Vector of sliding functions
$S$	:	Sliding Surface
$V(\sigma)$	:	Lyapunov function
<b>D</b>	:	Positive definite matrix
<b>G</b>	:	A matrix

$\mathbf{u}_{eq}$	:	Equivalent control
$\hat{\mathbf{u}}_{eq}$	:	Estimate of the equivalent control
$\mathbf{K}$	:	Positive diagonal matrix
$T_s$	:	Sampling time
$\mathbf{x}^r$	:	Reference state vector
$\zeta(\cdot)$	:	Estimate of the boundary layer around the sliding surface
$\mathbf{A}_N$	:	Nominal system matrix
$\mathbf{B}_N$	:	Nominal input matrix
$\Delta\mathbf{A}$	:	Uncertainty in system matrix
$\Delta\mathbf{B}$	:	Uncertainty in input matrix
$\mathbf{u}_d$	:	Disturbance vector
$\hat{\mathbf{x}}$	:	Estimate of the state vector
$\mathbf{u}_c$	:	Vector of observer control input
$H$	:	Hysteresis operator
$u_h$	:	Voltage due to hysteresis effect
$T_{em}$	:	Electromechanical transformation ratio
$C_e$	:	Equivalent electrical capacitance of a piezoelectric actuator
$q$	:	Charge in a piezoelectric actuator
$q_p$	:	Charge due to mechanical strain
$u_p$	:	Voltage due to piezoelectric effect
$F_p$	:	Transduced force from the electrical side
$F_{ext}$	:	Externally applied force
$a_h, b_h, \alpha_h$	:	Constants used in the hysteresis model
$D, D_{est}, D_f, D_x$	:	Positive constants
$K_u, K_{est}, K_f, K_x$	:	Tuning constants
$\theta(t)$	:	Angular position
$i(t)$	:	Current input to the DC-motor
$q_1, q_2$	:	Linear position of macroactuator and microactuator
$z$	:	Deflection of the piezoelectric actuator relative to the DC-drive
$\bar{p}$	:	Position of the top plate w.r.t the base
${}^A R_B$	:	Transformation matrix from the top plate to bottom plate
$\bar{u}, \bar{v}, \bar{w}$	:	Unit vectors
$\bar{a}_i, \bar{b}_i$	:	Location of the $i^{th}$ joint w.r.t the base and the top plate

## **LIST OF ABBREVIATIONS**

VSS	:	Variable Structure System
VSC	:	Variable Structure Control
SMC	:	Sliding Mode Control
PID	:	Proportional Integral Derivative Control
PZT	:	Lead Zirconium Titanate

# 1. INTRODUCTION

## 1.1 Objective

High precision motion control has become an essential requirement in today's advanced manufacturing systems such as machine tools, micro-manipulators, surface mounting robots, etc. As performance requirements become more stringent, classical controllers such as the PID controller, which has been the most favored controller and widely used in industry for generations, can no longer provide satisfactory results. Although various approaches to the design of better controllers have been proposed in the literature, control problems associated with system uncertainties, presence of high-order dynamics and system inherent nonlinearities remain big challenges for control engineers.

High precision motion control is first challenged by the presence of friction. Friction, as a highly complex, nonlinear phenomenon exists in almost every mechanical system involving relative motion between parts. Different characteristics of friction can appear in different types of contacting surfaces and the magnitude of friction depends on the physical properties of the interacting surfaces as well as the load. The problems caused by friction primarily result in unacceptable tracking/positioning errors which can not simply be eliminated by introducing an integral action in the controller. Particularly, when low-speed small-amplitude motion tasks are required, nonlinear friction in combination with integral action typically leads to so called stick-slip limit cycles.

In addition, other uncertainties which may also be regarded as parasitic effects are often present in real-world systems. These effects include:

- Parametric uncertainty, such as parameter changes due to, for example, different operating conditions and load changes.

- Actuator/sensor nonlinearities, such as hysteresis, dead-zone, saturation, input-output slope changes in operating ranges as well as the nonlinearity of quantization when using AD converters for digital-computer control
- Backlash and compliance in gear-trains
- Time delays

The research goal of this thesis is to develop a simplified control methodology for implementation into real systems that are required to have very high-precision motion. The main efforts are concentrated on handling internal nonlinear disturbances and friction of mechanical systems. The thesis focuses more on actual implementation than theoretical analysis.

## 1.2 Mechatronic Microsystems

Nowadays, novel trends can be seen in mechatronic systems technology: Micro mechatronic systems are being increasingly developed into stand-alone devices for multi-purpose applications, and these do not necessarily comprise of sensor elements but can also interact mechanically with the aid of micro actuators with their surroundings.

With dimensions of a few millimeters, piezo-driven valves and membrane pumps overcome fluid pressures up to 1000hPa. Electromagnetic motors generate torques of 7 to 100 $\mu$ m which are multiplied by adapted micro gears. Gear motors serve as a key unit for high force micro positioning systems or micro gear pumps which are first examples for the device level.

With the integration of electronics and optics the actuator performance can be considerably increased by establishing a feedback control and the systems really become mechatronic devices. Additionally, interface components such as electrical and fiber-optic connectors with pitches as small as 250 $\mu$ m, special gears and miniaturized clamping structures enable the implementation of complex optical fiber networks, micro robots or chemical micro reactors from these mechatronic devices in a construction kit.

Microsystems are widely used in all domains of our daily life but are hardly recognized. This is due to the fact that most of these devices are integrated into mass-products and specialized for the one application they are developed for. Airbag sensors

in passenger vehicles or laser heads in CD players illuminate that fact impressively. Another example are print heads of ink jet printers which only work in the specified printers and use only one type of fluid -ink. On the other hand ink printer heads are at least stand-alone micro devices in the geometrical sense. Printer heads interact, like more and more modern microsystems do, with their surroundings. The mechanical or fluidic interaction is executed by small but powerful actuators.

A promising actuation principle for application in microsystems is based on piezoelectricity. Piezoelectricity is a fundamental process in electromechanical energy conversion. It relates electric polarization to stress/strain in piezoelectric materials. Under the direct piezoelectric effect, an electric charge can be observed when the material is deformed. The inverse, or the reciprocal piezoelectric effect, is when the application of an electric field can cause mechanical stress/strain in the piezoelectric materials. There are numerous piezoelectric materials available today, including PZT (lead zirconate titanate), PLZT (lanthanum modified lead zirconate titanate), and PVDF (piezoelectric polymeric polyvinylidene flouride) to name a few.

Piezoelectric structures are widely used in applications that require electrical to mechanical energy conversion coupled with size limitations, precision, and speed of operation. Typical examples are microsensors, micropositioners, speakers, medical diagnostics, shutters and impact print hammers. In most applications bimorph or stack piezoelectric structures are used because of the relatively high stress/stain to input electric field ratio. These structures are mostly fabricated in a hybrid concept by combining advanced 3D micro fabrication methods with assembly and interconnection techniques.

### **1.2.1 Piezoelectric Actuator Driven Micromanipulators**

Micromanipulation technology is one of the most important key issues nowadays. The field of micromanipulation, which deals with objects from a few microns to hundreds of microns in size, places unique demands on the design of a manipulator. First, the dynamics of micro objects are different from that of conventional macro objects; in the micro world, surface forces such as surface tension, electrostatic force and viscous friction forces are dominant rather than inertial force. Second, the mechanism should be designed so that small actuator displacements can generate as

large workspace as possible. Furthermore, joint types and actuation methods which can be easily realized on miniature scale are required. In Figure 1.1, an example of a commercially available piezoelectric actuator driven system is shown.

## 1.2.2 Models of the Piezoelectric Actuator

In this section some models of the piezoelectric actuator that were encountered during this study are briefly described.

### 1.2.2.1 Continuous Model

The most widely recognized description of piezoelectric ceramic behavior published by a standards committee of the IEEE Ultrasonics, Ferroelectrics and Frequency Control Society originally in 1966 and most recently revised in 1987 [1]. This committee formulated linearized constitutive relations describing piezoelectric continua which form the basis of piezoelectric behavior that is presently in general use. The linearized relations are typically represented in a compressed matrix notation as follows:

$$\mathbf{S}_p = \mathbf{s}_{pq}^E \mathbf{T}_q + \mathbf{d}_{kp} \mathbf{E}_k \quad (1.1)$$

$$\mathbf{D}_i^E = \mathbf{d}_{iq} \mathbf{T}_q + \boldsymbol{\varepsilon}_{ik}^T \mathbf{E}_k \quad (1.2)$$



Figure 1.1. 3-Axis nanopositioning system, PI GmbH

Here  $\mathbf{S}$  represents the strain tensor,  $\mathbf{s}^E$  is the elastic compliance matrix when subjected to constant electric field,  $\mathbf{T}$  represents the stress tensor,  $\mathbf{d}$  is a matrix of piezoelectric material constants,  $\mathbf{E}$  is the electric field vector,  $\mathbf{D}^E$  is the electric displacement vector, and  $\boldsymbol{\epsilon}^T$  the permittivity measured at a constant stress. The compressed notation eliminates redundant terms by representing the symmetric stress and strain with single column vectors that incorporate elements representing both the diagonal and off-diagonal tensor terms. These equations essentially state that the material strain and electrical displacement exhibited by the PZT are both linearly affected by the mechanical stress and the electrical field to which ceramic is subjected. Aside from the awkward notation and the obvious difficulty in implementing these in real-time applications these relations fail to explicitly describe the nonlinearities that are present in all piezoelectric ceramics. Additionally, the derivation assumes a purely conservative energy field, and thus fails to describe the dissipative nature of these ceramics.

### 1.2.2.2 Preisach Model of Hysteresis

Preisach model was originally developed in the area of Magnetics. However, recently it has been increasingly used to model piezoelectric continua. The classical Preisach model equation relating piezoelectric expansion  $x(t)$  and input voltage  $u_{in}(t)$  is

$$x(t) = \iint_{\alpha \geq \beta} \mu(\alpha, \beta) \gamma_{\alpha\beta}[u_{in}(t)] d\alpha d\beta \quad (1.3)$$

where  $\gamma_{\alpha\beta}[u_{in}(t)]$  are elementary hysteresis operators whose values are determined by the input voltage signal  $u_{in}(t)$  (Figure 2).  $\alpha$  and  $\beta$  are extrema values of the input signal. They are defined such that  $\alpha$  corresponds to the maximum value of the input extrema and  $\beta$  corresponds to the minimum value of the input extrema. The function  $\mu(\alpha, \beta)$  is an arbitrary weighting function and is called the Preisach function (Mayergoyz, 1991). For stack actuators the piezoelectric hysteresis loop is only defined in the first quadrant of the  $u$ - $x$  plane. So the values of the hysteresis operator  $\gamma_{\alpha\beta}[u_{in}(t)]$  are selected as switching between 0 and 1 (see Figure 1.2). Knowing what the maximum and minimum values of the input are, the condition  $\alpha \geq \beta$  leads to a limiting triangle  $T_o$  on the  $\alpha$ - $\beta$  plane (Figure 1.3) which is defined such that the function  $\mu(\alpha, \beta)$  is equal to zero outside

$T_o$ . On the  $\alpha$ - $\beta$  half-plane, there is a one-to-one correspondence between operators  $\gamma_{\alpha\beta}[u_{in}(t)]$  and points  $(\alpha, \beta)$  which implies that each pair of values  $(\alpha, \beta)$  defines a unique operator  $\gamma_{\alpha\beta}[\cdot]$  with switching values  $\alpha$  and  $\beta$ . At each instant of time and as a result of applying an input  $u_i(t)$ , the limiting triangle in the half-plane can be divided into two areas,  $S_i^+(t)$  and  $S_i^-(t)$  (Figure 1.3). All operators  $\gamma_{\alpha\beta}[u_{in}(t)]$  that belong to  $S_i^+(t)$  are equal to 1 and those that belong to  $S_i^-(t)$  are equal to 0.

The solution of the Preisach model requires implementation of a cumbersome numerical technique in order to decide the weighing functions. Thus, it is not so favorable in this application in which high sampling rate would not allow implementation of such a numerical technique.

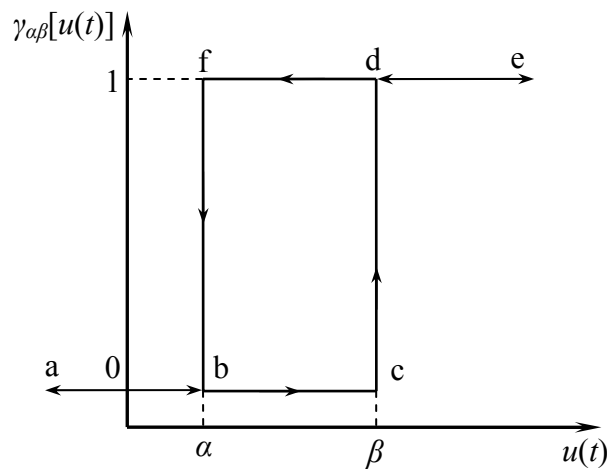


Figure 1.2. Hysteresis operator  $\gamma_{\alpha\beta}[u(t)]$

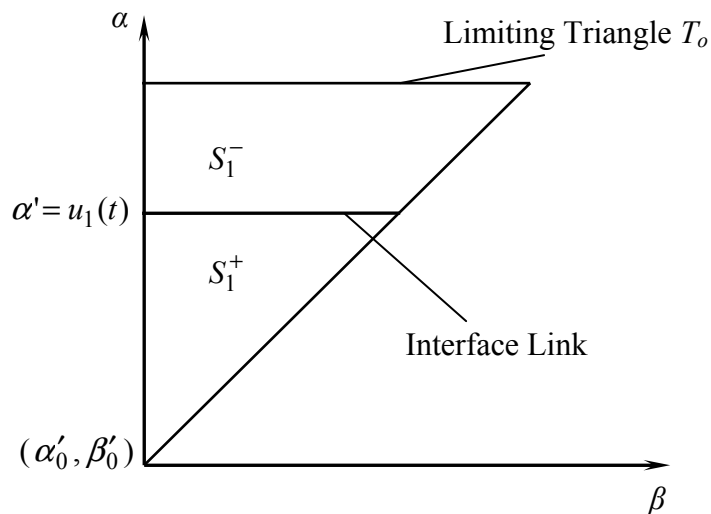


Figure 1.3. Monotonically increasing input  $u_1(t)$

### 1.3 Control Techniques

Numerous control techniques exist in the literature that can be implemented for the control of the piezoelectric actuators. But, one must keep in mind the high non-linearity that is inherent in these actuators. Thus, only control techniques found in the literature that were implemented on piezoelectric actuators will be mentioned.

#### 1.3.1 $H_\infty$ Almost Disturbance Decoupling Controller

This technique was implemented in the work of Chen [13]. The basic almost disturbance decoupling problem is to find an output feedback control law such that in the closed-loop system the disturbances are eliminated up to any specified degree of accuracy while maintaining internal stability. Such a problem was originally formulated by Willems [13] and termed almost disturbance decoupling problem with measurement feedback and internal stability.

For a system defined in the state-space form below

$$\begin{aligned}\dot{\mathbf{x}} &= \mathbf{A}\mathbf{x} + \mathbf{B}\mathbf{u} + \mathbf{H}\mathbf{w} \\ \mathbf{y} &= \mathbf{C}_1\mathbf{x} + \mathbf{D}_1\mathbf{w} \\ \mathbf{z} &= \mathbf{C}_2\mathbf{x}\end{aligned}\tag{1.4}$$

Here  $\mathbf{z}$  is the double integration of the error and  $\mathbf{w}$  is the disturbance. The  $H_\infty$  almost disturbance decoupling problem is to design a parameterized proper controller of the form where subscript  $c$  stands for controller

$$\begin{aligned}\dot{\mathbf{x}}_c &= \mathbf{A}_c(\varepsilon_1, \varepsilon_2)\mathbf{x}_c + \mathbf{B}_c(\varepsilon_1, \varepsilon_2)\mathbf{y} \\ \mathbf{u} &= \mathbf{C}_c(\varepsilon_1, \varepsilon_2)\mathbf{x}_c + \mathbf{D}_c(\varepsilon_1, \varepsilon_2)\mathbf{y}\end{aligned}\tag{1.5}$$

That has the following properties

- **Internal Stability:** There exists scalars  $\varepsilon_1^* > 0$  and  $\varepsilon_2^* > 0$  such that for all  $0 < \varepsilon_1 < \varepsilon_1^*$  and  $0 < \varepsilon_2 < \varepsilon_2^*$ , the closed-loop system comprising (1.4) and (1.5) is asymptotically stable. That is for all  $0 < \varepsilon_1 < \varepsilon_1^*$  and  $0 < \varepsilon_2 < \varepsilon_2^*$  the following matrix:

$$\mathbf{A}_{CL}(\varepsilon_1, \varepsilon_2) = \begin{bmatrix} \mathbf{A} + \mathbf{B}\mathbf{D}_c(\varepsilon_1, \varepsilon_2)\mathbf{C}_1 & \mathbf{B}\mathbf{C}_c(\varepsilon_1, \varepsilon_2) \\ \mathbf{B}_c(\varepsilon_1, \varepsilon_2)\mathbf{C}_1 & \mathbf{A}_c(\varepsilon_1, \varepsilon_2) \end{bmatrix} \quad (1.6)$$

Has all eigenvalues in the open left-half of the complex plane.

- Disturbance Rejection: The  $H_\infty$ -norm of the closed-loop transfer function matrix from the disturbance input  $\mathbf{w}$  to the output controlled  $\mathbf{z}$ , say  $\mathbf{G}_{zw}(\varepsilon_1, \varepsilon_2, s)$ , satisfying

$$\|\mathbf{G}_{zw}(\varepsilon_1, \varepsilon_2, s)\|_\infty \rightarrow 0 \text{ as } \varepsilon_1 \rightarrow 0 \text{ and } \varepsilon_2 \rightarrow 0 \quad (1.7)$$

In this technique the implementation requires the knowledge of some system parameters that are not possible to estimate and according to the results found in the literature, [13], it was not successful in producing very high precision motion as would be expected from piezoelectric actuators. Furthermore, disturbance rejection was done based on a hysteresis model which is impractical.

### 1.3.2 Neural Networks Based Controller

The main premise here is to take advantage of the capability of neural networks to model non-linear functions and model the hysteresis non-linearity of the piezoelectric actuator. Introducing closed-loop control in addition to neural networks model should result in achieving the necessary requirements.

Model of the hysteresis using neural networks is constructed from extensive measurements of the piezoelectric actuator dynamics. The resulting model is inverted allowing overall linearization of the system. The closed-loop control is added to compensate modeling errors. The overall control strategy is depicted in Figure 1.4.

This technique is cumbersome as it requires a lot of testing to fit the neural network to the hysteresis.

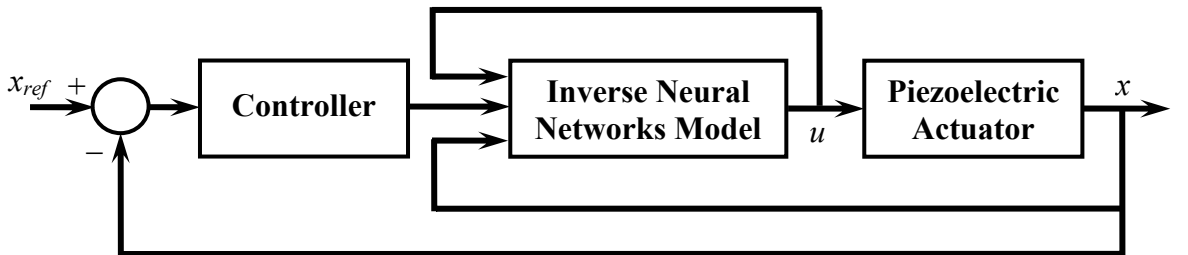


Figure 1.4. Closed-loop neural network controller

## 1.4 Motivation behind using Sliding-Mode Control

There is no unique solution to different control problems. Some methods may be more attractive for certain control problems, while others may also be acceptable. As far as internal hysteresis or friction compensation is concerned, the effectiveness of model based compensation has been proved in many reports, of which some will be mentioned below. The used models include both advanced dynamic models and simple static models. It is known that both hysteresis and friction identification is usually a tough and time consuming work. Moreover, using more complicated models may not always lead to better compensation results than just using a simple model, e.g., the model of Coulomb friction, since the quality of compensation depends not only on the model, but also on the implementation constraints. As already mentioned, how accurate the parameters can be identified and how accurate the system state variables, such as velocity, can be measured or estimated are also key factors. Small error in velocity may possibly result in very inaccurate compensation both in magnitude and direction, which in turn seriously deteriorates the performance. This is another reason that the dynamic friction models so far have mostly been applied only in simulation analysis and at laboratory stages, [4].

It is concluded that a more effective but applicable compensation method must be developed. Note that even in the same type of series manufactured machines, differences in parameters among individual machines are present uncertainties, e.g., uncertainty in friction parameters due to time-varying friction characteristics, operating condition changes, load changes, etc. It is highly desired that the same control settings should meet the control specification for all machines of the same type, i.e., without individual tuning. However, this goal is difficult to fulfill with the existing compensation techniques, due to the limitations related to both fixed model based and on-line identification based compensation. This difficulty leads to the necessity of finding a methodology that produces a robust controller that can be designed by considering only nominal process parameters. At the same time, the designed controller should have good disturbance rejection such that high precision motion can be achieved without calling for complicated modeling and identification methods. Furthermore,

unmodeled dynamics should also be appropriately handled to avoid causing serious performance degradation.

The theory of variable structure systems (VSS) opened up a wide new area of development for control designers, [4]. Variable structure control (VSC), which is frequently known as sliding mode control (SMC), is characterized by a discontinuous control action which changes structure upon reaching a set of predetermined switching surfaces. This kind of control may result in a very robust system and thus provides a possibility for achieving the previously stated goals.

### 1.5 Stewart Platform for Flexible Six-dof Motion

Parallel manipulators were first introduced by Gough and Whitewall in tire testing equipment, [23]. Later, Stewart, [23], proposed to use a parallel mechanism as a motion base for a flight simulator. The rationale for the use of this kind of manipulator was its high stiffness and dexterity required to impart large accelerations to a heavy load with six degrees of freedom. This architecture soon gained popularity and can now be found in virtually all modern flight simulators. The use of these mechanisms has also extended to other applications such as precision machining, vibration isolation and precision pointing.

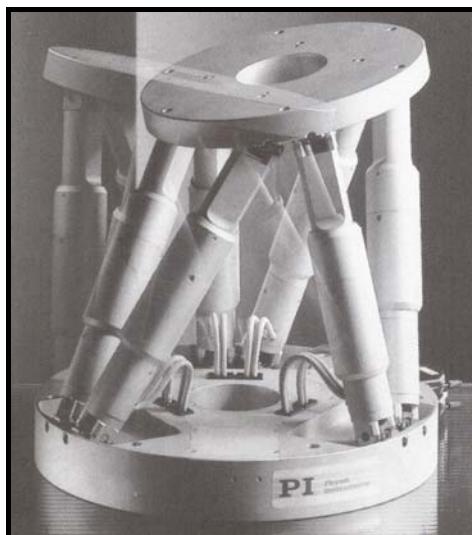


Figure 1.5. Six-dof Stewart platform, PI GmbH



Figure 1.6. Experimental Stewart platform

Because of the unique architecture of a Stewart Platform it offers the following advantages over serial manipulators:

- The load capacity is high: Indeed the load on the platform is supported by all the legs and furthermore the stress in the leg is only tension or compression and not bending as in serial manipulators. This explains the reason why such mechanisms are used for tasks that involve motion of heavy loads.
- The positioning accuracy is good: Indeed the errors on the positioning of the platform are only in some sense an average of the errors on the measurement of the leg lengths.
- They are easily scalable: A Stewart Platform may be used as a huge flight simulator or as a device performing motion in the range of a few micrometers or even nanometers.

These advantages make the use of these manipulators in applications that require precision positioning and force control very suitable.

## 2. SLIDING-MODE VARIABLE STRUCTURE CONTROL

### 2.1 Introduction

Variable structure systems (VSS) first appeared in the late fifties in Russia, as a special class of nonlinear systems. At the very beginning, VSS were studied for solving several specific control tasks in second-order linear and nonlinear systems (Utkin, [3]). The most distinguishing property of VSS is that the closed loop system is completely insensitive to system uncertainties and external disturbances. However, VSS did not receive wide acceptance among engineering professionals until the first survey paper was published by Utkin, [24]. Since then, and especially during later 80's, the control research community has shown significant interest in VSS. This increased interest is explained by the fact that robustness has become a major requirement in modern control applications. A great deal of efforts has been put on establishing both theoretical VSS concepts and practical applications. Some of the concepts and theoretical advances of VSS are covered in, e.g., DeCarlo, et al. [25], Slotine & Li [26], Utkin [3], Hung, et al. [27] and Zinober [28]. Due to its excellent invariance and robustness properties, variable structure control has been developed into a general design method and extended to a wide range of system types including multivariable, large-scale, infinite-dimensional and stochastic systems. The applications include control of aircraft and spacecraft flight, control of flexible structures, robot manipulators, electrical drives, electrical power converters and chemical engineering systems.

## 2.2 Sliding-Mode in Variable Structure Systems

Sliding mode control (SMC), which is sometimes known as variable structure control (VSC), is characterized by a discontinuous control action which changes structure upon reaching a set of predetermined switching surfaces. This kind of control may result in a very robust system and thus provides a possibility for achieving the goals of high-precision and fast response. Some promising features of SMC are listed below:

- The order of the motion can be reduced
- The motion equation of the sliding mode can be designed linear and homogenous, despite that the original system may be governed by non-linear equations.
- The sliding mode does not depend on the process dynamics, but is determined by parameters selected by the designer.
- Once the sliding motion occurs, the system has invariant properties which make the motion independent of certain system parameter variations and disturbances. Thus the system performance can be completely determined by the dynamics of the sliding manifold.

Consider the system defined below

$$\dot{\mathbf{x}} = \mathbf{f}(\mathbf{x}, t) + \mathbf{B}(\mathbf{x}, t)\mathbf{u}(\mathbf{x}, t), \quad \mathbf{x} \in \mathcal{R}^n, \quad \mathbf{u} \in \mathcal{R}^m \quad (2.1)$$

here  $\mathbf{f}(\mathbf{x}, t)$  and  $\mathbf{B}(\mathbf{x}, t)$  are assumed continuous and bounded and the rank of  $\mathbf{B}(\mathbf{x}, t)$  is  $m$ . The discontinuous control is given by

$$\mathbf{u} = \begin{cases} \mathbf{u}^+(\mathbf{x}, t) & \text{if } \boldsymbol{\sigma}(\mathbf{x}) > 0 \\ \mathbf{u}^-(\mathbf{x}, t) & \text{if } \boldsymbol{\sigma}(\mathbf{x}) < 0 \end{cases} \quad (2.2)$$

$$\boldsymbol{\sigma}(\mathbf{x})^T = \{\sigma_1(\mathbf{x}), \sigma_2(\mathbf{x}), \dots, \sigma_m(\mathbf{x})\}, \quad \boldsymbol{\sigma}(\mathbf{x}) = \mathbf{G}(\mathbf{x}^r - \mathbf{x})$$

here  $\mathbf{u}^+(\mathbf{x}, t)$ ,  $\mathbf{u}^-(\mathbf{x}, t)$  and  $\boldsymbol{\sigma}(\mathbf{x})$  are continuous functions. Since  $\mathbf{u}(\mathbf{x}, t)$  undergoes discontinuity on the surfaces  $\sigma_i(x) = 0$ ,  $\sigma_i(x) = 0$  is called the *switching surface* or the *switching hyperplane*.

Let  $S = \mathbf{x} |_{\boldsymbol{\sigma}(\mathbf{x})=0}$  be a switching surface that includes the origin  $\mathbf{x} = 0$ . If, for any  $\mathbf{x}_0$  in  $S$ ,  $\mathbf{x}(t)$  is in  $S$  for all  $t > t_0$ , then  $\mathbf{x}(t)$  is a sliding mode of the system and the switching

surface  $S$  is called a sliding surface or sliding manifold. A sliding mode exists, if in the vicinity of the switching surface  $S$ , the tangent or the velocity vectors of the state trajectory always point towards the switching surface.

Existence of a sliding mode requires stability of the state trajectory towards the sliding surface  $S = \mathbf{x}|_{\sigma(\mathbf{x})=0}$  at least in the neighborhood of  $S$ , i.e., the representative point must approach the sliding surface at least asymptotically. This sufficient condition for sliding mode is called reaching condition and state trajectory under the reaching condition is called the reaching mode or reaching phase. The largest neighborhood of  $S$  for which the reaching condition is satisfied is called the region of attraction.

In order to guarantee desired behavior of the closed-loop system, the sliding mode controller requires infinitely fast switching mechanism. However, due to physical limitations in real-world systems, directly applying the above control will always lead to some oscillations in some vicinity of the sliding surface, i.e., the so called chattering problem. The main limitations come from the implementation of controllers in digital computers which work on discrete-time principles and cannot allow infinitely fast switching. Since modern controllers are most likely implemented in digital computers, it is unavoidable to approach a practical SMC design in discrete-time.

### **2.3 Sliding-Mode Controller Design and Realization of Discrete-time Control**

The VSS theory was originally developed from a continuous time perspective. It has been realized that directly applying the continuous-time SMC algorithms to discrete-time systems will lead to some unconquerable problems, such as the limited sampling frequency, sample/hold effects and discretization errors. Since the switching frequency in sampled-data systems can not exceed the sampling frequency, a discontinuous control does not enable generation of motion in an arbitrary manifold in discrete-time systems. This leads to chattering along the designed sliding surface, or even instability in case of a too large switching gain. Fig 2.2 illustrates that in discrete-time systems, the state moves around the sliding surface in a zigzag manner at the sampling frequency.

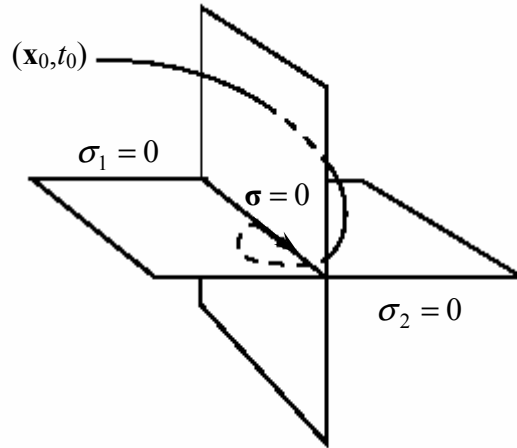


Figure 2.1. Geometric interpretation of two intersecting switching surfaces

So far the developed sliding mode has always been associated with discontinuities in motion equations. To cope with the sampling frequency limitations of sampled-data controllers, Drakunov & Utkin [7] introduced a new concept of “sliding mode” for an arbitrary finite-dimensional discrete-time system. The essence of sliding modes in dynamic systems is that a motion exists in some manifold of state trajectories, and that the time to achieve this motion is finite.

Derivation of the control law starts with the selection of the Lyapunov function,  $V(\boldsymbol{\sigma})$ , and an appropriate form of the derivative of the Lyapunov function,  $\dot{V}(\boldsymbol{\sigma})$ .

Selecting the Lyapunov function such that it is positive definite

$$V(\boldsymbol{\sigma}) = \frac{\boldsymbol{\sigma}^T \boldsymbol{\sigma}}{2} \quad (2.3)$$

Hence the derivative of the Lyapunov function is

$$\dot{V}(\boldsymbol{\sigma}) = \boldsymbol{\sigma}^T \dot{\boldsymbol{\sigma}} \quad (2.4)$$

The derivative of the Lyapunov function is selected to be

$$\dot{V}(\boldsymbol{\sigma}) = -\boldsymbol{\sigma}^T \mathbf{D} \boldsymbol{\sigma} \quad (2.5)$$

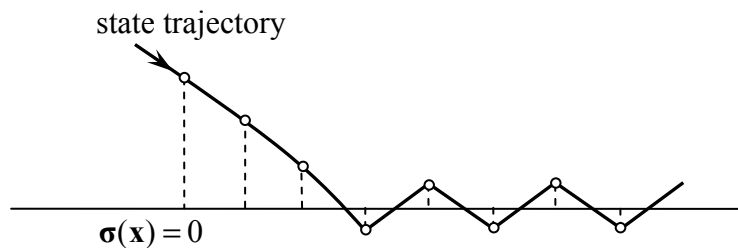


Figure 2.2. Discrete-time system with discontinuous control

here  $\mathbf{D}$  is a positive definite symmetric matrix of dimension  $m \times m$ . Hence, the derivative of the Lyapunov function is negative definite in order to ensure stability. If (2.4) and (2.5) are combined the following result is obtained

$$\boldsymbol{\sigma}^T (\dot{\boldsymbol{\sigma}} + \mathbf{D}\boldsymbol{\sigma}) = 0 \quad (2.6)$$

A solution for (2.6) is as follows

$$\dot{\boldsymbol{\sigma}} + \mathbf{D}\boldsymbol{\sigma} = 0 \quad (2.7)$$

The derivative of the sliding function combined with (2.1) leads to following

$$\dot{\boldsymbol{\sigma}} = G(\dot{\mathbf{x}}^r - \dot{\mathbf{x}}) + \frac{\partial \boldsymbol{\sigma}}{\partial t} = \mathbf{G}\dot{\mathbf{x}}^r - \mathbf{G}\mathbf{f} + \frac{\partial \boldsymbol{\sigma}}{\partial t} - \mathbf{G}\mathbf{B}\mathbf{u}(t) \quad (2.8)$$

Rewriting (2.8) to get

$$\dot{\boldsymbol{\sigma}} = \underbrace{\mathbf{G}\dot{\mathbf{x}}^r - \mathbf{G}\mathbf{f} + \frac{\partial \boldsymbol{\sigma}}{\partial t}}_{\mathbf{G}\mathbf{B}\mathbf{u}_{eq}} - \mathbf{G}\mathbf{B}\mathbf{u}(t) = \mathbf{G}\mathbf{B}(\mathbf{u}_{eq} - \mathbf{u}(t)) \quad (2.9)$$

If (2.9) is inserted in (2.7) and the result is solved for the control

$$\mathbf{u}(t) = \mathbf{u}_{eq} + (\mathbf{G}\mathbf{B})^{-1} \mathbf{D}\boldsymbol{\sigma} \quad (2.10)$$

It can be seen from (2.9) that  $\mathbf{u}_{eq}$  is difficult to calculate if information about  $\mathbf{f}(\mathbf{x})$  is not available. Using the fact that  $\mathbf{u}_{eq}$  is a smooth function, then (2.9) can be written as, [4],

$$\mathbf{u}_{eq} \cong \mathbf{u}(t^-) + (\mathbf{G}\mathbf{B})^{-1} \dot{\boldsymbol{\sigma}} = \hat{\mathbf{u}}_{eq} \quad (2.11)$$

here

$$t^- = t - \Delta, \quad \Delta \rightarrow 0 \quad (2.12)$$

and  $\hat{\mathbf{u}}_{eq}$  is the estimate of the equivalent control. If (2.11) is inserted back into (2.10) an approximation of the control is obtained

$$\mathbf{u}(t) = \mathbf{u}(t^-) + (\mathbf{G}\mathbf{B})^{-1} (\mathbf{D}\boldsymbol{\sigma} + \dot{\boldsymbol{\sigma}}) \Big|_{t=t^-} \quad (2.13)$$

Thus, the term  $(\mathbf{G}\mathbf{B})^{-1} (\mathbf{D}\boldsymbol{\sigma} + \dot{\boldsymbol{\sigma}}) \Big|_{t=t^-}$  is used in updating the control in a recursive formula. Note that once on the sliding manifold,  $\mathbf{u}(t^-)$  becomes the same as the equivalent control.

Although (2.13) is an approximation of (2.9) in discrete-time, it can be used to push  $\boldsymbol{\sigma}$  to zero such that (2.7) is satisfied and stability is reached. During implementation, the control defined by (2.13) is used with a nominal value of  $\mathbf{B}$  instead of its exact value since it is difficult to obtain. When actual implementation is done, a tuning term  $\mathbf{K}$  is introduced before  $(\mathbf{G}\mathbf{B})^{-1} (\mathbf{D}\boldsymbol{\sigma} + \dot{\boldsymbol{\sigma}}) \Big|_{t=t^-}$  such that the control becomes

$$\mathbf{u}(t) = \mathbf{u}(t^-) + \mathbf{K}(\mathbf{GB})^{-1}(\mathbf{D}\boldsymbol{\sigma} + \dot{\boldsymbol{\sigma}})\Big|_{t=t^-} \quad (2.14)$$

and for a general system,  $\mathbf{K}$  is a positive diagonal matrix. It is possible to rewrite (2.14) for discrete-time implementation as follows

$$\mathbf{u}((k+1)T_s) = \mathbf{u}(kT_s) + \mathbf{K}(\mathbf{GB})^{-1}(\mathbf{D}\boldsymbol{\sigma} + \dot{\boldsymbol{\sigma}})\Big|_{t=kT_s} \quad (2.15)$$

here  $T_s$  is the sampling time of the controller and the derivative of the sliding surface is obtained from the backward difference as shown

$$\dot{\boldsymbol{\sigma}}(kT_s) \approx \frac{\boldsymbol{\sigma}(kT_s) - \boldsymbol{\sigma}((k-1)T_s)}{T_s} \quad (2.16)$$

Details of the analysis shown above can be found in [5].

For a discrete-time system, the discrete sliding mode can be interpreted as that the states are only required to be kept on the sliding surface at each sampling instant. Between the samples, the states are allowed to deviate from the surface within a boundary layer, see Figure 2.3.

Note that the control defined by (2.15) is continuous unlike the case for continuous-time. Thus chattering is no longer a matter of concern. This is the most striking contrast between discrete-time sliding mode and continuous-time sliding mode. Furthermore, in continuous-time systems with continuous control, the sliding manifold of state trajectories can be reached only asymptotically, while in discrete time systems with continuous control, sliding motion with state trajectories in some manifold may be reached within a finite time interval, Utkin [2]. Estimation of the boundary layer is explained in section 2.4.

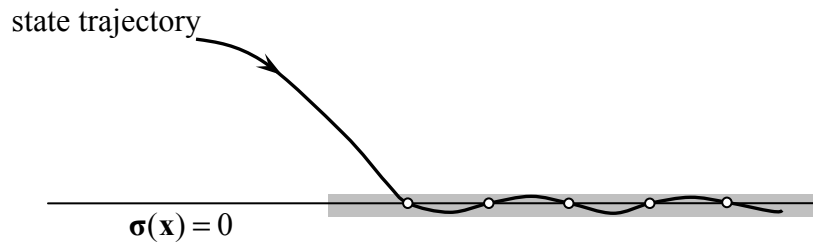


Figure 2.3. Discrete-time Sliding mode in sampled-data systems

## 2.4 Calculation of the Boundary Layer in Discrete-Time Sliding-Mode Control

After designing the controller, it is necessary to analyze the robustness of the controller or, in other words, whether it satisfies the condition defined by (2.7). The analyses that will be shown are concerned with a general system affine with control such as (2.1).

Consider the system defined below

$$\dot{\mathbf{x}} = \mathbf{f}(\mathbf{x}, t) + \mathbf{B}(\mathbf{x}, t)\mathbf{u}(\mathbf{x}, t) \quad (2.17)$$

as in (2.1),  $\mathbf{f}(\mathbf{x}, t)$  and  $\mathbf{B}(\mathbf{x}, t)$  are assumed to be continuous and bounded. The derivative of the sliding surface is given by

$$\frac{d\boldsymbol{\sigma}(t)}{dt} = \mathbf{G}(\dot{\mathbf{x}}^r - \dot{\mathbf{x}}) + \frac{\partial \boldsymbol{\sigma}(t)}{\partial t} = \mathbf{G}\dot{\mathbf{x}}^r(t) - \mathbf{G}\mathbf{f}(t) - \mathbf{G}\mathbf{B}\mathbf{u}(t) + \frac{\partial \boldsymbol{\sigma}(t)}{\partial t} \quad (2.18)$$

If instead of  $u(t)$  the control defined by (2.13) is used, the following result is obtained

$$\frac{d\boldsymbol{\sigma}(t)}{dt} = \mathbf{G}\dot{\mathbf{x}}^r(t) - \mathbf{G}\mathbf{f}(t) - \mathbf{G}\mathbf{B}\left(\mathbf{u}(t^-) + (\mathbf{G}\mathbf{B})^{-1}(\mathbf{D}\boldsymbol{\sigma} + \dot{\boldsymbol{\sigma}})\Big|_{t^-}\right) + \frac{\partial \boldsymbol{\sigma}(t)}{\partial t} \quad (2.19)$$

here  $t^- = t - T_s$  for discrete-time applications with  $T_s$  as the sampling time. Further simplifications of (2.19) lead to

$$\frac{d\boldsymbol{\sigma}(t)}{dt} = \mathbf{G}\dot{\mathbf{x}}^r(t) - \mathbf{G}\mathbf{f}(t) - \mathbf{G}\mathbf{B}\mathbf{u}(t^-) + \frac{\partial \boldsymbol{\sigma}(t)}{\partial t} - \left(\mathbf{D}\boldsymbol{\sigma} + \frac{d\boldsymbol{\sigma}}{dt}\right)\Big|_{t^-} \quad (2.20)$$

Finally, (2.20) can be written as

$$\frac{d\boldsymbol{\sigma}(t)}{dt} = \frac{d\boldsymbol{\sigma}(t^-)}{dt} - \frac{d\boldsymbol{\sigma}(t^-)}{dt} - \mathbf{D}\boldsymbol{\sigma}(t) + \underbrace{\mathbf{G}\Delta\dot{\mathbf{x}}^r - \mathbf{G}\Delta\mathbf{f} + \Delta\left(\frac{\partial \boldsymbol{\sigma}}{\partial t}\right) - \mathbf{D}\Delta\boldsymbol{\sigma}}_{\xi(T_s)} \quad (2.21)$$

here

$$\begin{aligned} \Delta\dot{\mathbf{x}}^r &= \dot{\mathbf{x}}^r(t) - \dot{\mathbf{x}}^r(t^-); \Delta\mathbf{f} = \mathbf{f}(t) - \mathbf{f}(t^-); \Delta\boldsymbol{\sigma} = \boldsymbol{\sigma}(t) - \boldsymbol{\sigma}(t^-); \\ \Delta\left(\frac{\partial \boldsymbol{\sigma}}{\partial t}\right) &= \frac{\partial \boldsymbol{\sigma}(t)}{\partial t} - \frac{\partial \boldsymbol{\sigma}(t^-)}{\partial t} \end{aligned} \quad (2.22)$$

Hence,

$$\frac{d\boldsymbol{\sigma}(t)}{dt} + \mathbf{D}\boldsymbol{\sigma}(t) = \xi(T_s) \quad (2.23)$$

Since  $\mathbf{f}(t)$ ,  $\mathbf{x}'(t)$  and  $\boldsymbol{\sigma}(t)$  are smooth functions, then  $\zeta(T_s)$  has order  $O(T_s)$ . Hence, the states will remain within an  $O(T_s)$  boundary layer of the sliding surface.

## 2.5 Disturbance Observers based on Sliding-Mode Control

In most systems that are encountered in control engineering, some form of disturbance exists. This could include internal nonlinearities, external forces, parameter uncertainties, etc. Hence, it is necessary to compensate for the disturbance while using closed-loop control in order to improve the robustness of the overall control. Estimation of plant disturbances are done with the aid of disturbance observers that are based on the so called nominal plant model.

Consider the linear system with disturbance shown below

$$\dot{\mathbf{x}} = \mathbf{A}\mathbf{x} + \mathbf{B}\mathbf{u}(t) + \mathbf{d}, \quad \mathbf{x} \in \mathfrak{R}^n, \quad \mathbf{u} \in \mathfrak{R}^m \quad (2.24)$$

If  $\mathbf{A} = \mathbf{A}_N + \Delta\mathbf{A}$  and  $\mathbf{B} = \mathbf{B}_N + \Delta\mathbf{B}$  are inserted in (2.24)

$$\dot{\mathbf{x}} = \mathbf{A}_N\mathbf{x} + \mathbf{B}_N\mathbf{u}(t) + \Delta\mathbf{A}\mathbf{x} + \Delta\mathbf{B}\mathbf{u}(t) + \mathbf{d} \quad (2.25)$$

here  $\mathbf{A}_N$  and  $\mathbf{B}_N$  are the nominal state and input matrices while  $\Delta\mathbf{A}$  and  $\Delta\mathbf{B}$  are the uncertainties involved in those matrices. The disturbance  $\mathbf{d}$  is assumed continuous and bounded. The analysis hereafter is for the case where it is possible to write the disturbance term as  $\mathbf{B}_N\mathbf{u}_d(t) = \Delta\mathbf{A}\mathbf{x} + \Delta\mathbf{B}\mathbf{u}(t) + \mathbf{d}$ . Thus (2.25) can be written as

$$\dot{\mathbf{x}} = \mathbf{A}_N\mathbf{x} + \mathbf{B}_N\mathbf{u}(t) + \mathbf{B}_N\mathbf{u}_d(t) \quad (2.26)$$

The structure of the observer is as follows

$$\dot{\hat{\mathbf{x}}} = \mathbf{A}_N\hat{\mathbf{x}} + \mathbf{B}_N\mathbf{u}(t) + \mathbf{B}_N\mathbf{u}_c(t) \quad (2.27)$$

here  $\hat{\mathbf{x}}$  is the estimated state vector and  $\mathbf{u}_c(t)$  is the observer control input to force  $\hat{\mathbf{x}}$  to track  $\mathbf{x}$ . If (2.27) is subtracted from (2.26)

$$\left(\dot{\mathbf{x}} - \dot{\hat{\mathbf{x}}}\right) = \mathbf{A}_N(\mathbf{x} - \hat{\mathbf{x}}) + \mathbf{B}_N\mathbf{u}_d(t) - \mathbf{B}_N\mathbf{u}_c(t) \quad (2.28)$$

If the sliding manifold is selected to be  $\boldsymbol{\sigma} = \mathbf{G}(\mathbf{x} - \hat{\mathbf{x}})$  and condition (2.7) is used

$$\mathbf{G}\left(\dot{\mathbf{x}} - \dot{\hat{\mathbf{x}}}\right) + \mathbf{D}\mathbf{G}(\mathbf{x} - \hat{\mathbf{x}}) = 0 \quad (2.29)$$

Inserting (2.28) in (2.29) to get

$$\mathbf{G}\mathbf{A}_N(\mathbf{x} - \hat{\mathbf{x}}) + \mathbf{D}\mathbf{G}(\mathbf{x} - \hat{\mathbf{x}}) + \mathbf{G}\mathbf{B}_N\mathbf{u}_d(t) - \mathbf{G}\mathbf{B}_N\mathbf{u}_c(t) = 0 \quad (2.30)$$

Finally, the control input is

$$\mathbf{u}_c(t) = \mathbf{u}_d(t) + (\mathbf{GB}_N)^{-1}(\mathbf{GA}_N + \mathbf{DG})(\mathbf{x} - \hat{\mathbf{x}}) \quad (2.31)$$

It can be seen that if  $\sigma \rightarrow 0$  then  $\hat{\mathbf{x}} \rightarrow \mathbf{x}$  and  $\mathbf{u}_c \rightarrow \mathbf{u}_d$ . Thus, all that is required is for condition (2.7) to be satisfied for the observer. The control defined by (2.14) or (2.15) can be used to satisfy condition (2.7). Implementation is depicted in Figure 2.4. In the implementation  $\mathbf{u}_0$  is the uncompensated control input.

As it can be seen the above control algorithm is simple to implement. The only drawback is that for constructing the observer plant parameters must be known. Experimental implementation of the above control algorithm to different systems will be shown in coming chapters.

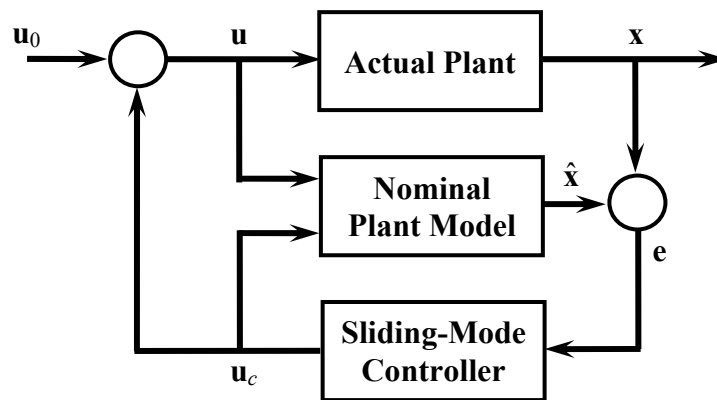


Figure 2.4. Disturbance observer implementation

### **3. MODEL OF THE PIEZOELECTRIC ACTUATOR**

#### **3.1 Introduction**

Micromanipulator applications require control actuators that can provide both accurate position tracking performance in addition to robustly stable force control. These objectives are significantly compromised by the presence of backlash and Coulomb friction in the control plant, the effects of which are exaggerated in small scales. Since PZT stack actuators are monolithic and have no sliding or rolling parts, they exhibit no significant mechanical stiction or backlash. Additionally, a typical PZT stack actuator can perform step movements in nanometer resolutions with bandwidths on the order of a kilohertz. Consequently, PZT actuators are well suited for use as precision microactuators for micropositioning devices.

An inherent non-linearity in piezoceramic actuators is hysteresis. This hysteresis non-linearity is usually 15-20% of the output thereby greatly reducing the performance of the actuators. Additionally, many attempts of modeling this behavior have been fruitless due to its peculiarities. In [12] and [14] attempts were made to model the voltage-to-displacement behavior of PZT actuators using Bond-Graph and Priesach models. These models proved effective, however, these models failed to explain the physical behavior of the actuators. In [1] and [9] models were made based on the physics of the actuators and these models proved to be effective in modeling the behavior of these actuators under different excitations. Additionally, they claim that the hysteresis behavior exists in the electrical domain of the actuator and is between voltage and charge. In [9], a simple differential equation was used to model the voltage-charge hysteresis behavior. This model proved simple to implement in real-time applications due to the simplicity of the equation representing the hysteresis. In Figure 3.1, the actuators used in the experiments are shown.

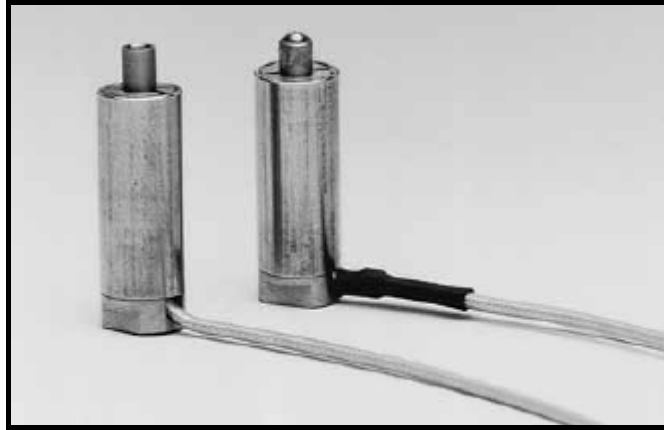


Figure 3.1. Stack actuators used in the experiments

### 3.2 Structure of the Piezoelectric Actuator

Dielectric materials are insulators, thus, there is an electrical relation between electrical voltage and electrical charge. Piezoelectric materials are a special type of dielectric in the sense that, in piezoelectric materials, an externally applied force induces an electrical charge. Conversely, an applied electrical charge induces a force. The former effect is known as the piezoelectric effect and was discovered in 1880 by the Curies. The latter effect is the inverse piezoelectric effect. The word “piezo” derives from the Greek word “piezen,” which means “to push.” The effect was discovered when a pushing force or, in other words pressure, was applied to the material. In the beginning, both pressure electricity and piezoelectricity were used to describe the same phenomenon. Besides the piezoelectric and inverse piezoelectric effect, we have the already mentioned electrical relation between voltage and charge, and a mechanical relation between force and elongation.

In naturally occurring piezoelectric materials, such as quartz, the (inverse) piezoelectric effect is too small to be of practical use. Man-made piezoelectric polycrystalline ceramics are much more suitable for actuator purposes because the useful properties, such as maximum elongation, can be influenced by the proper mixture of ingredients. A disadvantage of man-made piezoelectric ceramics is that a hysteresis effect is encountered between electrical voltage and electrical charge. The piezoelectric effect (or the piezo effect for short) and the hysteresis effect play an important role in the dynamical behavior of these actuators.

The fundamental component of a PZT stack actuator is a wafer of piezoelectric material sandwiched between two electrodes. Prior to fabrication, the wafer is polarized uniaxially along its thickness, and thus exhibits significant piezoelectric effect in this direction only. A typical PZT stack actuator is formed by assembling several of the wafer elements in series mechanically and connecting the electrodes so that the wafers are parallel electrically, as illustrated in Figure 3.2. The nominal quasi-static behavior of a PZT stack actuator is a steady-state output displacement that is monotonically related to the voltage input.

### 3.3 Model of the Piezoelectric Actuator

In this section, a model for PZT actuators that was selected after an extensive search of the literature will be presented. This model was selected based on ease of implementation and accuracy of estimating the actual behavior of these actuators.

#### 3.3.1 The Selected Model

A fairly accurate overall electromechanical model of a PZT actuator is given in [1]. It is reproduced in Figure 3.3. Here, the hysteresis and piezoelectric effect are separated.  $H$  represents the hysteresis effect and  $u_h$  is the voltage due to this effect. The piezoelectric effect is represented by  $T_{em}$ , which is an electromechanical transducer with transformer ratio  $T_{em}$ . The capacitance  $C_e$  represents the sum of the capacitances of the individual PZT wafers, which are electrically in parallel. The total current flowing through the circuit is  $\dot{q}$ . Furthermore,  $q$  may be seen as the total charge in the PZT actuator. The charge  $q_p$  is the transduced charge from the mechanical side. The voltage  $u_p$  is due to the piezo effect. The total voltage over the PZT actuator is  $u_{in}$ ,  $F_p$  is the transduced force from the electrical side,  $F_{ext}$  is the externally applied force, and the resulting elongation of the PZT actuator is denoted by  $x$ . The mechanical relation between  $F_p$  and  $x$  is denoted by  $M$ . Note that we have equal electrical and mechanical energy at the ports of interaction, i.e.  $u_p q_p = F_p x$ .

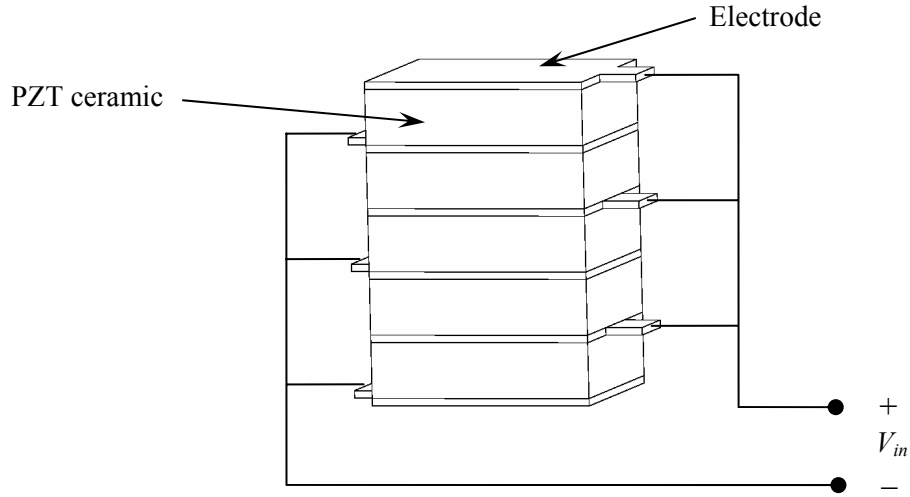


Figure 3.2. Illustration of a PZT stack actuator

The piezoelectric ceramic has elasticity modulus  $E$ , viscosity  $\eta$ , and mass density  $\rho$ . Furthermore, the geometrical properties of the PZT actuator are length  $L$  and cross-sectional area  $A_p$ . Mass  $m_p$ , stiffness  $k_p$ , and damping coefficient  $c_p$  can be calculated from the material and geometrical properties as follows:

$$m_p = \rho AL \quad (3.3)$$

$$k_p = \frac{EA_p}{L} \quad (3.4)$$

$$c_p = \frac{\eta A}{L} \quad (3.5)$$

Though, it will be safer to experimentally measure those using FRF analysis, since, some of the parameters needed above are not easily available.

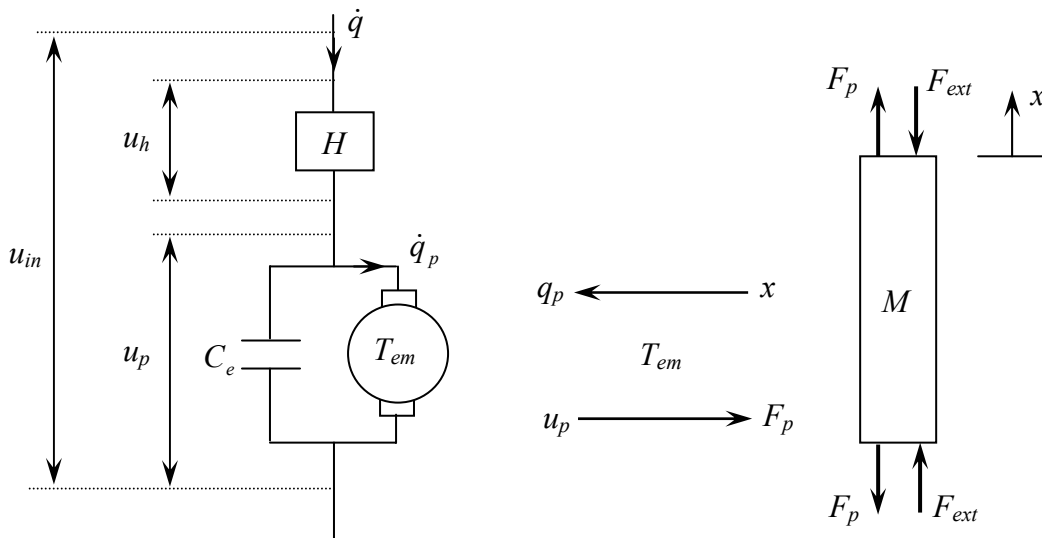


Figure 3.3. Electromechanical model of the PZT actuator, [1]

The complete electromechanical equations are defined by (3.6) thru (3.11). The model can also be described by the block diagram given in Figure 3.4.

$$u_p = u_{in} - u_h \quad (3.6)$$

$$u_h = H(q) \quad (3.7)$$

$$q = C_e u_p + q_p \quad (3.8)$$

$$q_p = T_{em} x \quad (3.9)$$

$$F_p = T_{em} u_p \quad (3.10)$$

$$m_p \ddot{x} + c_p \dot{x} + k_p x = F_p - F_{ext} \quad (3.11)$$

We must stress that the mechanical part of the actuator is more accurately described by a PDE that takes into account the continuous nature of the PZT actuator. However, for simplicity and due to the fact that the first natural frequency of the actuator is much higher than our allowable bandwidth, (3.11) is a fairly good representation of the mechanical behavior.

### 3.3.2 Hysteresis Model

By definition, a hysteretic effect is dynamic, rate-independent and nonlinear. By rate-independent, it is meant that it is time independent. In [1], this effect is modeled by a combination of elements that were called elasto-slide elements. The accuracy of the model was improved by using larger numbers of those elements, and hence the number of parameters involved was large.

In [9], a differential equation with three parameters is used as a hysteresis model. A differential equation is also more attractive when it comes to using this model as a basis for controller design. A brief description of this differential equation will be done here, but, a more comprehensive discussion may be found in [10].

A hysteresis loop is defined as the stationary loop in the input-output plane for a quasi-static monotone oscillating input such as a low-frequency sinusoid. The equation under consideration is a first-order differential equation that is proposed in [9]. It was initially developed to model magnetic hysteresis, but in [10], it has been experimentally verified that this differential equation is also suitable for describing electric hysteresis

such as that in PZT actuators. The model between the hysteresis effect between  $u_h$  and  $q$  is given by

$$\dot{q} = \alpha_h |\dot{u}_h| (f(u_h) - q) + \dot{u}_h g(u_h) \quad (3.12)$$

where  $f(u_h)$  and  $g(u_h)$  are functions which are used to “shape” the hysteresis loop. In [10], it has been proven that, for a sinusoid with offset  $u_{h,c}$ , the center point of a hysteresis loop is given by  $q_c = f(u_{h,c})$ . Furthermore, it has been proven that the average slope of a hysteresis loop is equal to  $g(u_{h,c})$ .

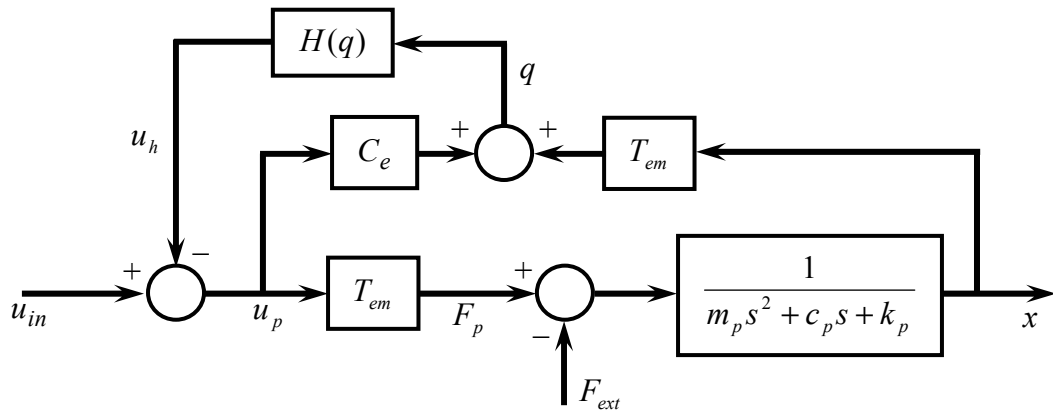


Figure 3.4. Block-Diagram representation of the electromechanical model

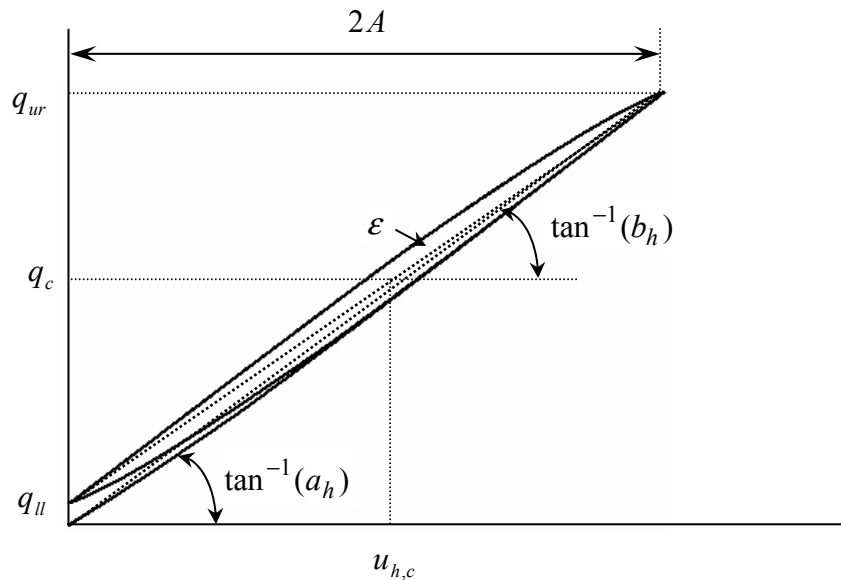


Figure 3.5. A hysteresis loop

In theory, PZT actuators show lengthening saturation. In practice, however, we stay far away from saturation, i.e., we deal with hysteresis loops that are similar in shape to the one in Figure 3.5. Therefore, the functions  $f(u_h)$  and  $g(u_h)$  may be chosen as

$$f(u_h) = a_h u_h \quad (3.13)$$

$$g(u_h) = b_h \quad (3.14)$$

where  $a_h$  and  $b_h$  are constants.

Using the previously mentioned results, the equations for the center point and the average slope of a hysteresis loop are given by

$$q_c = a_h u_{h,c} \quad (3.15)$$

$$q_{ur} - q_{ll} = b_h \cdot 2A \quad (3.16)$$

where  $q_c$  and  $q_{ll}$  are the upper right- and lower left-hand-side points of a hysteresis loop, respectively, and  $A$  is the input amplitude.

In (3.12), (3.13) and (3.14) there are three independent parameters, namely  $\alpha_h$ ,  $a_h$  and  $b_h$ . This means that there should be three independent characteristic quantities in a hysteresis loop. Besides the center point and the average slope in [9], a relation has been derived for the hysteresis area for relatively small amplitudes of the sinusoidal input (Figure 3.5)

$$\varepsilon = \frac{4}{3}(a_h - b_h)\alpha_h A^3 \quad (3.17)$$

Having experimentally determined  $a_h$  and  $b_h$  from center points and average slopes, the parameter  $\alpha_h$  can then be experimentally determined from hysteresis areas.

### 3.3.3 Simulation Results

The above model was used to estimate the response of the PZT actuator to two sinusoidal inputs each having an offset equal to the amplitude of the signal. The resulting outputs are depicted in Figure 3.6 and 3.7. It is possible to see that the model is able to estimate the residual displacement when the input goes to zero quite nicely. The most important task this model has to perform however is the ability to estimate an externally applied force. The parameters used in the simulation are listed in Table 3.1.

Table 3.1. Parameters of the PZT model

Parameter	Value	Parameter	Value
$m_p$	$9.24 \times 10^{-4}$ kg	$C_e$	2.4 $\mu$ F
$c_p$	685 Ns/m	$a_h$	5
$k_p$	$8.0 \times 10^6$ N/m	$b_h$	4.5
$T_{em}$	3.9 N/V	$\alpha_h$	1.8

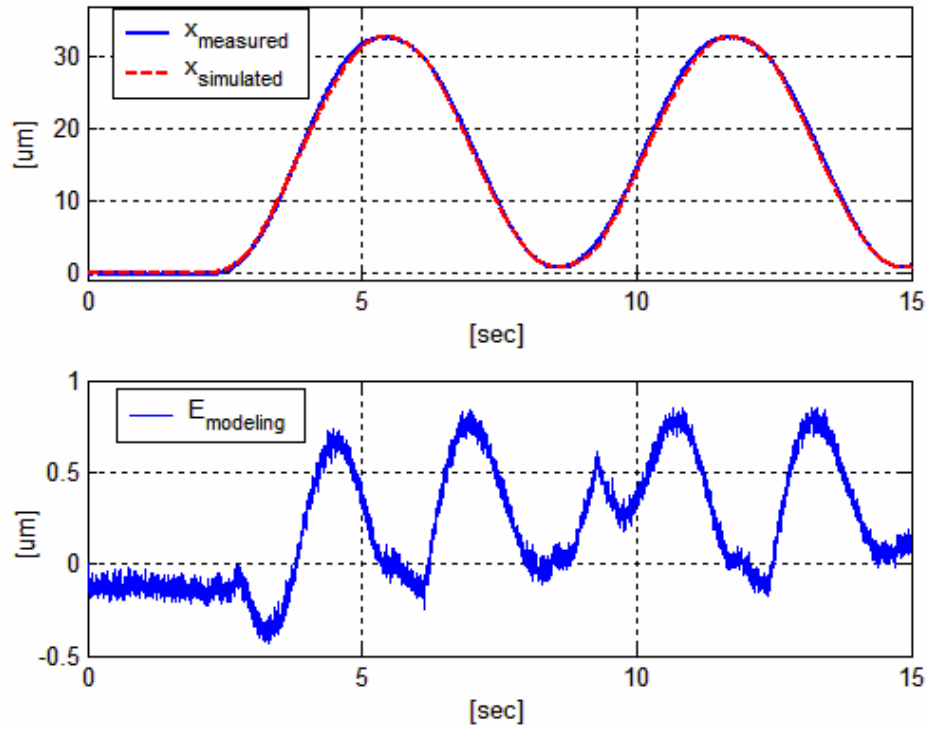


Figure 3.6. Response to  $u = 40 + 40\sin(t)$  and corresponding modeling error

### 3.4 Open-Loop Control of the Actuator

As previously stated, the model estimated the behavior of the actuator quite well. Conversely, this model should be able to estimate the necessary input to the actual plant in order to follow a certain reference. This can be represented in the block diagram of Figure 3.8. This technique was applied experimentally to test its capabilities.

The open-loop results are depicted in the figures below. From the results we see that the inverse model works quite well. It must be stressed that the results below are for zero external force. In the case of an externally applied force, it must be added to  $F_p$ .

This means that the force has to be known before hand. Thus, this method would prove fruitless in the face of an unknown external force.

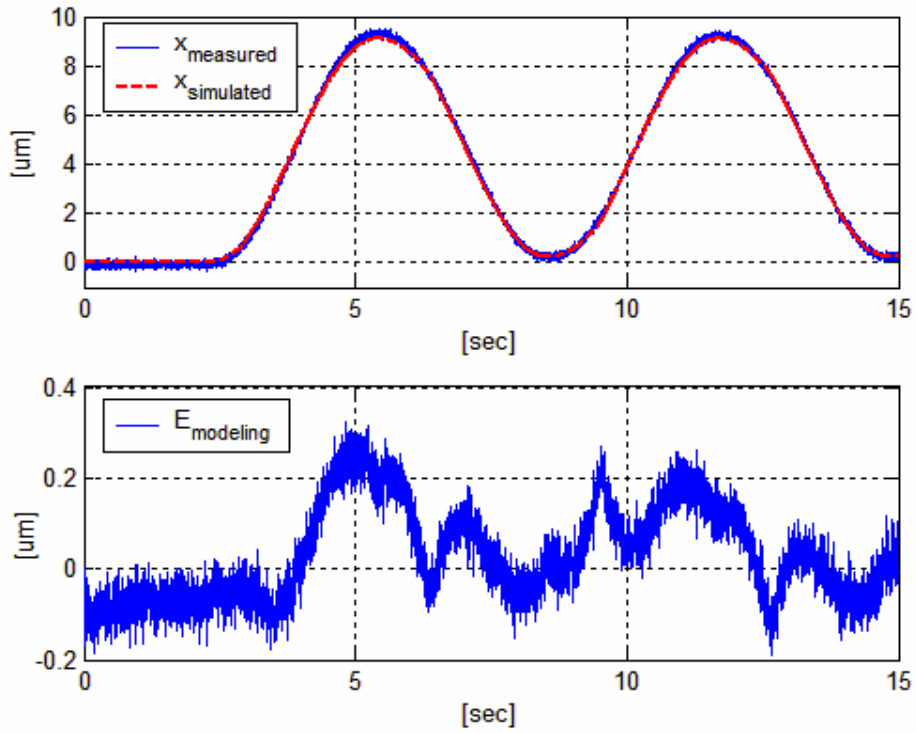


Figure 3.7. Response to  $u = 15 + 15\sin(t)$  and corresponding modeling error

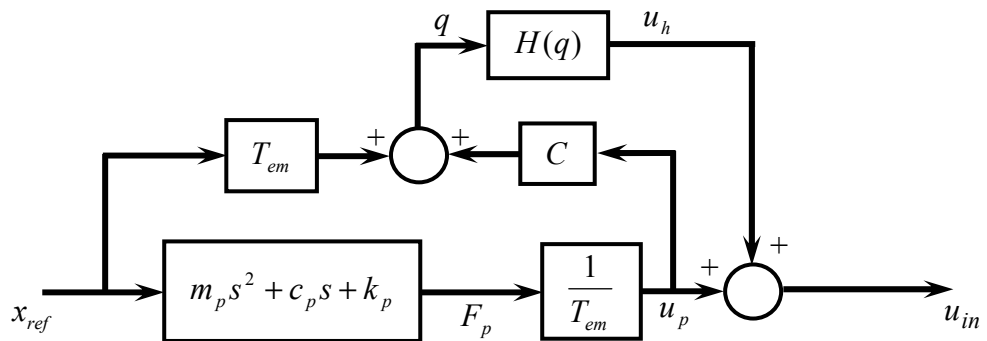


Figure 3.8. Inverse model of the PZT actuator

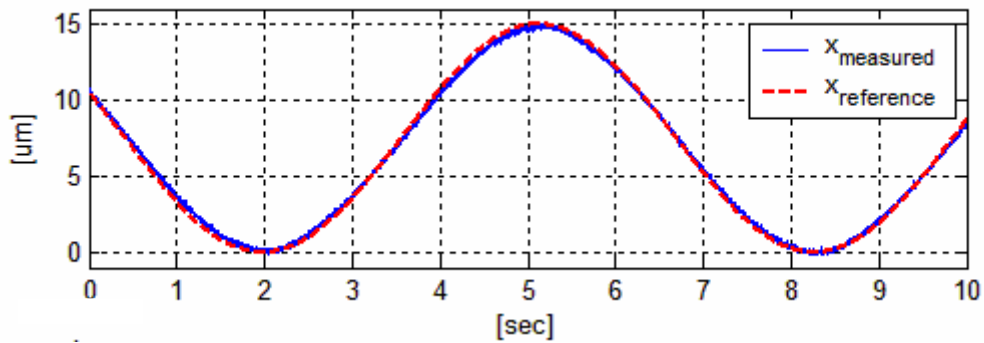


Figure 3.9. Response to  $x_r = 7.5 + 7.5\sin(t)$

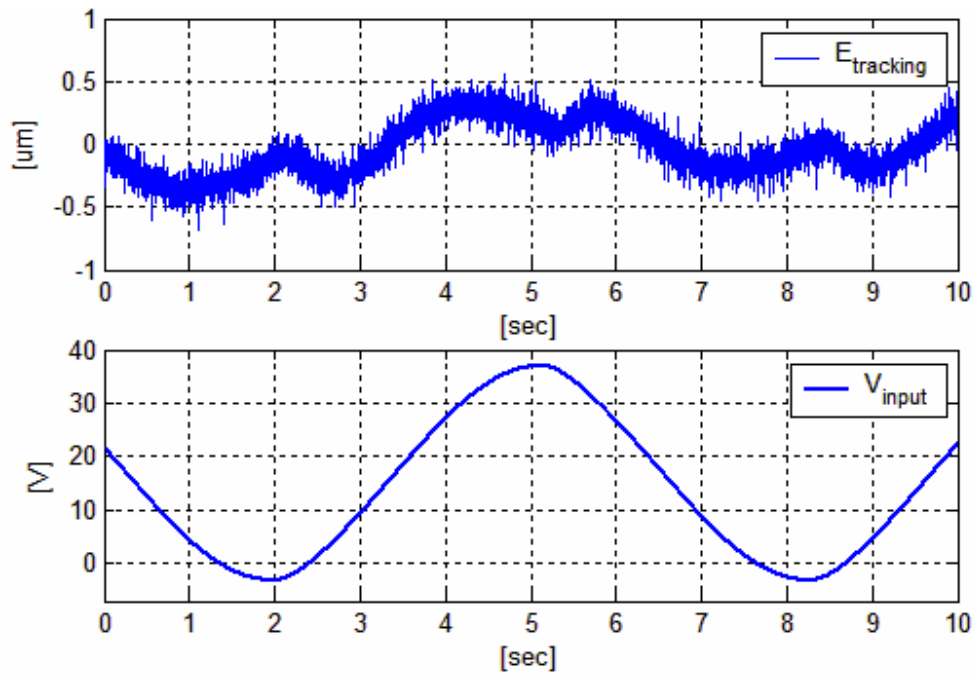


Figure 3.10. Open-loop tracking error and input voltage for  $x_r = 7.5 + 7.5 \sin(t)$

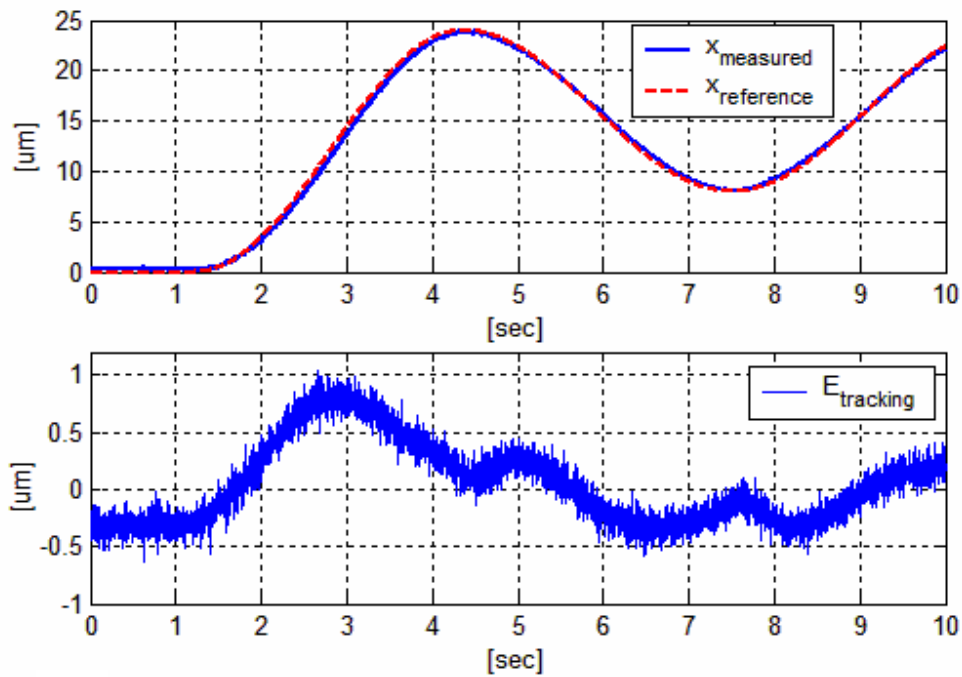


Figure 3.11. Response to a varying amplitude sine reference

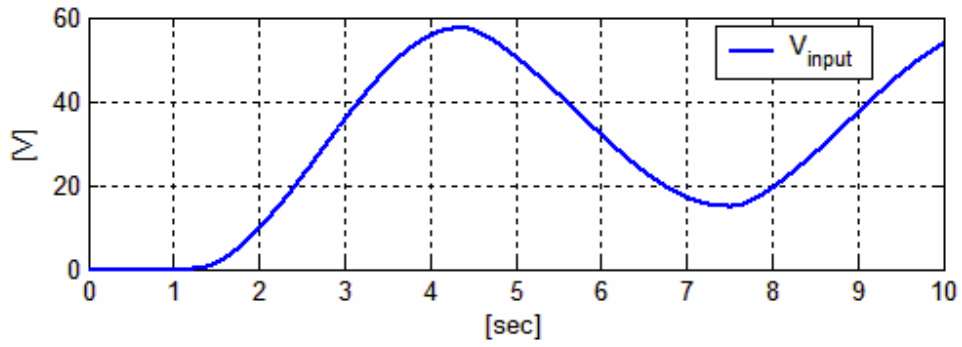


Figure 3.12. Input voltage for a varying amplitude sine reference (contd.)

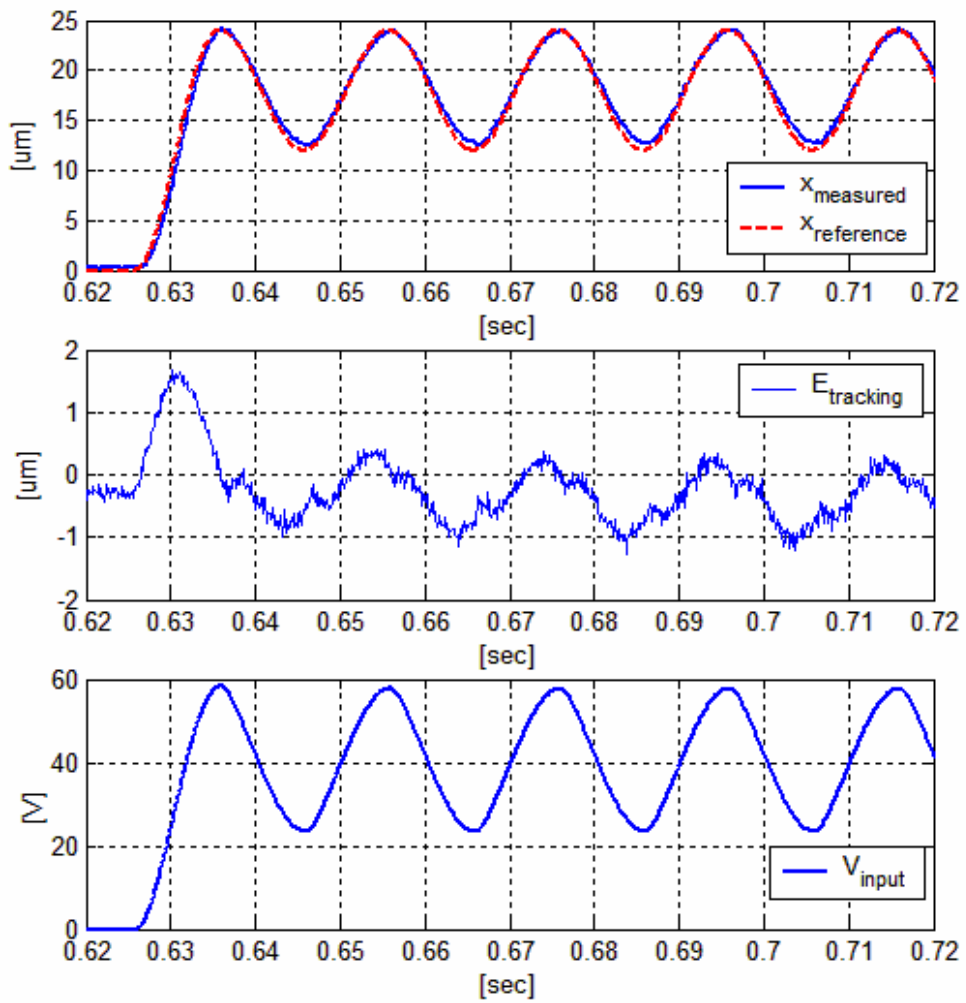


Figure 3.13. Response to a high frequency varying amplitude sine reference

## 4. IMPLEMENTATION OF SMC TO A PIEZOELECTRIC ACTUATOR

### 4.1 Introduction

The use of piezoelectric actuators (PZT) for accurate and stable control of manipulator position and/or force is greatly facilitated by model-based control system analysis and design. Inherent nonlinearities composed primarily of hysteresis in piezoelectric actuators pose as an obstacle to these objectives. In [11], a piezoelectric actuator is used as a secondary actuator in a hard disk drive to increase the precision of read/write head positioning. The control used is based on charge rather than voltage which eliminated the problem of hysteresis. However, charge based control is harder to realize due to the difficulties involved in the hardware realization. Hence, techniques based on voltage control must compensate for the hysteresis.

By far, open-loop techniques have not been successful in providing good results due to the difficulties involved in modeling the actuator precisely. In [12], open-loop control is used, resulting in position errors as much as 100nm. This is clearly not acceptable in applications where high precision positioning is required. In [13], disturbance compensation based on a hysteresis model is used. However, unmodeled disturbances required the addition of a robust controller such as  $H_\infty$ .

Usage of the hysteresis model for the design of the position control of PZT needs high accuracy of modeling and adjustment but it offers advantage since it does not require measurement of mechanical coordinates. In this work we aim to design a motion controller for PZT having position sensor based on the assumption that the PZT can be modeled as a linear lumped parameters ( $m_p, c_p, k_p$ ) second order electromechanical system with voltage as input and position as output coordinates. Furthermore we assume that the parameters of the model are constant and have some so-called nominal values ( $m_N, c_N, k_N$ ). A sliding mode observer based disturbance observer is used then in the framework of disturbance compensation method.

In many applications such as precise assembly, micromachining, or in minimum invasive surgery that involve micromotion and/or micromanipulation, force measurement and/or force control may be required. In general applications that require force control, force sensors are used. But they are constrained by limited detectable point and narrow bandwidth due to the natural frequency of the sensor [15]. It is also difficult to incorporate force sensors in micromanipulation systems that are required to be as compact as possible. Hence, it is more desirable to have force estimation rather than direct measurement. Thus, using the disturbance observer concept, a force observer is constructed based on the electromechanical model with the inclusion of the hysteresis model proposed in [9].

Force control is accomplished in the sliding-mode control (SMC) framework and in this chapter results for the case of force sensor feedback as well as force observer feedback are depicted.

## 4.2 Design of the Observers

In this section, the structure of the disturbance observer will be discussed as well as an attempt to use the disturbance information to estimate the external force acting on the actuator. Theory presented will be backed by actual experimental results to demonstrate the effectiveness of the concept.

### 4.2.1 Total Disturbance Estimation

The structure of the observer is based on (3.11). Here we propose that all the plant parameter uncertainties, nonlinearities and external disturbances as a single disturbance which leads to the following structure

$$m_N \ddot{x} + c_N \dot{x} + k_N x = T_{em_N} u_{in} - \underbrace{(T_{em_N} u_h + \Delta m \cdot \ddot{x} + \Delta c \cdot \dot{x} + \Delta k \cdot x + F_{ext})}_{F_d} \quad (4.1)$$

$$m_N \ddot{x} + c_N \dot{x} + k_N x = T_{em_N} u_{in} - F_d$$

here  $m_N$ ,  $c_N$ ,  $k_N$  and  $T_{em_N}$  are the nominal plant parameters. The proposed observer is then of the following form

$$m_N \ddot{\hat{x}} + c_N \dot{\hat{x}} + k_N \hat{x} = T_{em_N} u_{in} - u \quad (4.2)$$

Here  $\hat{x}$  is the estimated position  $u_{in}$  is the plant control input and  $u$  is the observer control input. It is obvious that if we can force  $\hat{x}$  to track  $x$  then  $F_d = u$ . Let us select the sliding manifold as  $\sigma = \dot{x} - \dot{\hat{x}} + C(x - \hat{x})$ . Selecting the Lyapunov function as  $v_L = \sigma^2 / 2$  which is clearly positive definite. Selecting the derivative of the Lyapunov function as  $-D\sigma^2$  such that it is negative definite. Equating the above results and simplifying

$$\dot{v}_L = \sigma \dot{\sigma} = -D\sigma^2 \Rightarrow \dot{\sigma} + D\sigma = 0 \quad (4.3)$$

Plugging  $\sigma = \dot{x} - \dot{\hat{x}} + C(x - \hat{x})$  in (4.3) and simplify we get

$$(\ddot{x} - \ddot{\hat{x}}) + (C + D)(\dot{x} - \dot{\hat{x}}) + CD(x - \hat{x}) = 0 \quad (4.4)$$

Subtracting (4.2) from (4.1) and plug the result into (4.4), we get

$$u = F_d + [c_N - m_N(C + D)](\dot{x} - \dot{\hat{x}}) + [k_N - m_N CD](x - \hat{x}) \quad (4.5)$$

which is the necessary control to ensure sliding mode. From here it is seen that if  $\sigma \rightarrow 0$  then  $\dot{x} - \dot{\hat{x}} + C(x - \hat{x}) \rightarrow 0$  and  $x - \hat{x} \rightarrow 0$  thus assuring that the estimation error is zero, hence,  $u \rightarrow F_d$ . In the actual implementation, a discrete form of the sliding mode control is used which is given by

$$u_{(k)} = u_{(k-1)} + K_u \left( D\sigma_{(k)} + \frac{\sigma_{(k)} - \sigma_{(k-1)}}{T_s} \right) \quad (4.6)$$

here  $K_u$  is a design parameter which can be tuned to optimize the controller. The observer implementation is best described by the block diagram of Figure 4.1. The systems defined by Figure 4.1 are as follows

$$m_N \ddot{x} + b_N \dot{x} + k_N x = T_{em} u_{in} - F_d \quad (4.7)$$

$$m_N \ddot{\hat{x}} + b_N \dot{\hat{x}} + k_N \hat{x} = T_{em_N} u_{in} - u \quad (4.8)$$

$$u_{in} = u_0 + \alpha \frac{u}{T_{em_N}} \quad (4.9)$$

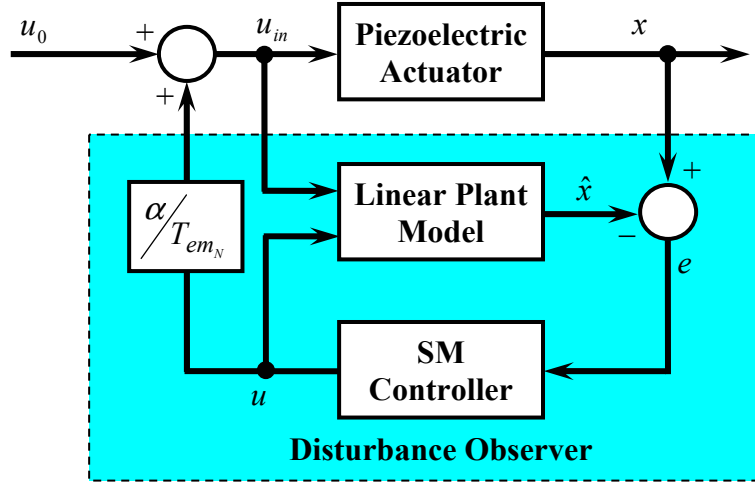


Figure 4.1. Observer implementation

From (4.7), (4.8) and (4.9) we get the following

$$u = \frac{T_{em_N}}{T_{em_N} + \alpha\Delta T_{em}} F_d - \frac{T_{em_N} \Delta T_{em}}{T_{em_N} + \alpha\Delta T_{em}} u_0 \quad (4.10)$$

If we plug (4.10) in (4.7) we get

$$m_N \ddot{x} + b_N \dot{x} + k_N x = T_{em} \left( \frac{T_{em_N}}{T_{em_N} + \alpha\Delta T_{em}} \right) + \frac{\alpha T_{em} - (T_{em_N} + \alpha\Delta T_{em})}{T_{em_N} + \alpha\Delta T_{em}} F_d \quad (4.11)$$

From here we see that if  $\alpha \rightarrow 1$  then

$$m_N \ddot{x} + b_n \dot{x} + k_N x = T_{em_N} u_0 \quad (4.12)$$

Thus, the system is compensated and closed loop controller can be designed based on this model. Since this model has the same structure as disturbance observer it is easy to show that by selecting sliding mode manifold  $\sigma_x = (\dot{x}^{ref} - \dot{x}) + C_x(x^{ref} - x)$  controller (4.6) will provide motion  $\ddot{\epsilon}_x + (C_x + D_x)\dot{\epsilon}_x + C_x D_x \epsilon_x = 0$  with  $x^{ref} - x = \epsilon_x$ . The open-loop and closed loop behavior of the system with the proposed observer is shown below.

The above concept was applied to the actuator. In all the experiments below, the reference position was computed from the compensated model and is given by

$$x_{ref} = \frac{1}{m_N s^2 + c_N s + k_N} \cdot T_{em_N} u \quad (4.13)$$

In the results that will be shown below, the observer parameters were:  $C = 800$ ,  $D = 2000$ ,  $K_u = 20$  and  $\alpha = 1$ .

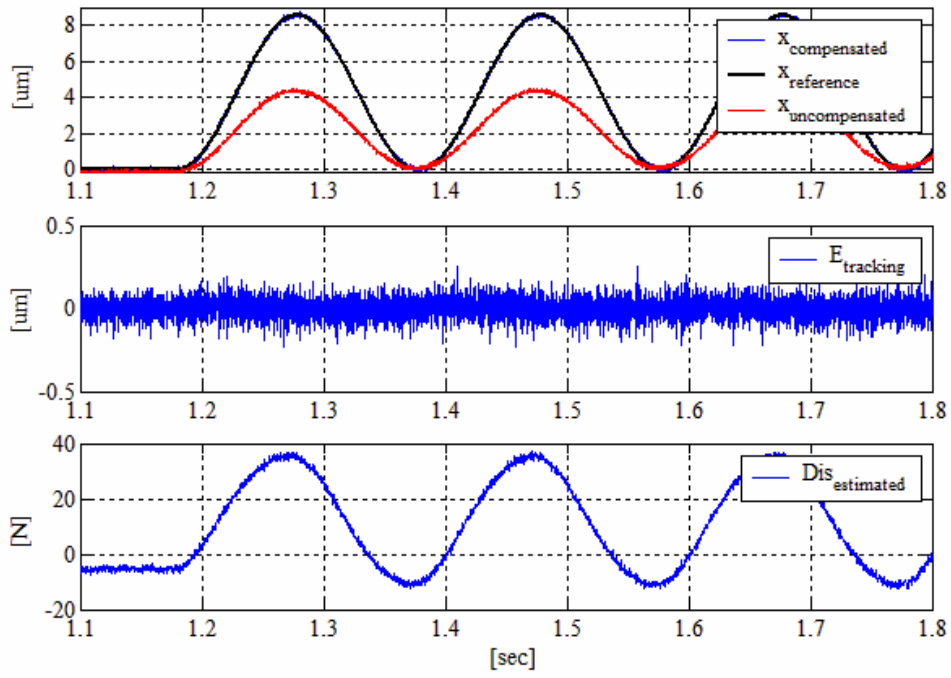


Figure 4.2. Response to  $u_0 = 7.5 \sin(10\pi t) + 7.5$

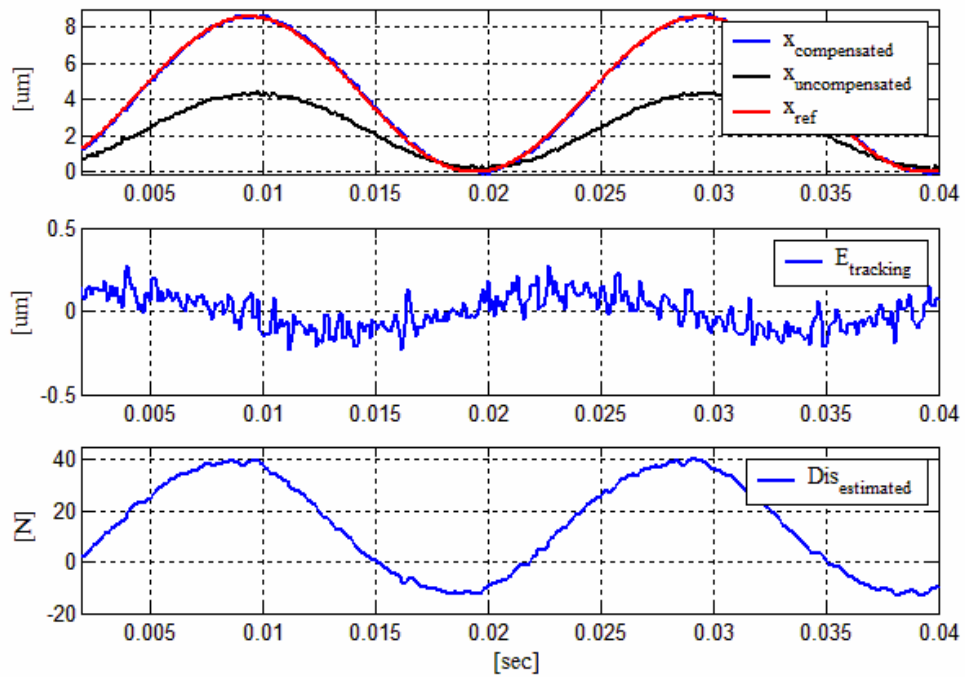


Figure 4.3. Response to  $u_0 = 7.5 \sin(100\pi t) + 7.5$  with disturbance compensation

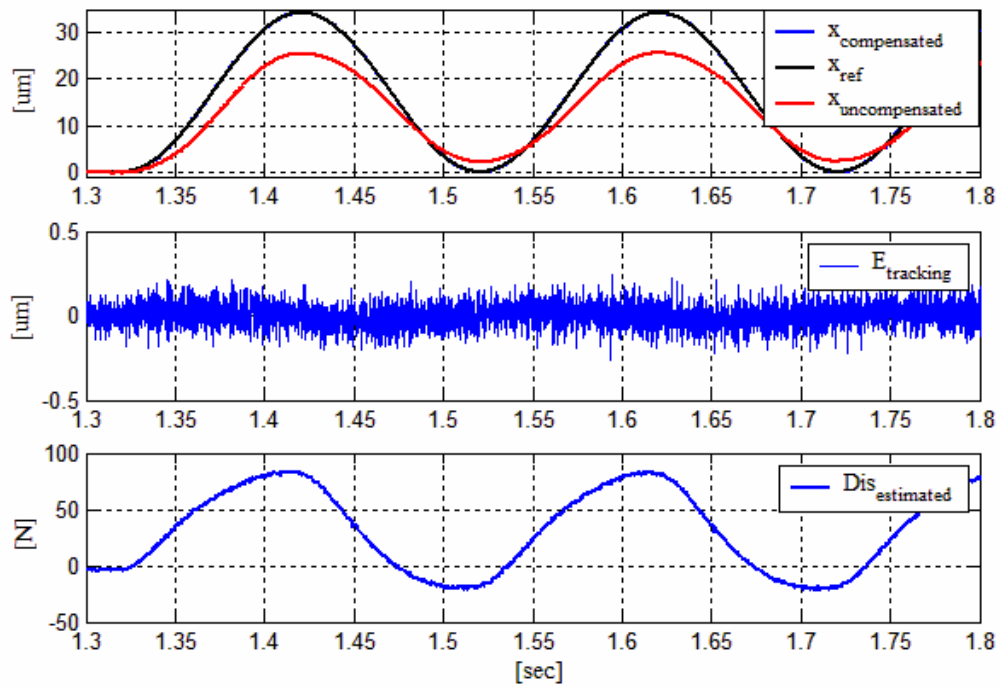


Figure 4.4. Response to  $u_0 = 30 \sin(10\pi t) + 30$  with disturbance compensation

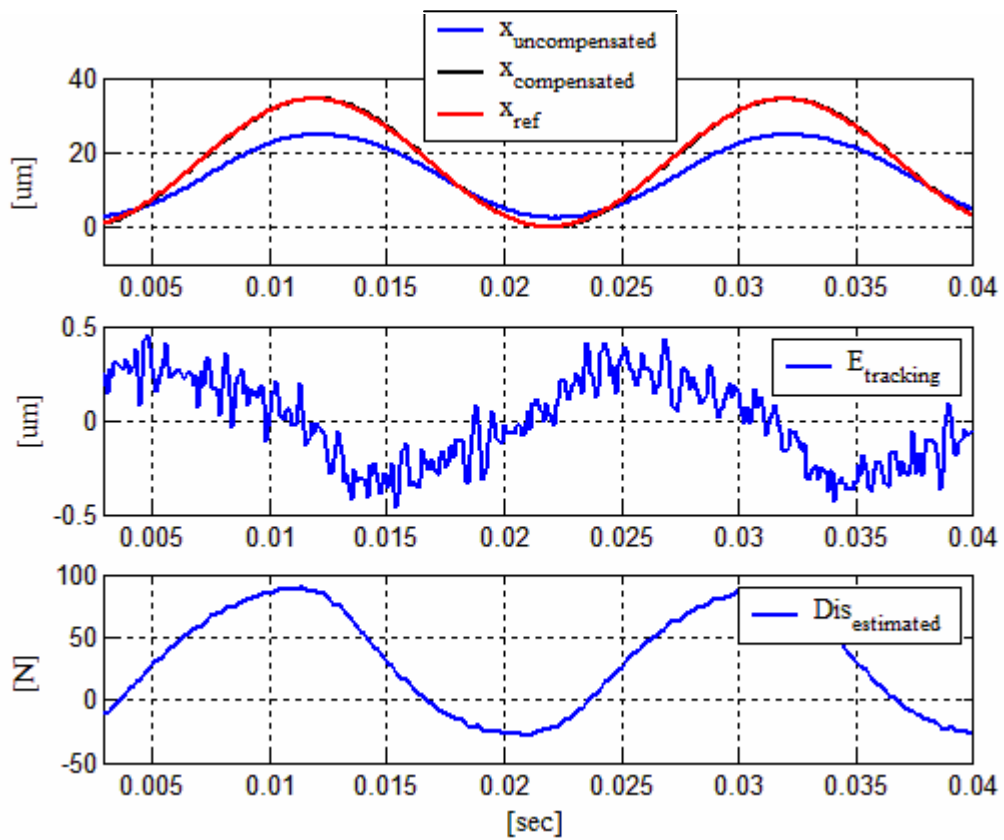


Figure 4.5. Response to  $u_0 = 30 \sin(100\pi t) + 30$  with disturbance compensation

## 4.2.2 Force Observer

From the structures (3.10) and (3.11) defined previously, the mechanical side of the actuator can be written as

$$m_N \ddot{x} + c_N \dot{x} + k_N x = T_N u_p - F_{ext} \quad (4.14)$$

Note that any parameter uncertainties are neglected with the assumption that the nominal plant parameters are as precise as possible. Hence, a disturbance observer based on the complete model of the actuator that includes hysteresis estimates the external force only. Based on the same principles defined for the total disturbance observer an observer based on the non-linear model of the actuator is constructed as follows

$$m_N \ddot{\hat{x}} + c_N \dot{\hat{x}} + k_N \hat{x} = T_N u_p - u_{force} \quad (4.15)$$

As before, if  $\hat{x}$  is forced to track  $x$  then  $F_{ext} = u_{force} = \hat{F}_{ext}$ . Note that  $u_p$  is not measured directly, but, is computed from  $x$  and  $u_{in}$  using equations (3.6) to (3.9). Similar to the previous case the controller used will be in the SMC framework. Using the sliding manifold  $\sigma_{est} = (\dot{x} - \dot{\hat{x}}) + C_{est}(x - \hat{x})$  and since this is a discrete-time application the following control is used.

$$u_{(k)} = u_{(k-1)} + K_{est} \left( D_{est} \sigma_{est(k)} + \frac{\sigma_{est(k)} - \sigma_{est(k-1)}}{T_s} \right) \quad (4.16)$$

The observer implementation is depicted in figure 3.6. The results of the force observer are shown below.

Experiments were carried out with the force observer in an attempt to test its capacity of estimating the external forces acting on the system. Figure 4.7a shows the measured and estimated force for a step motion shown in Figure 4.7b. The position tracking was not the main concern but the concern was to have reasonable force estimation. The force estimation depends on the accuracy of the model. Hence, any inaccuracies in the model will cause errors in the force estimation. The difficulties in the model arise from the hysteresis estimation which has some inaccuracies. The inaccuracies obtained are in the order of 1-10%. The force observer parameters were the same as the disturbance observer and are:  $C_{est} = 800$ ,  $D_{est} = 2000$  and  $K_{est} = 20$ .

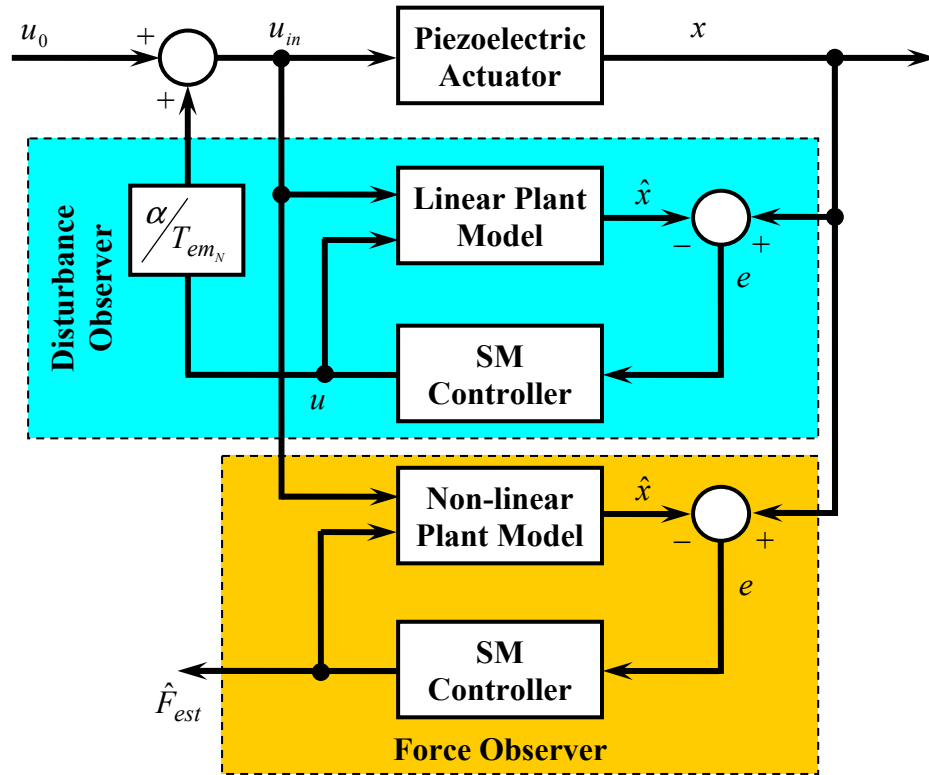


Figure 4.6. Block-diagram for external force estimation

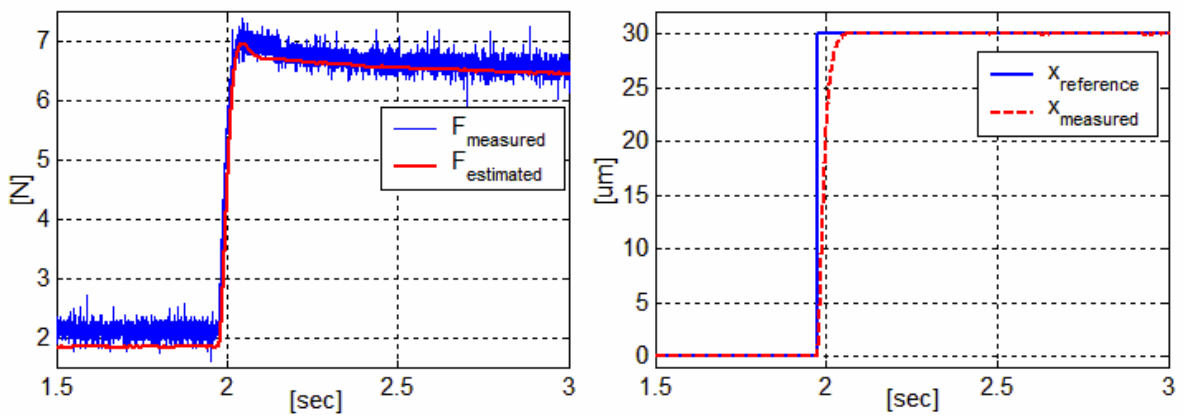


Figure 4.7. Results of the Force Observer Experiments

### 4.3 Results of Closed-Loop Control Experiments

The experimental setup consists of a PSt150/5/60 stack actuator ( $x_{\max} = 60 \mu\text{m}$ ,  $F_{\max} = 800 \text{N}$ ,  $v_{\max} = 150 \text{V}$ ) produced by Piezomechanik connected to SVR150/3 low-voltage, low-power amplifier. The piezoelectric actuator has built-in strain-gages

for position measurement. Force measurement is accomplished by the help of a load cell that is placed against the actuator as shown in Figure 4.8. Any motion on the part of the actuator will exert a force on the load cell which is equal and opposite of the force on the actuator. Hence, the force measured by the load cell is nothing but the force acting on the actuator. The entire setup is connected DS1103 module hosted in a PC with dSpace software Control Desk v.2.0. In Figure 4.9 a simplified structure of the experimental setup is shown.

### 4.3.1 Position Control

The disturbance compensation scheme was incorporated with closed-loop control algorithm using SMC as depicted by Figure 4.10. As it can be seen from the results in Figure 4.11, the use of closed-loop control with disturbance compensation gives good results. The results that are shown in Figure 4.11 are for a reference trajectory of the form  $x_{ref} = 11 + 11\sin(2\pi t)$ .

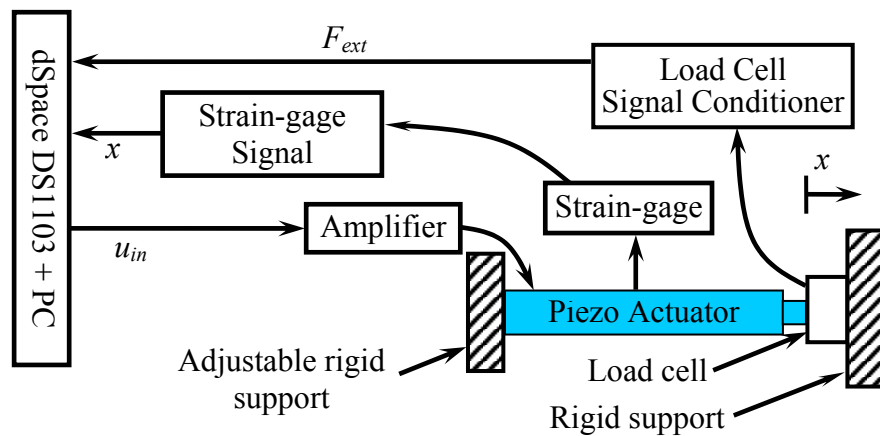


Figure 4.8. Sketch of the experimental setup

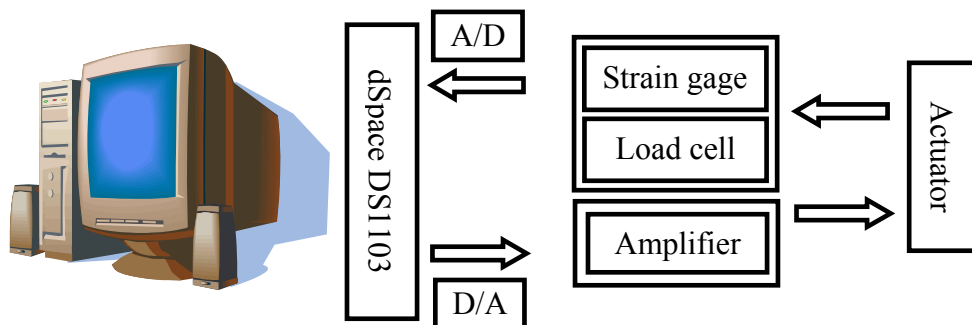


Figure 4.9. Structure of the experimental setup

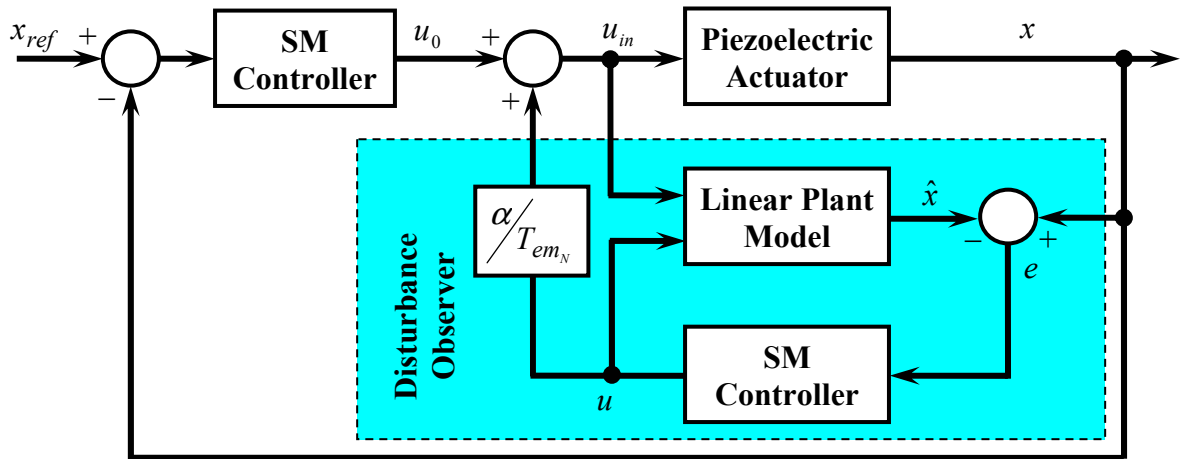


Figure 4.10. Closed-loop control scheme

In the experiments shown below the controller parameters were:  $C_x = 800$ ,  $D_x = 2000$  and  $K_x = 25$ .

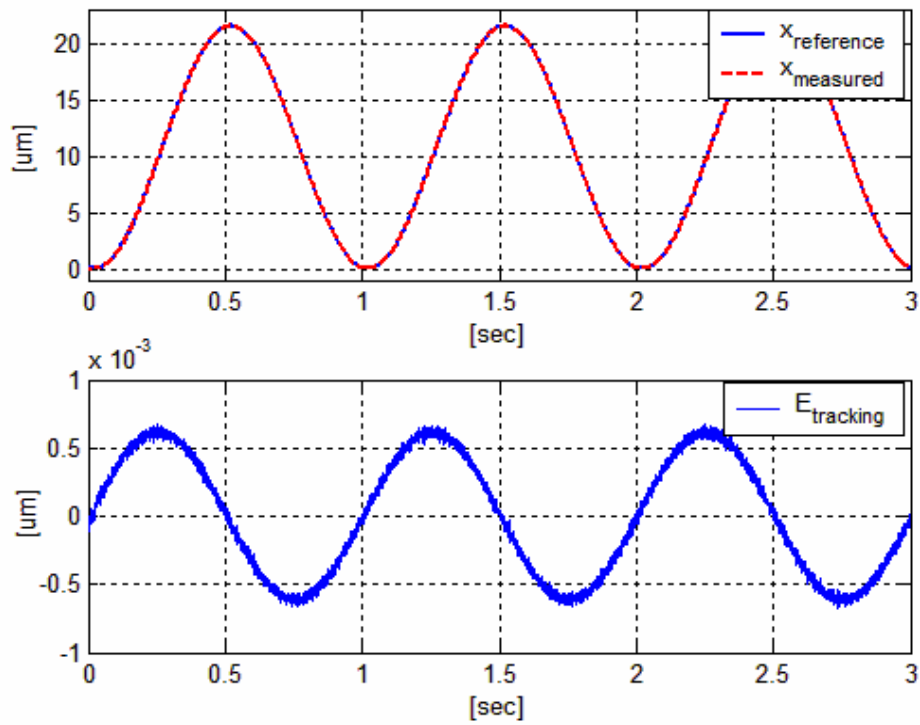


Figure 4.11. Closed-loop response to a 1Hz sinusoidal reference

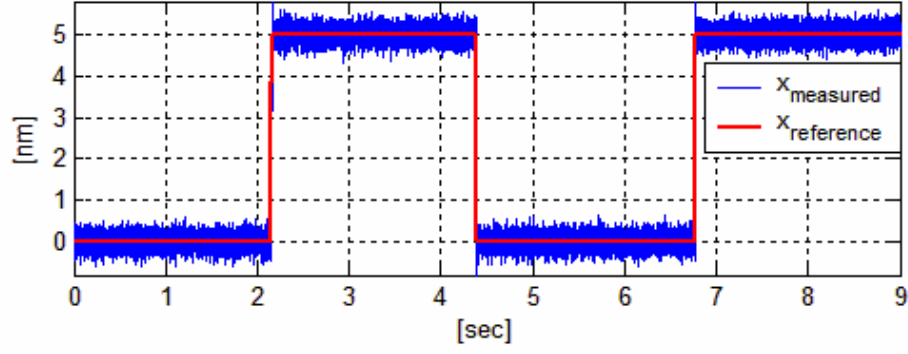


Figure 4.12. 5nm step motion

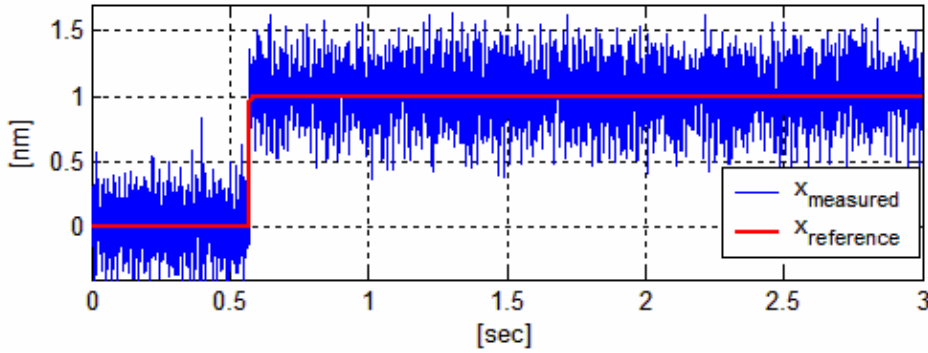


Figure 4.13. 1nm step motion

Very small incremental step motions are also possible with this technique. Figure 4.13 shows that step motions as small as 1nm are possible.

### 4.3.2 Force Control

The force controller is based on SMC framework. Here, the environment was modeled as stiffness and damping as follows, [16]

$$F_{ext} = K_{ext}x + B_{ext}\dot{x} \quad (4.17)$$

Here  $K_{ext}$  and  $B_{ext}$  are the environmental stiffness and damping and are in all cases unknown before hand. Let the force control error be defined as  $\sigma_f = F_{ref} - F_{ext}$  and sliding mode be established at  $\sigma_f = 0$ , such that the solution  $\sigma_f = 0$  is stable. Also selecting the Lyapunov function as  $v_L = \sigma_f^2/2$  and selecting the derivative of the Lyapunov function as  $-D_f\sigma_f^2$  with  $D_f > 0$ . Equating the above results and simplifying

$$\dot{v}_L = \sigma_f \dot{\sigma}_f = -D_f \sigma_f^2 \Rightarrow \dot{\sigma}_f + D_f \sigma_f \Big|_{\sigma_f \neq 0} = 0 \quad (4.18)$$

Inserting  $\sigma_f = F_{ref} - F_{ext}$  and simplifying further

$$\dot{F}_{ref} - \dot{F}_{ext} + D_f(F_{ref} - F_{ext}) = 0 \quad (4.19)$$

Using (4.1), (4.17) and (4.19) the final form of the equivalent control with  $u_{eq} = u_{in}$  is as follows

$$u_{eq} = \frac{m_N}{T_N B_{ext}} (\dot{F}_{ref} + D_f F_{ref} + A\dot{x} + Bx) + \frac{1}{T_N} F_d$$

$$A = B_{ext} \frac{c_N}{m_N} - K_{ext} - D_f B_{ext} \quad (4.20)$$

$$B = B_{ext} \frac{k_N}{m_N} - D_f K_{ext}$$

Finally, the control necessary to insure  $\sigma_f(\dot{\sigma}_f + D_f \sigma_f) = 0$  when  $\sigma_f \neq 0$  is given by

$$u_c = u_{eq} + D_f \text{sgn}(\sigma_f) \quad (4.21)$$

The transients of the closed-loop control system are defined by  $D_f$ . As before, for discrete-time applications the following control is used

$$u_{(k)} = u_{(k-1)} + K_f \left( D_f \sigma_{f(k)} + \frac{\sigma_{f(k)} - \sigma_{f(k-1)}}{T_s} \right) \quad (4.22)$$

Here  $K_f$  is a design parameter which can be tuned to optimize the controller and  $T_s$  is the sampling interval of the discrete-time control. The closed-loop system is best described by the block diagram of Figure 4.14.

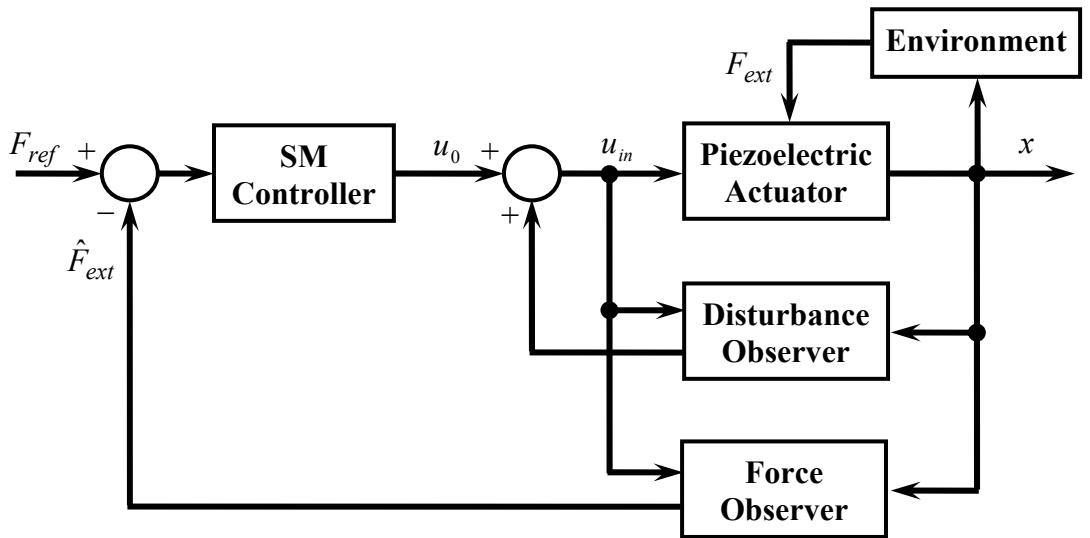


Figure 4.14. Block-diagram of force control system

Experiments using both a force sensor and the force observer were conducted. The experiments prove that the technique works well. For the results in Figure 4.15, the control scheme using a force sensor for feedback was used. However, large noise in the sensor measurement prevented the use of higher gains in the controller. Thus, a slow rise time for the force controller was generated. Also, using force sensors is not very feasible in most applications. Thus, emphasis must be made on the use of force estimation techniques.

The results in Figure 4.16 are for the case when force observer feedback is used. The results show that the force observer works quite well. For the case of sensor based force control, the following controller parameters were used:  $D_f = 400$  and  $K_f = 0.1$ . For the case of sensor based force control, the following controller parameters were used:  $D_f = 400$  and  $K_f = 0.1$ . For the sensorless case  $D_f = 1000$  and  $K_f = 1$ .

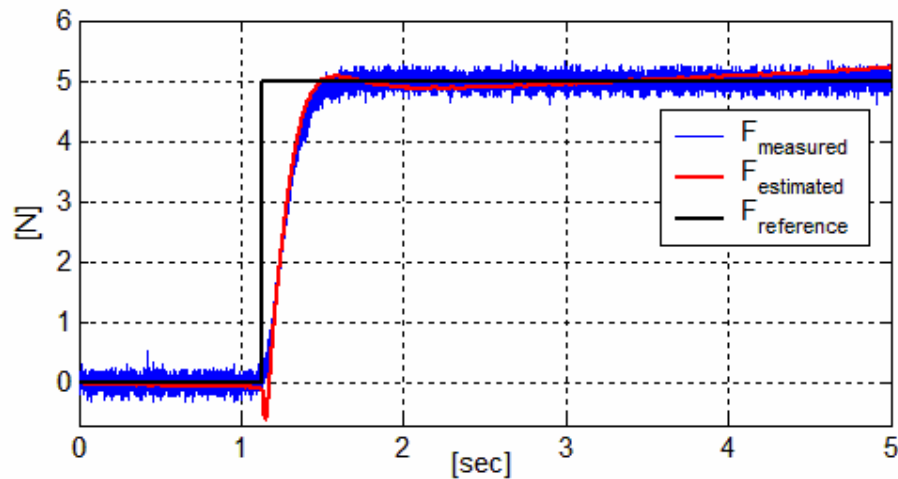


Figure 4.15. Sensor based force control

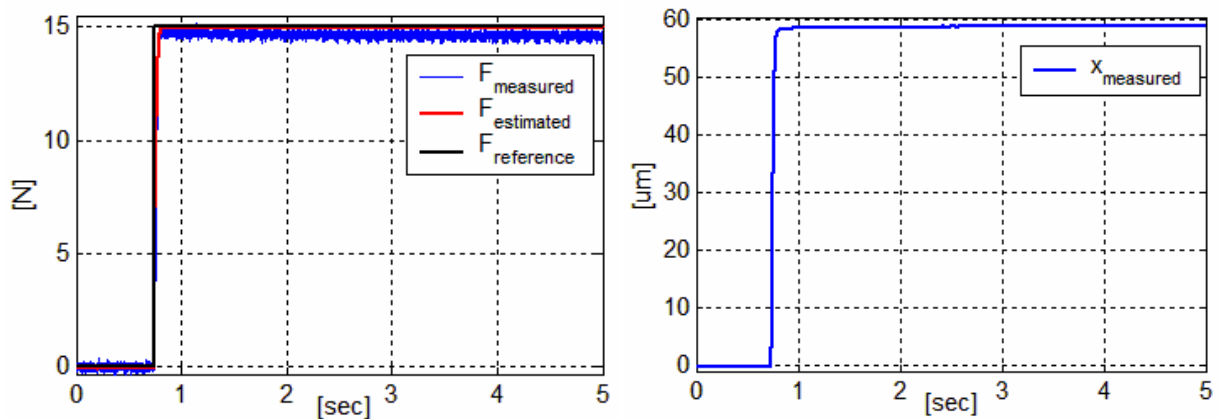


Figure 4.16. Observer based force control

## 5. A DUAL-STAGE SERVO SYSTEM

### 5.1 Introduction

As the industrial need for high speed and high accuracy positioning devices increases, a new concept of servo system emerged: the dual-stage servo system, which is defined as combination of coarse/fine (or macro/micro) actuation stages for fast and precise positioning. In dual-stage systems, the coarse actuator is used for coarse and large motions while the fine actuator for fine and small range motions. Usually, the fine actuators have the characteristic of low power and small range but the frequency band is very high. In coarse actuators, the situation is the reverse. So, by adopting the advantages of both actuators for one purpose, a desirable system satisfying the purpose can be constructed.

The conventional actuator (e.g., electrical motor) has the following limitations: mechanical resonance at high frequencies and large bearing friction at low speed. Especially, the nonlinear friction around zero velocity is the main source of hindering the fine positioning. The fine actuator such as piezoelectric actuator is a solution to increase the servo bandwidth and positioning resolution, although it is limited in motion range and power.

Many systems exist that incorporate the dual actuation concept. Examples of such systems are disk drives [11], macro/micro robotic manipulators [21], and 2-axis linear positioning tables [22]. In this work the control of a dc-motor driven ball-screw actuator with a piezo actuator attached on the tip will be considered. This is the building block to controlling a Stewart-Platform manipulator that is considered as the end result of this work.

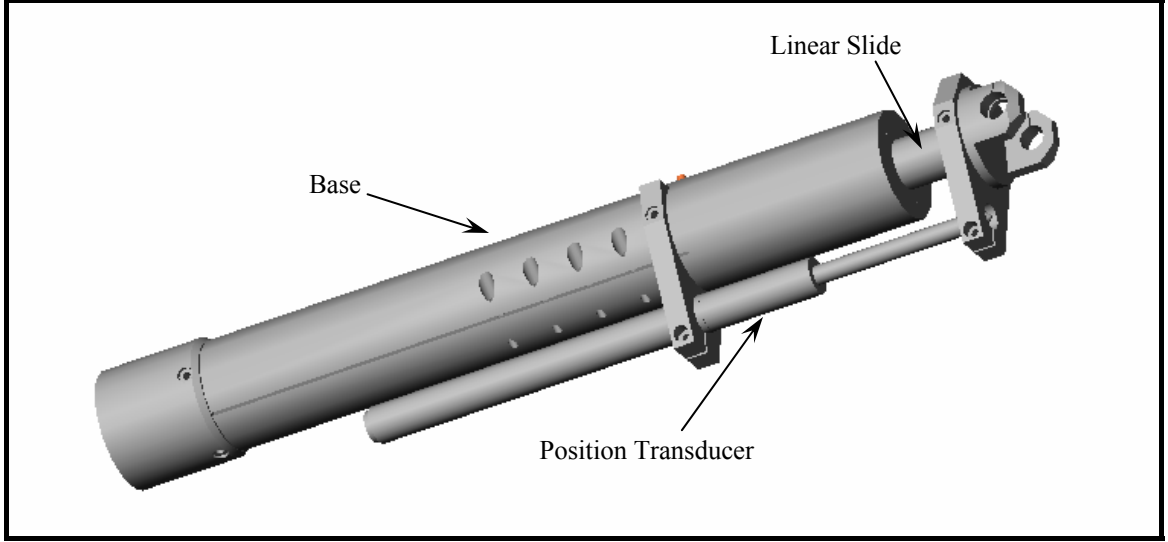


Figure 5.1. CAD model of the dual-stage system

## 5.2 Structure of the System

In this work the dc-motor driven ball-screw actuator with a piezo actuator attached at the tip is used to drive a slider as seen in Figure 5.1 and Figure 5.2. Motion of the ball-screw is measurable via an encoder attached to the dc-motor and the combined motion of the actuator is measured via a linear capacitance based transducer. The maximum repeatability of the ball-screw drive is  $5\mu\text{m}$  while that of the piezo-drive is  $0.1\text{nm}$ . Thus, with proper control it is possible to achieve repeatability in the sub-nanometer range.

For the modeling of the system, the ball-screw drive will be modeled as a dc-motor with a disturbance term that will include the dynamics of the ball-screw, the piezo-drive coupling dynamics and friction. The piezo-drive will be modeled as described in chapter 2 and the coupling dynamics will be included along with the hysteresis and external forces in the disturbance term. The equations of motion for the two systems when independent are as follows

$$J\ddot{\theta}(t) = K_T i(t) - T_D \quad (5.1)$$

$$m_p \ddot{x} + c_p \dot{x} + k_p x = T_{em} u_{in}(t) - F_d \quad (5.2)$$

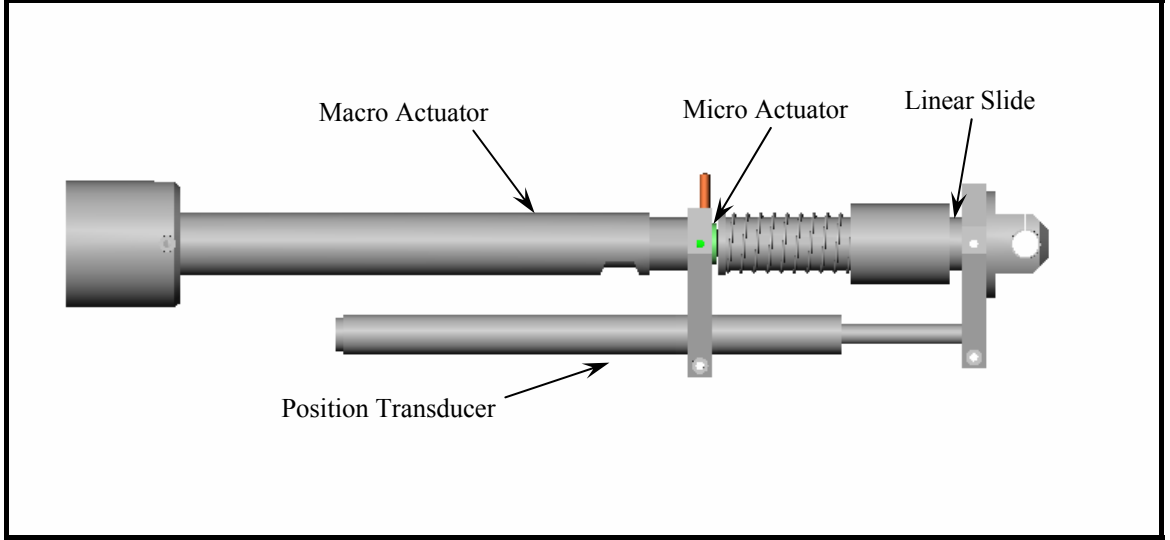


Figure 5.2. Anatomy of the dual-stage system

In (5.1) and (5.2),  $J$  is the motor inertia,  $\theta(t)$  is the angular position of the motor shaft,  $K_T$  is the motor torque constant,  $i(t)$  is the current input to the motor,  $T_D$  is the disturbance torque on the motor shaft,  $m_p$  is the equivalent mass of the piezo-drive,  $c_p$  is the equivalent damping of the piezo-drive,  $k_p$  is the equivalent stiffness of the piezo-drive,  $x$  is the deflection of the piezo-drive,  $T_{em}$  is the electromechanical transformation constant,  $u_{in}(t)$  is the voltage input to the piezo-drive and  $F_d$  is the disturbance force acting on the piezo-drive. The above equations can be written differently in terms of the global coordinates of the equivalent masses of each drive  $q_1$  and  $q_2$  as follows

$$\frac{J}{n^2} \ddot{q}_1(t) = \frac{K_T}{n} i(t) - \frac{T_D}{n} \Rightarrow m_m \ddot{q}_1(t) = K_m i(t) - f_1(q_1, q_2) \quad (5.3)$$

$$m_p \ddot{q}_2 + c_p (\dot{q}_2 - \dot{q}_1) + k_p (q_2 - q_1) = T_{em} u_{in}(t) - f_2(q_1, q_2) \quad (5.4)$$

here  $n$  is the rotation-to-linear transformation constant and  $f_1$  along with  $f_2$  are the disturbances that contain the coupling dynamics, external forces and nonlinearities of each drive and are, hence, functions of both coordinates. The model of the system is depicted in Figure 5.3. The force  $f_1$  includes  $f_D$  and coupling effects due to  $k_p$  and  $c_p$ .

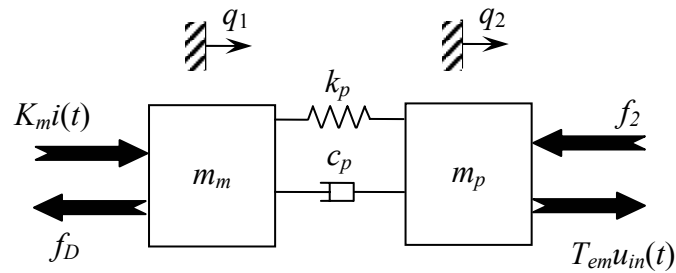


Figure 5.3. Model representation of the system

It is possible to write (5.4) in terms of the relative motion between  $m_p$  and  $m_m$ . This will be necessary in the control algorithm that will be shown in the later section. Note that the relative motion between mp and mm is  $q_2 - q_1$  and this will be represented by  $z$ . Hence, equation (5.4) becomes

$$m_p \ddot{z} + b_p \dot{z} + k_p z = T_{em} v(t) - \tilde{f}_2(q_1, q_2) \quad (5.5)$$

here  $\tilde{f}_2$  contains the dynamics due to  $q_1$ . The system can be written into state-space form to simplify the analysis as follows

$$\begin{aligned} \dot{x}_1 &= \dot{q}_1 = x_2 \\ \dot{x}_2 &= \ddot{q}_1 = \frac{K_m}{m_m} i - \frac{1}{m_m} f_1 \\ \dot{x}_3 &= \dot{z} = x_4 \\ \dot{x}_4 &= \ddot{z} = -\frac{k_p}{m_p} x_3 - \frac{b_p}{m_p} x_4 + \frac{T_{em}}{m_p} v(t) - \frac{1}{m_p} \tilde{f}_2 \end{aligned} \quad (5.6)$$

The task here is to force  $q_2$  which is the sum of the states  $x_1$  and  $x_3$  to track a desired reference trajectory. The control algorithm for handling this task will be discussed in section 5.4.

### 5.3 Results with Single-Stage Servo

In order to test the capacity of the single-stage, composed of the DC-motor ball-screw drive, it was necessary to conduct some reference tracking experiments. Various types of references were used on the system with the actuation of only a single-stage. The controller of the drive was in the SMC framework in discrete-time and the structure of the overall control for the single-stage is depicted in Figure 5.4.

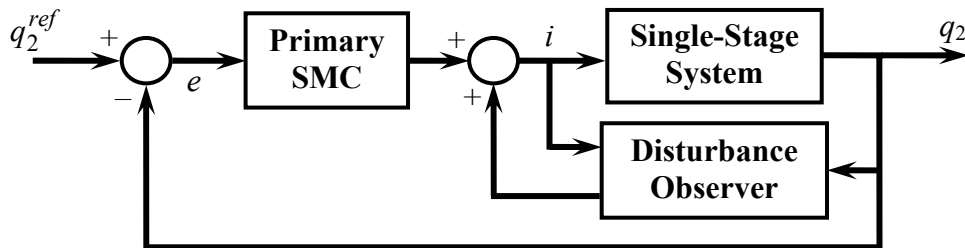


Figure 5.4. Single-stage controller scheme

Numerous experiments on the actuator were conducted using the simple algorithm shown above. The results of those experiments are depicted below. For the experiments shown below, the following controller parameters were used:

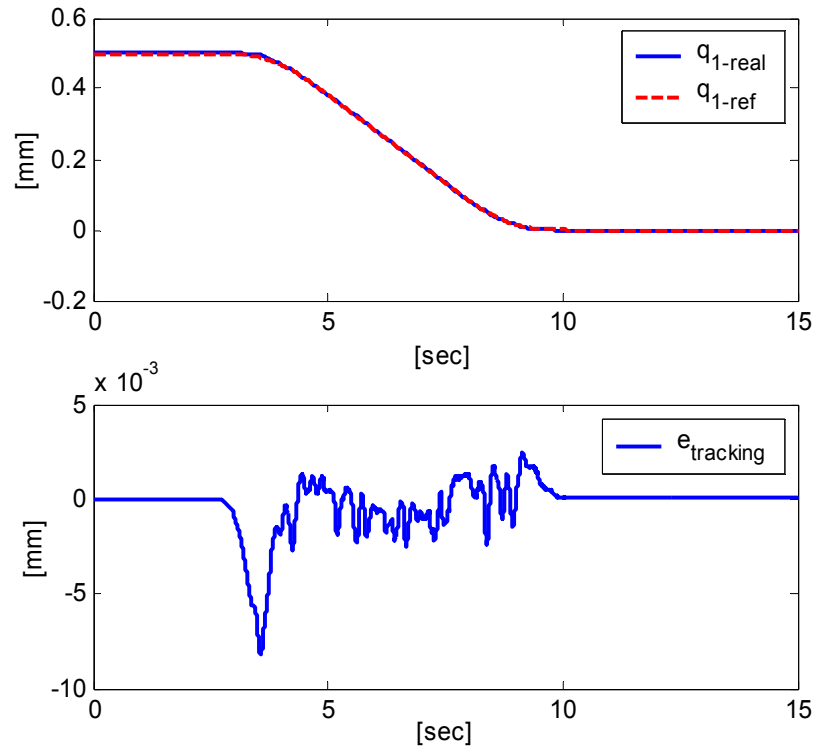


Figure 5.5. Single-stage 0.5mm sigmoid reference tracking

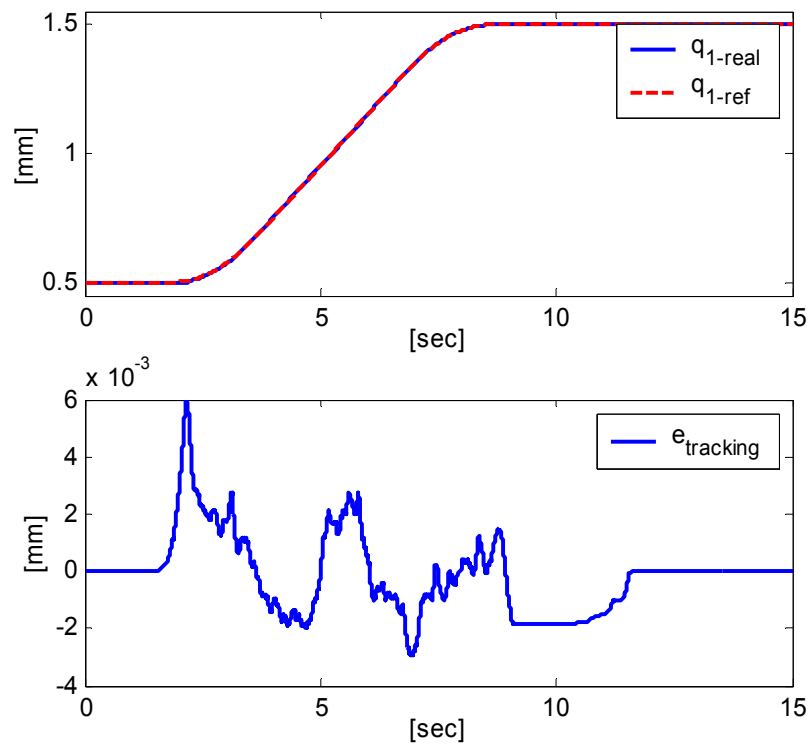


Figure 5.6. Single-stage 1mm sigmoid reference tracking

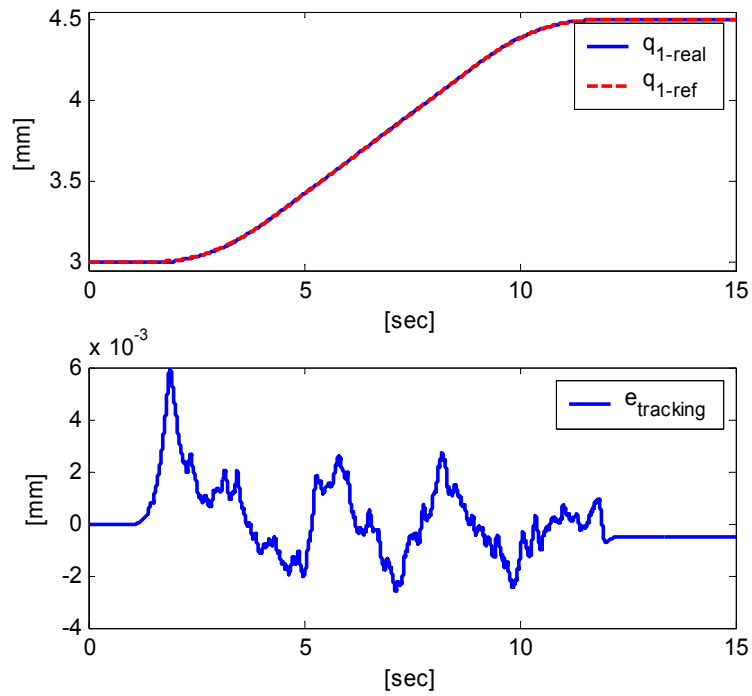


Figure 5.7. Single-stage 1.5mm sigmoid reference tracking

#### 5.4 Proposed Controller

Control of the dual-stage system is based on a simple algorithm in which each stage has independent control. The reference position for the ball-screw drive is the final tip position of the piezo-drive. The error of tracking of the ball-screw drive is then sent to the piezo-drive as a reference. Thus, whatever discrepancies that exist during the reference tracking are compensated by the piezo-drive. This is shown by Figure 5.5.

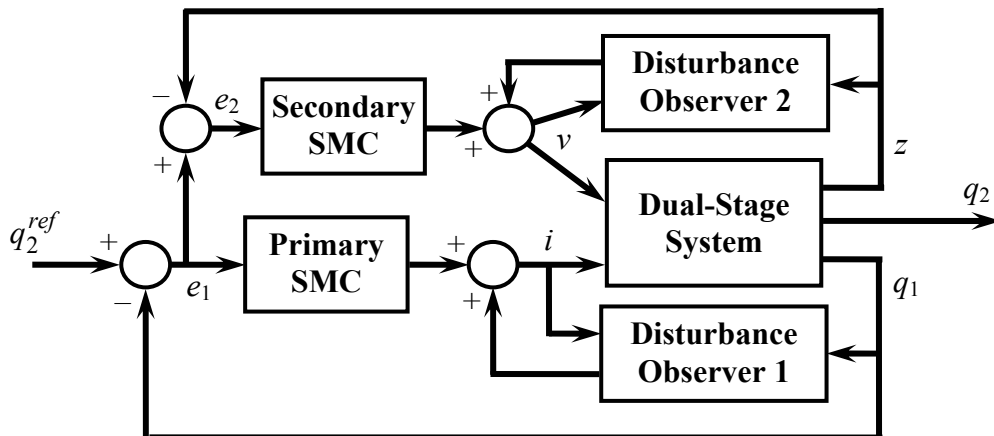


Figure 5.8. Dual-stage Controller scheme

## 5.5 Results with Dual-Stage Servo

As in all cases, the proposed control scheme is implemented on an actual dual-stage system to test its capacity. References used in these experiments are the same as those used for the single-stage experiments in order to be able to compare the two schemes. The figures shown below verify that the overall tracking performance can be greatly enhanced if a secondary microactuator is included at the tip position of the linear drive system.

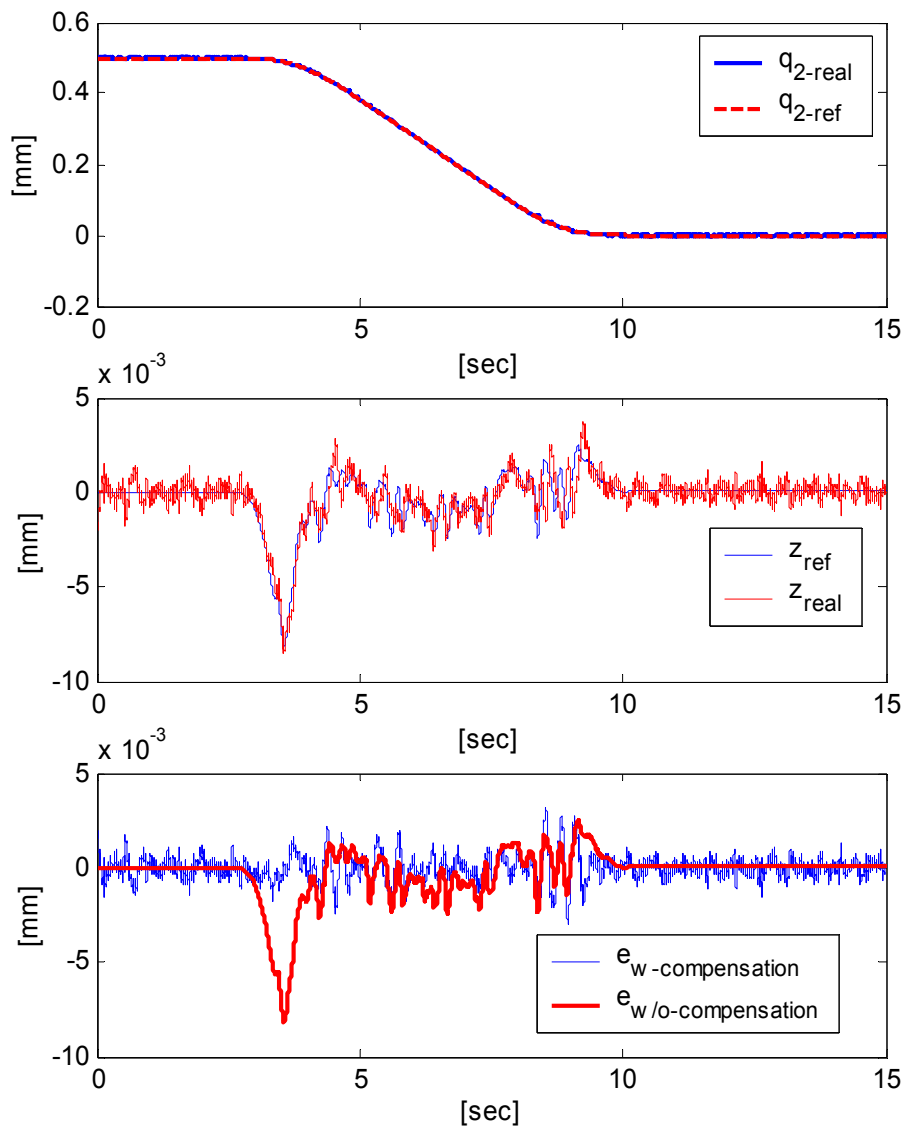


Figure 5.9. Dual-stage 0.5mm sigmoid reference tracking

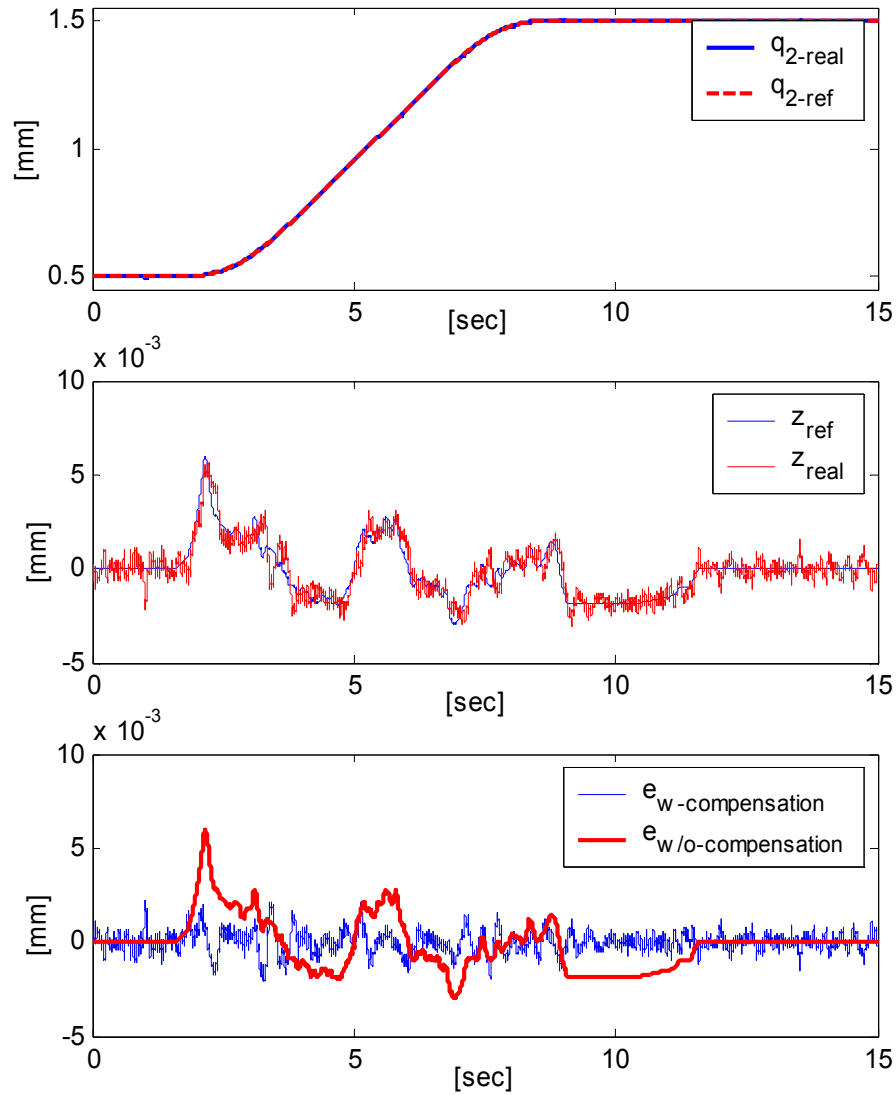


Figure 5.10. Dual-stage 1mm sigmoid reference tracking

Note that due to some noise in the tip position measurement tracking of the piezo-drive is somehow compromised.

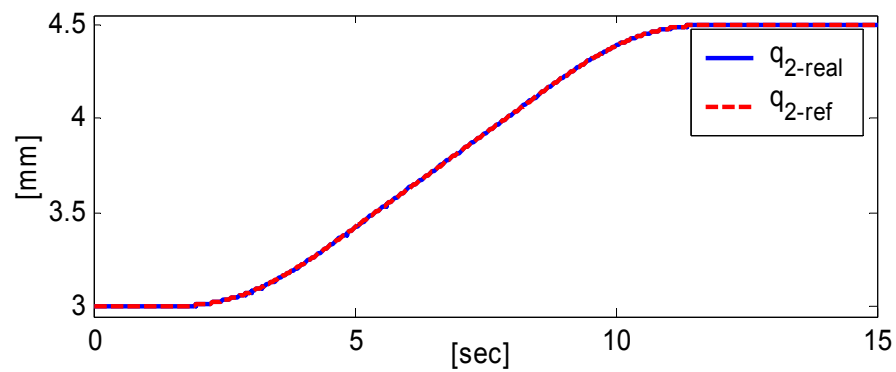


Figure 5.11. Dual-stage 1.5mm sigmoid reference tracking

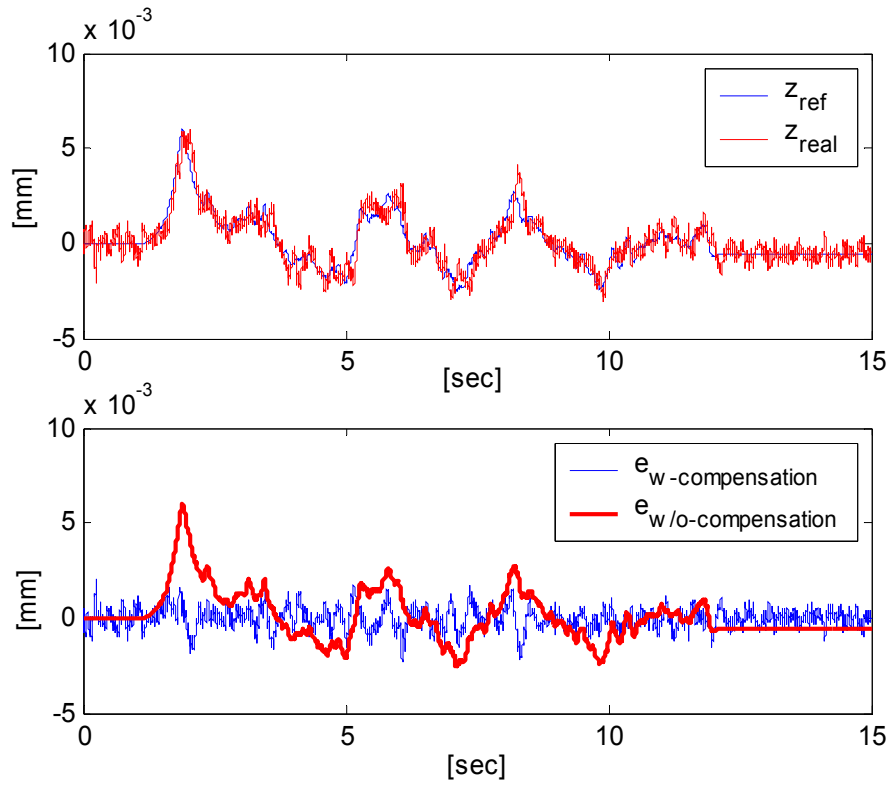


Figure 5.12. Dual-stage 1.5mm sigmoid reference tracking (contd.)

From the above figures it can be concluded that the concept works well. However, improvements in the measurement should allow higher resolution tuning as compared to that shown above. Due to the non-availability of such sensors, it will not be shown in this thesis.

## **6. ANALYSIS OF THE KINEMATICS OF A 6-DOF STEWART-GOUGH MANIPULATOR**

### **6.1 Introduction**

The kinematics of a Stewart-Gough manipulator will be described in this chapter. A Stewart-Gough platform is a special type of manipulator that belongs to a class of mechanisms known as parallel manipulators. Parallel manipulators are classified as planar, spherical, or spatial manipulators in accordance with their motion characteristics.

As shown in Figure 6.1, a parallel manipulator consists of a moving platform that is connected to a fixed base by several limbs or legs. Typically, the number of degrees of freedom is equal to the number of legs such that every leg is controlled by one actuator and all actuators can be mounted at or near the fixed base. For this reason, parallel manipulators are sometimes called platform manipulators. Because the external load can be shared by the actuators, parallel manipulators tend to have a large load-carrying capacity.

Parallel manipulators can be found in many applications, such as airplane simulators, adjustable articulated trusses, mining machines, pointing devices and walking machines. Recently, it has been developed as a high-speed, high-precision, multi-dof machining center, shown in Figure 6.1.

The design of parallel manipulators goes back to 1962, when Gough and Whitehall devised a six-linear jack system for use as a universal tire-testing machine. Stewart (1965) designed a platform manipulator for use as an aircraft simulator in 1965. Hunt (1983) made a systematic study of the kinematic structure of parallel manipulators. Since then, parallel manipulators have been studied extensively by numerous researchers, [23].

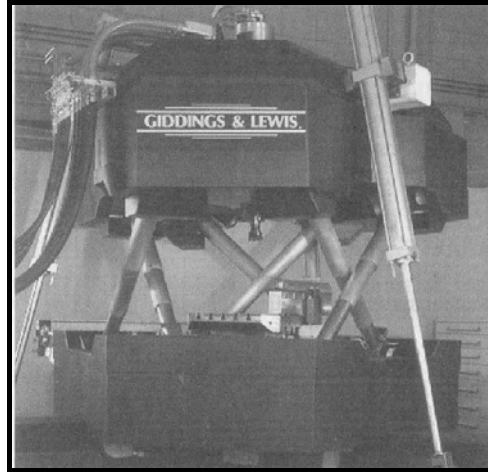


Figure 6.1. VARIAX<sup>®</sup> machining center, Giddings and Lewis machine tools

Most of the 6-dof parallel manipulators studied to date consist of six extensible limbs. These parallel manipulators possess the advantages of high stiffness, low inertia and large payload capacity. However, they suffer the problems of relatively small workspaces and design difficulties. Furthermore, their direct kinematics is a difficult problem. Perhaps, the only six-limbed, 6-dof parallel manipulators for which closed-form direct kinematic solutions have been reported in the literature are special forms of the Stewart-Gough platform.

## 6.2 Description of the Stewart-Gough Manipulator

The Stewart-Gough manipulator used in this study is of the symmetrical type. A parallel manipulator is said to be symmetrical if it satisfies the following conditions:

- The number of limbs is equal to the number of degrees of freedom of the moving platform.
- The type and number of joints in all the limbs are arranged in an identical pattern.
- The number and location of actuated joints in all the limbs are the same.

Figure 6.2 shows a spatial 6-dof, 6SPS (Spherical-Prismatic-Spherical) symmetric Stewart-Gough platform. Six identical limbs connect the moving platform to the fixed base by spherical joints at points  $B_i$  and  $A_i, i = 1, 2, \dots, 6$  respectively. Each limb consists of an upper member and a lower member connected by a prismatic joint. Ball screws or hydraulic jacks can be used to vary the lengths of the prismatic joints and therefore to control the location of the moving platform. In the case of the Stewart-Gough platform

used in this study, serially connected ball screws and piezoelectric-ceramic actuated translators are used to vary the length of the limbs, but for simplicity reasons, a single actuator will be considered in each limb.

Note that in Figure 6.2, the attachment points  $A_i$  for  $i=1$  to 6 are sketched in a plane on the fixed base. Similarly,  $B_i$  for  $i=1$  to 6 are sketched in a plane on the moving platform. There are 14 links connected by 6 prismatic joints and 12 spherical joints. Hence the number of degrees of freedom of the mechanism is

$$F = \lambda(n - j - 1) + \sum_i f_i = 6(14 - 18 - 1) + (6 + 3 \times 12) = 12 \quad (6.1)$$

However, there are 6 passive degrees of freedom associated with the six *SPS* limbs. Therefore, the moving platform possesses 6 degrees of freedom. Since the limbs are connected to the moving platform and the fixed base by spherical joints, no bending moments or twisting torques will transmit to the limbs. The force acting on the limb is directed along the longitudinal axis of the limb. Consequently, these limbs can be made of hollow cylindrical rods to produce a light-weight, high-stiffness, high-speed manipulator.

### 6.3 Geometry of the Stewart-Gough Manipulator

For the purpose of analysis, two Cartesian coordinate systems, frames  $A(x,y,z)$  and  $B(u,v,w)$  as shown in Figure 6.2, are attached to the fixed base and the moving platform.

The transformation from the moving platform to the fixed base can be described by the position vector  $\vec{p}$  of the centroid  $P$  and the rotation matrix  ${}^A R_B$  of the moving platform. Let  $\vec{u}, \vec{v}$  and  $\vec{w}$  be three unit vectors defined along the  $u, v$  and  $w$  axis of the moving coordinate system; then the rotation matrix can be written as

$${}^A R_B = \begin{bmatrix} u_x & v_x & w_x \\ u_y & v_y & w_y \\ u_z & v_z & w_z \end{bmatrix} \quad (6.2)$$

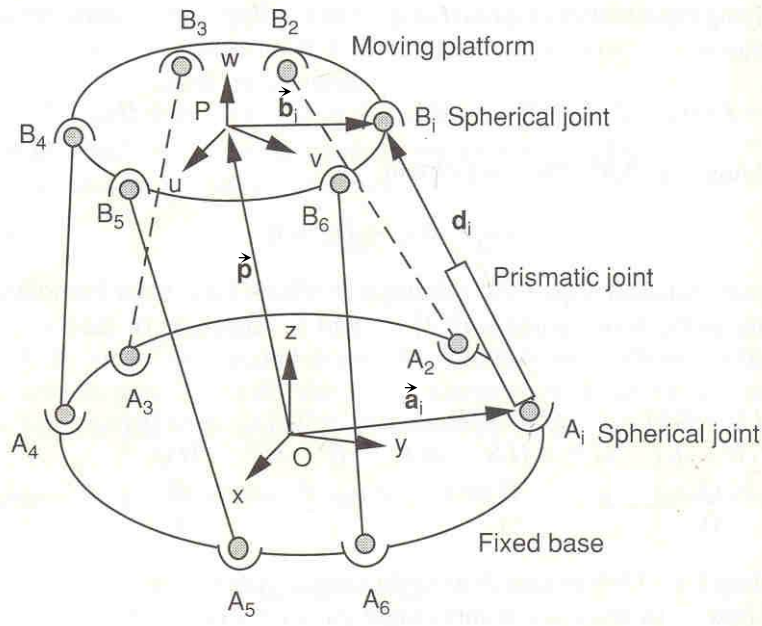


Figure 6.2. Spatial 6-dof, 6SPS parallel manipulator

The elements of the transformation matrix  ${}^A R_B$  must satisfy the following orthogonal conditions:

$$u_x^2 + u_y^2 + u_z^2 = 1 \quad (6.3)$$

$$v_x^2 + v_y^2 + v_z^2 = 1 \quad (6.4)$$

$$w_x^2 + w_y^2 + w_z^2 = 1 \quad (6.5)$$

$$u_x v_x + u_y v_y + u_z v_z = 0 \quad (6.6)$$

$$u_x w_x + u_y w_y + u_z w_z = 0 \quad (6.7)$$

$$v_x w_x + v_y w_y + v_z w_z = 0 \quad (6.8)$$

As shown in Figure 6.2, let  $\vec{a}_i = [a_{i_x} \ a_{i_y} \ a_{i_z}]^T$  and  ${}^B \vec{b}_i = [b_{i_u} \ b_{i_v} \ b_{i_w}]^T$  be the position vectors of points  $A_i$  and  $B_i$  in the coordinate frames  $A$  and  $B$ . A vector-loop equation for the  $i^{\text{th}}$  limb of the manipulator can be written as follows:

$$\overline{A_i B_i} = \vec{p} + {}^A R_B {}^B \vec{b}_i - \vec{a}_i \quad (6.9)$$

The length of the  $i^{\text{th}}$  limb is obtained by taking the dot product of the vector  $\overline{A_i B_i}$  with itself:

$$d_i^2 = [\vec{p} + {}^A R_B {}^B \vec{b}_i - \vec{a}_i]^T [\vec{p} + {}^A R_B {}^B \vec{b}_i - \vec{a}_i] \quad \text{for } i = 1, 2, \dots, 6 \quad (6.10)$$

Where  $d_i$  denotes the length of the  $i^{\text{th}}$  limb. Expanding (6.10) yields

$$d_i^2 = \vec{p}^T \vec{p} + [{}^B\vec{b}_i]^T [{}^B\vec{b}_i] + \vec{a}_i^T \vec{a}_i + 2\vec{p}^T [{}^A R_B {}^B\vec{b}_i] - 2\vec{p}^T \vec{a}_i - 2[{}^A R_B {}^B\vec{b}_i]^T \vec{a}_i \quad (6.11)$$

Writing (6.11) six times, once for each  $i = 1, 2, \dots, 6$ , yields six equations describing the location of the moving platform with respect to the fixed base. Note that  ${}^B\vec{b}_i$  and  $\vec{a}_i$  are constant vectors defined by the geometry of the manipulator.

#### 6.4 Direct Kinematics of the Stewart-Gough Manipulator

For the direct kinematics problem, the limb lengths  $d_i$ , for  $i = 1, 2, \dots, 6$ , are given, and the position vector  $\vec{p} = [p_x \ p_y \ p_z]^T$  and the rotation matrix  ${}^A R_B$  of the moving platform are to be found. The position vector contains three scalar unknowns, while the rotation matrix contains nine scalar unknowns. However, the nine scalar unknowns in ARB are related by the six orthogonal conditions given by (6.3) through (6.8). Without losing generality, the following assumptions can be made

- The origin  $O$  of the fixed frame is located at the center of the spherical joint  $A_1$ .
- The origin  $P$  of the moving frame is located at the center of the spherical joint  $B_1$ .

Based on the assumptions above,  $a_{1_x} = a_{1_y} = a_{1_z} = 0$  and  $b_{1_u} = b_{1_v} = b_{1_w} = 0$ . Hence (6.11) for  $i = 1$  reduces to

$$d_1^2 = p_x^2 + p_y^2 + p_z^2 \quad (6.12)$$

For the manipulator considered here,  $a_{i_z} = b_{i_w} = 0$  for  $i = 1, 2, \dots, 6$ . Keeping this in mind and expanding (6.11) for  $i = 2, 3, \dots, 6$ , and then subtracting (6.12) from each of the resulting equations yields

$$b_{i_u} \xi_1 + b_{i_v} \xi_2 - a_{i_x} p_x - a_{i_y} p_y - a_{i_x} b_{i_u} u_x - a_{i_y} b_{i_u} u_y - a_{i_x} b_{i_v} v_x - a_{i_y} b_{i_v} v_y + k_i = 0 \quad (6.13)$$

where  $k_i = (a_{i_x}^2 + a_{i_y}^2 + b_{i_u}^2 + b_{i_v}^2 - d_i^2 + d_1^2)/2$  and the variables  $\xi_1$  and  $\xi_2$  are defined as follows:

$$\xi_1 = p_x u_x + p_y u_y + p_z u_z \quad (6.14)$$

$$\xi_2 = p_x v_x + p_y v_y + p_z v_z \quad (6.15)$$

It can be noted that the unit vector  $\bar{w}$  disappears from (6.13). Hence only three of the six orthogonal conditions are needed for the analysis. By considering  $\xi_1$  and  $\xi_2$  as intermediate variables, we have a system of 11 equations in 11 unknowns. The system of equations consists (6.3), (6.4), (6.6), (6.12), (6.13) for  $i = 2, 3, \dots, 6$ , (6.14), and (6.15). The unknowns are  $p_x$ ,  $p_y$ ,  $p_z$ ,  $u_x$ ,  $u_y$ ,  $u_z$ ,  $v_x$ ,  $v_y$ ,  $v_z$ ,  $\xi_1$ , and  $\xi_2$ . Equations (6.13) for  $i = 2, 3, \dots, 6$  are linear, while the remaining equations are second-degree polynomials.

In what follows, we derive six polynomial equations in three unknowns:  $u_x$ ,  $u_y$  and  $v_y$ . First, rewriting (6.3), (6.4), and (6.12) as a group, and (6.6), (6.14), and (6.15) as another group, as follows:

$$u_z^2 = 1 - u_x^2 - u_y^2 \quad (6.16)$$

$$v_z^2 = 1 - v_x^2 - v_y^2 \quad (6.17)$$

$$p_z^2 = d_1^2 - p_x^2 - p_y^2 \quad (6.18)$$

and

$$u_z v_z = -u_x v_x - u_y v_y \quad (6.19)$$

$$p_z u_z = \xi_1 - p_x u_x - p_y u_y \quad (6.20)$$

$$p_z v_z = \xi_2 - p_x v_x - p_y v_y \quad (6.21)$$

Next, we substitute (6.16) through (6.21) into the following six identities:

$$\left(u_z^2\right)\left(v_z^2\right) - \left(u_z v_z\right)^2 = 0 \quad (6.22)$$

$$\left(u_z^2\right)\left(p_z^2\right) - \left(u_z p_z\right)^2 = 0 \quad (6.23)$$

$$\left(p_z^2\right)\left(v_z^2\right) - \left(p_z v_z\right)^2 = 0 \quad (6.24)$$

$$\left(u_z v_z\right)\left(p_z^2\right) - \left(p_z v_z\right)\left(p_z u_z\right) = 0 \quad (6.25)$$

$$\left(u_z p_z\right)\left(v_z^2\right) - \left(u_z v_z\right)\left(p_z v_z\right) = 0 \quad (6.26)$$

$$\left(v_z p_z\right)\left(u_z^2\right) - \left(u_z v_z\right)\left(p_z u_z\right) = 0 \quad (6.27)$$

This results in six equations free of the variables  $u_x$ ,  $v_x$  and  $p_x$ .

Equation (6.13),  $i = 2, 3, \dots, 6$ , represent five linear equations in eight unknowns. Hence it is possible to solve five unknowns in terms of the remaining three. For example, it is possible to express  $p_x$ ,  $p_y$ ,  $v_x$ ,  $\xi_1$ , and  $\xi_2$  in terms of  $u_x$ ,  $u_y$ , and  $v_y$  as follows:

$$\xi_1 = e_{11}u_x + e_{12}u_y + e_{13}v_y + e_{14} \quad (6.28)$$

$$\xi_2 = e_{21}u_x + e_{22}u_y + e_{23}v_y + e_{24} \quad (6.29)$$

$$p_x = e_{31}u_x + e_{32}u_y + e_{33}v_y + e_{34} \quad (6.30)$$

$$p_y = e_{41}u_x + e_{42}u_y + e_{43}v_y + e_{44} \quad (6.31)$$

$$v_x = e_{51}u_x + e_{52}u_y + e_{53}v_y + e_{54} \quad (6.32)$$

where  $e_{i,j}$ 's are constants that can be found by solving (6.13) for  $i = 2,3,\dots,6$ .

Upon substitution of (6.28) through (6.32) into (6.22) through (6.27), obtaining six fourth-degree polynomials in three unknowns:  $u_x$ ,  $u_y$ , and  $u_z$ . Any of the three polynomials can be used to solve for the three unknowns. This system of equations has at most 64 solutions. Zhang and Song (1994) applied the Sylvester dialytic method to further reduce the six polynomial equations to a 20<sup>th</sup> degree polynomial in one unknown and showed that after back substitution there are at most 40 direct kinematics solutions. Closed-form solutions of this manipulator have also been derived by Wen and Liang (1994), [23].

## 6.5 Inverse Kinematics of the Stewart-Gough Manipulator

For the inverse kinematics problem, the position vector  $\vec{p}$  and the rotation matrix  ${}^A R_B$  of the frame  $B$  with respect to  $A$  are given and the limb lengths  $d_i$ ,  $i=1,2,\dots,6$ , are to be found. The solution is very straight forward. Taking the square root of (6.11) to obtain

$$d_i = \sqrt{\vec{p}^T \vec{p} + [{}^B \vec{b}_i]^T [{}^B \vec{b}_i] + \vec{a}_i^T \vec{a}_i + 2\vec{p}^T [{}^A R_B {}^B \vec{b}_i] - 2\vec{p}^T \vec{a}_i - 2[{}^A R_B {}^B \vec{b}_i]^T \vec{a}_i} \quad (6.33)$$

for  $i=1,2,\dots,6$ . For simplicity it is assumed that the center of frame  $A$  is at the origin. Thus, the position vector of the of the frame  $B$  with respect to  $A$  is given as

$$\vec{p} = \{x \quad y \quad z + z_0\}^T \quad (6.34)$$

where  $x$ ,  $y$  and  $z$  are the required displacements of frame  $B$  with respect to  $A$  while  $z_0$  is the initial elevation of frame  $B$  with respect to  $A$ . Similarly, the rotation matrix  ${}^A R_B$  can be written in terms of the required Euler angles  $\varphi$ ,  $\theta$  and  $\psi$  of frame  $B$  as shown in Figure 6.3.

$${}^A R_B = \begin{bmatrix} c\varphi c\theta c\psi - s\varphi s\psi & -c\varphi c\theta s\psi - s\varphi c\psi & c\varphi s\theta \\ s\varphi c\theta c\psi + c\varphi s\psi & -s\varphi c\theta s\psi + c\varphi c\psi & s\varphi s\theta \\ -s\theta c\psi & s\theta s\psi & c\theta \end{bmatrix} \quad (6.35)$$

Hence, corresponding to each given location of the moving platform, there are generally two possible solutions for each limb. However, the negative limb length is physically not feasible. When the solution of  $d_i$  becomes a complex number, the location of the moving platform is not reachable.

### 6.5.1 Simulation Results for the Proposed Manipulator

The proposed manipulator was constructed on MSC.ADAMS™ dynamics simulation program for the purpose of analyzing the kinematics behavior.

The manipulator used in the simulations is only used for the purpose of verifying the inverse kinematics model that will be used in the actual prototype and does not necessarily reflect the topology of the final design. The joint locations on frame  $A$  with respect to  $A$  and the joints on frame  $B$  with respect to  $B$  are tabulated below.

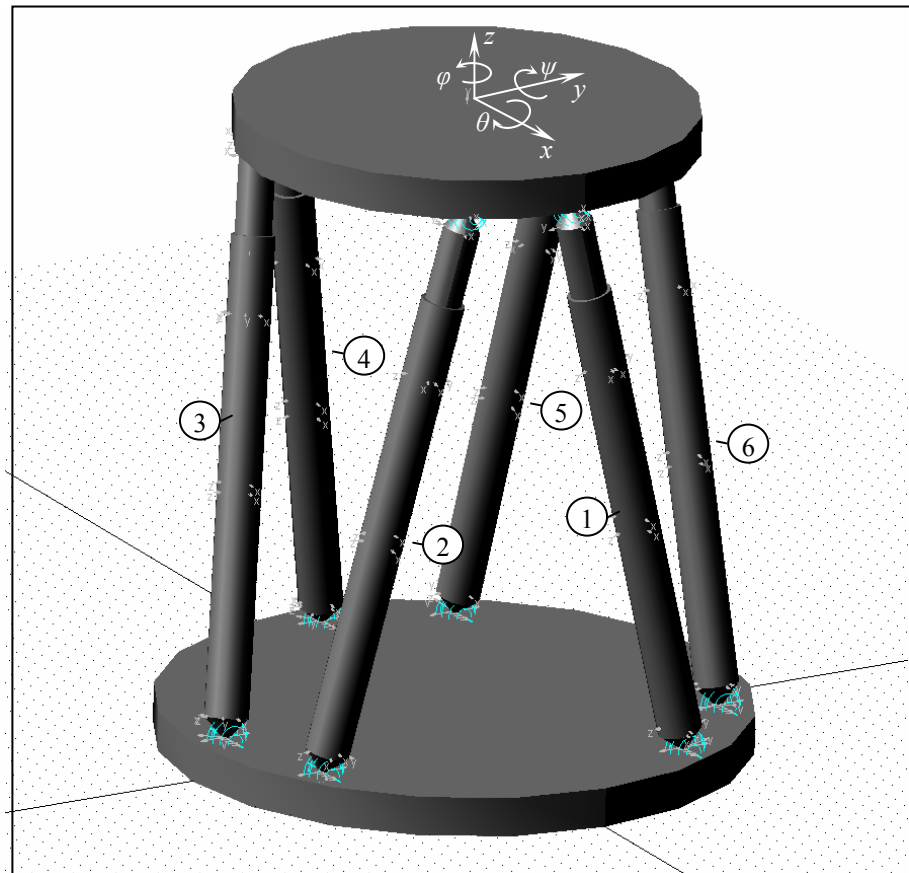


Figure 6.3. MSC.ADAMS CAD model of the proposed manipulator

Table 6.1. Manipulator joint coordinates

Frame $A(x,y,z)$		Frame $B(u,v,w)$	
Joint	Coordinate	Joint	Coordinate
$A_1$	(121.2mm, 70mm, 0mm)	$B_1$	(110mm, 0mm, 0mm)
$A_2$	(70mm, -121.2mm, 0mm)	$B_2$	(95.3mm, -55mm, 0mm)
$A_3$	(0mm, -140mm, 0mm)	$B_3$	(-55mm, -95.3mm, 0mm)
$A_4$	(-140mm, 0mm, 0mm)	$B_4$	(-95.3mm, -55mm, 0mm)
$A_5$	(-121.2mm, 70mm, 0mm)	$B_5$	(-55mm, 95.3mm, 0mm)
$A_6$	(70mm, 121.2mm, 0mm)	$B_6$	(0mm, 110mm, 0mm)

The initial elevation of frame  $B$  is set to  $z_0 = 300$  mm. After defining the necessary topological parameters of the manipulator it is possible to study its kinematics in response to different trajectories of the limbs. Using the inverse kinematics model defined previously, limb trajectories are calculated using reference trajectories for the centre point of frame  $B$ . The first set of reference trajectories for point  $P$  are shown in Figure 6.4 and Figure 6.5.

Here, it is required that point  $P$  moves 20mm in the  $x$  direction while all the other directions are forced to be zero. Thus, the required limb elongations for the trajectories in Figure 6.4 and 6.5 are calculated and shown in Figure 6.6.

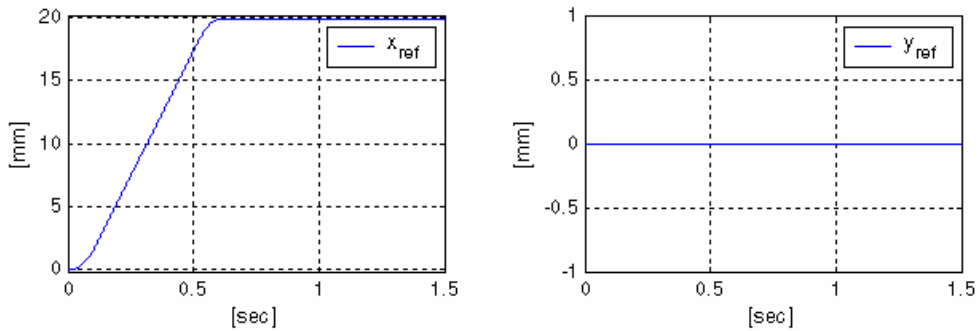


Figure 6.4. First set of reference trajectories for point  $P$

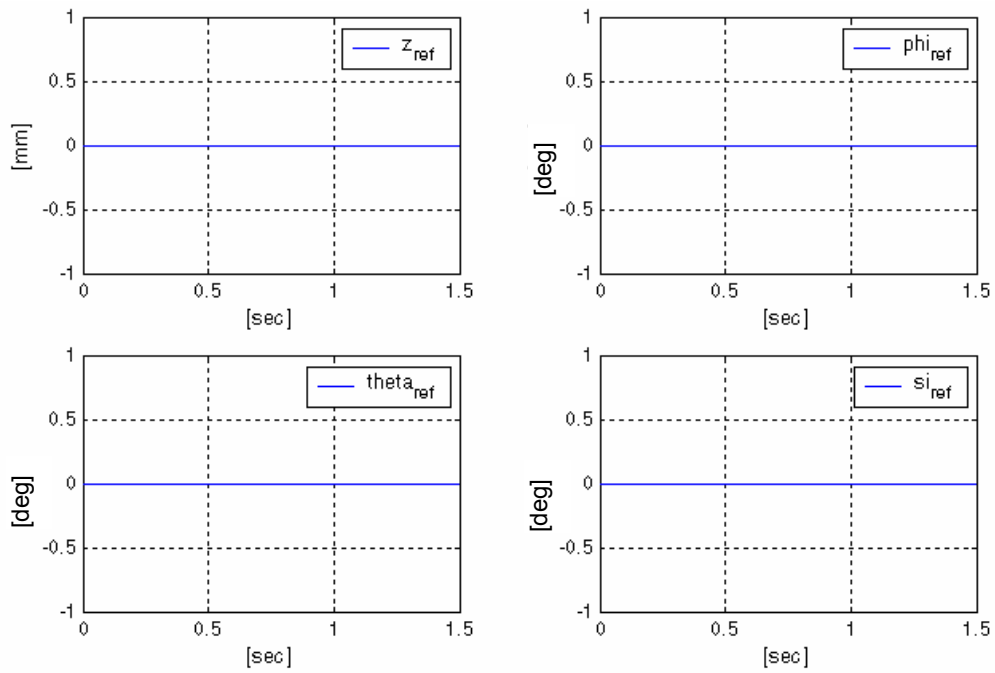


Figure 6.5. First set of reference trajectories for point  $P$

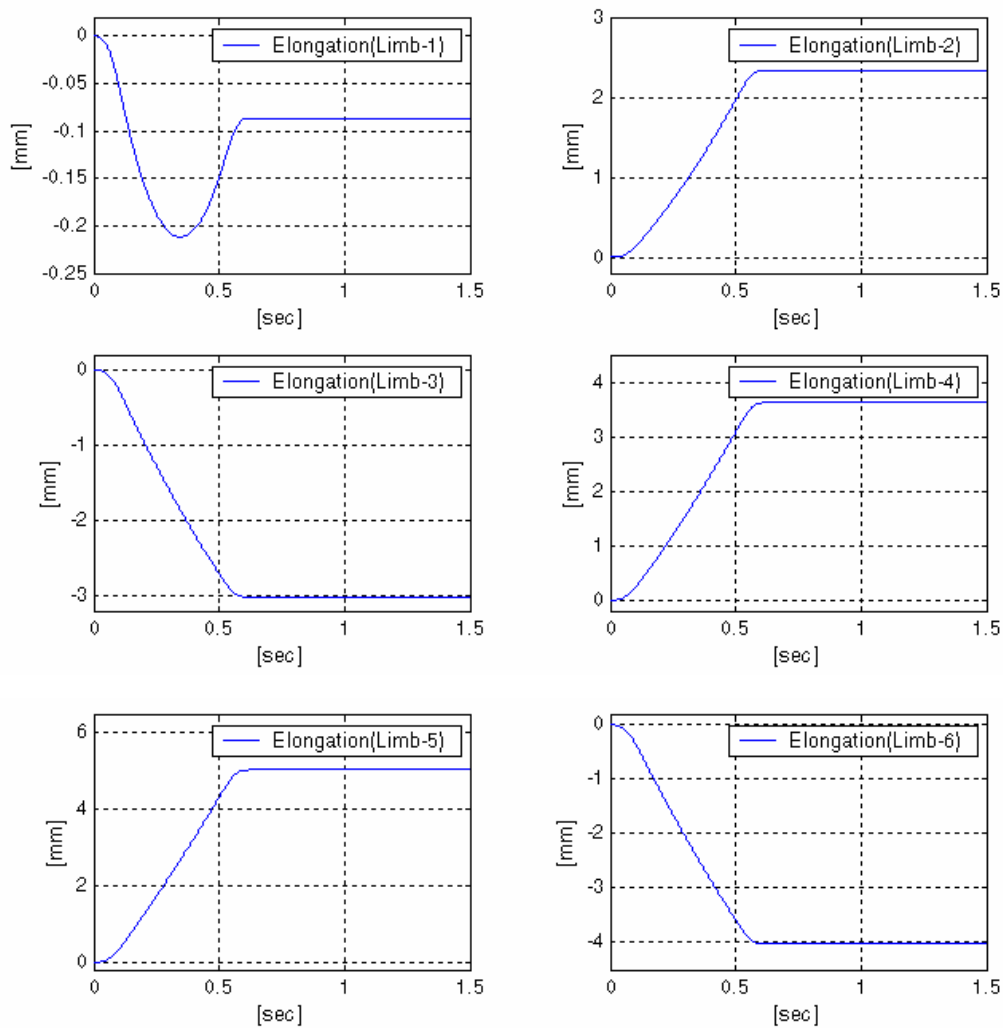


Figure 6.6. Required limb elongations for the first set of trajectories

The above limb elongations are used in the CAD model to verify the inverse kinematics model. The result of the CAD model motion compared with reference trajectories is shown in Figure 6.7.

As it can be seen from Figure 6.7, the inverse kinematics model works. The errors seen in the CAD model response are associated with problems of the simulation tool and are not related to the inverse kinematics model.

Using a second set of trajectories shown in Figure 6.8, the response of the CAD model is studied.

For this case it is required that point  $P$  moves 10mm in the  $x$  and  $y$  while motion in all other directions are forced to be zero. Using the inverse kinematics model, the required limb elongations are computed for the required motion of point  $P$ . The results are shown in Figure 6.9 and Figure 6.10.

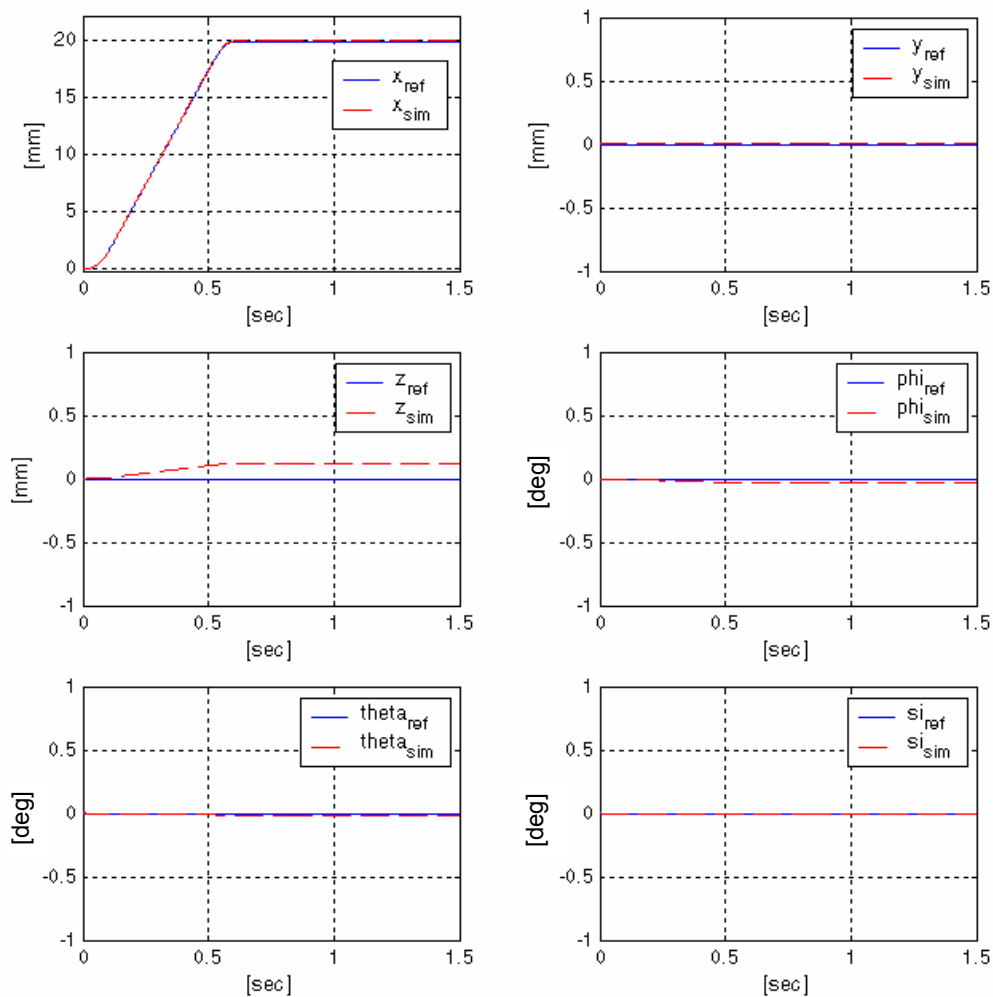


Figure 6.7. CAD model response to the first set of trajectories

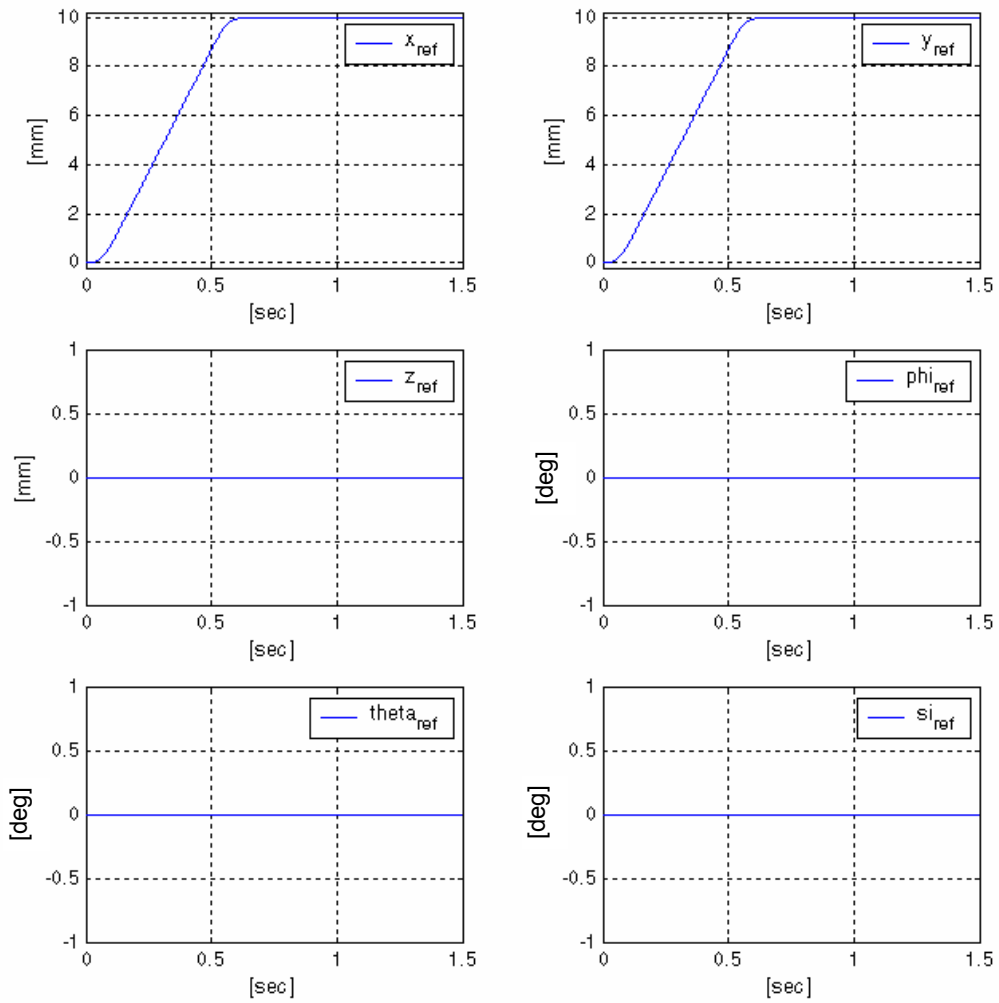


Figure 6.8. Second set of reference trajectories for point  $P$

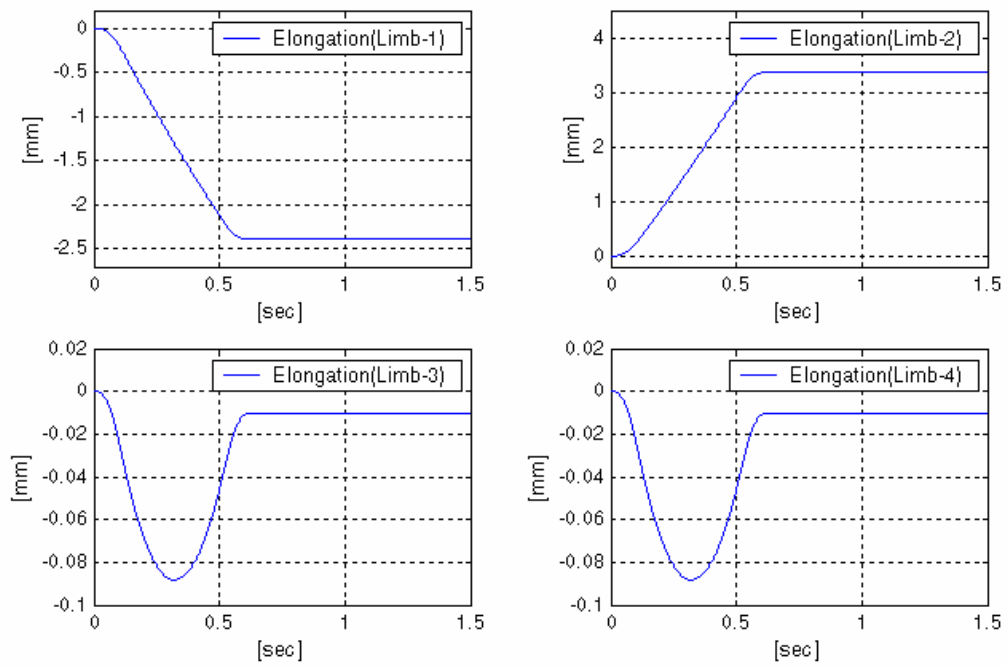


Figure 6.9. Limb elongations for the second set of trajectories

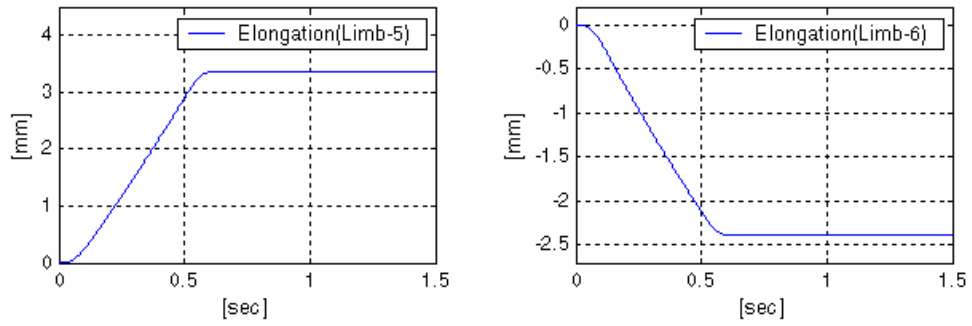


Figure 6.10. Limb elongations for the second set of trajectories (contd.)

As it was done for the first case, the limb elongations are used in the CAD model to verify the inverse kinematics model. The results compared with the reference trajectories of point  $P$  are shown in Figure 6.11.

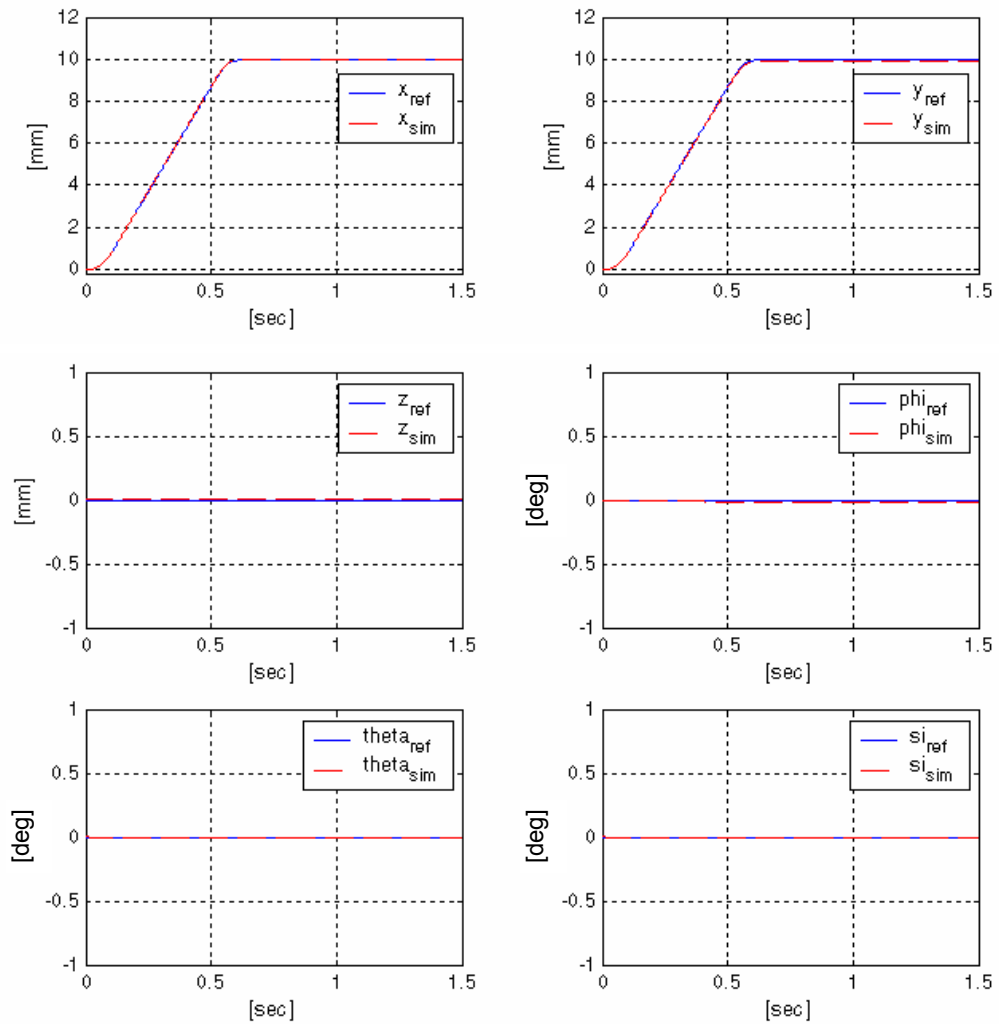


Figure 6.11. CAD model response to the second set of trajectories

## **7. EXPERIMENTS ON AN ACTUAL STEWART PLATFORM**

### **7.1 Introduction**

A culmination of this research is the implementation of the described algorithms to a system of reasonable complexity. The system used is a 6-dof Stewart platform such as the one described in the previous chapter. However, in this case the limbs of the actuator are dual-actuated. The aim here is to test the effectiveness of macro/micro motion actuators on the overall tracking capacity of complicated manipulators such as Stewart platforms. The experimental Stewart platform was designed and built as a part of the research.

In the experiments, independent joint control will be used since measurement only exists for the limbs. Limb trajectories will be generated based on the inverse kinematics of the platform as it was shown and simulated in the previous chapter.

### **7.2 Structure of the Experimental Stewart Platform**

The experimental Stewart platform used was of the symmetrical 6SPS as was described in the previous chapter. The limbs of the actuator are dual-actuated as described in chapter 5. The macroactuator is a DC-Ball screw drive produced by PI, GmbH that has a maximum stroke of 25mm with maximum repeatability of 5 $\mu$ m. The microactuator is a piezo drive with a maximum stroke of 20 $\mu$ m and repeatability as good as 0.1nm. The position of the DC-Ball screw is measured via 2024-pulse encoders while the tip position of the piezo drive is measured via SLVC (Super Linear Variable Capacitor) transducer that has a measuring range of 50mm with a resolution of 1 $\mu$ m. The limb of the platform is shown in Figure 7.1.



Figure 7.1. Limb of the experimental system

The control references for the actuators are generated by DSpace™ DS1103 controller card with the control routine executed in C-code. A simplified sketch of the experimental setup is shown in Figure 7.2.

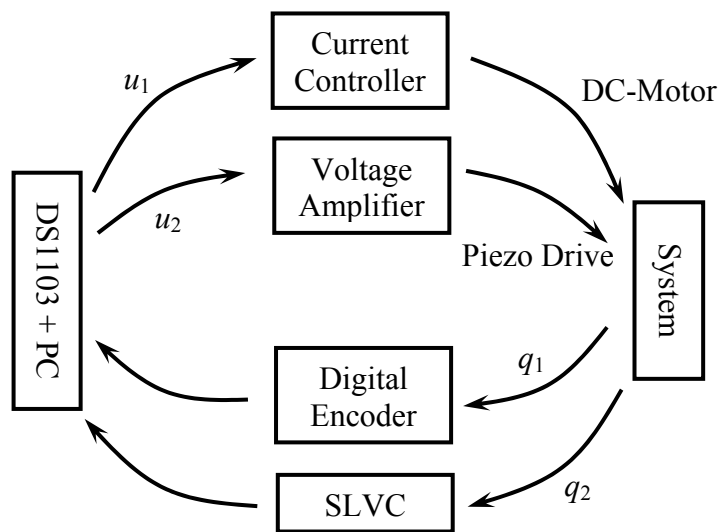


Figure 7.2. Sketch of the system

Unfortunately, due to the limitation on the number of DAC (Digital to Analog Converter) channels on the DS1103 it will not be possible to demonstrate the dual-actuation principle for the entire platform. Only the DC-Ball screw drives will be used in the platform experiments. The experimental Stewart platform can be seen in Figure 7.3.



Figure 7.3. Experimental Stewart platform

### 7.3 Experimental Results

In this section some of the experimental results on the Stewart platform will be shown. The experiments consisted of several types of trajectories for the top plate and generation of the limb elongation trajectories in order to satisfy the required plate motion. The motion of the plate in one direction is measured via a laser sensor with a resolution of 1-4 $\mu$ m. The figures below are for sigmoid references for the  $p_x$  coordinate while all other coordinates are maintained at zero.

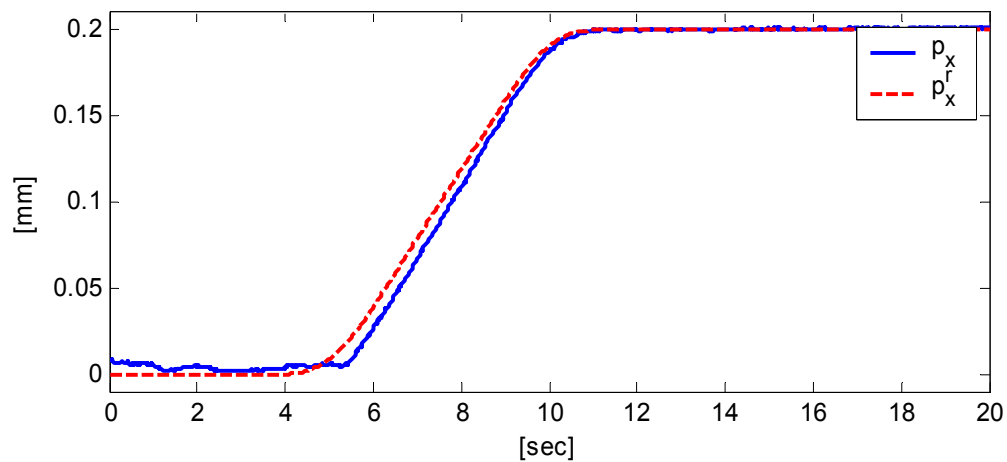


Figure 7.4. 0.2mm reference trajectory for  $p_x$  and measured motion

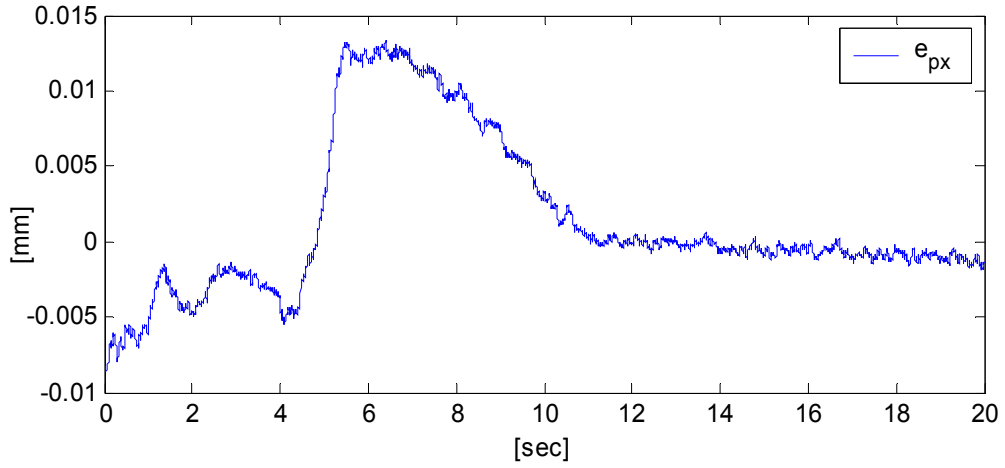


Figure 7.5. Corresponding tracking error for the 0.2mm sigmoid

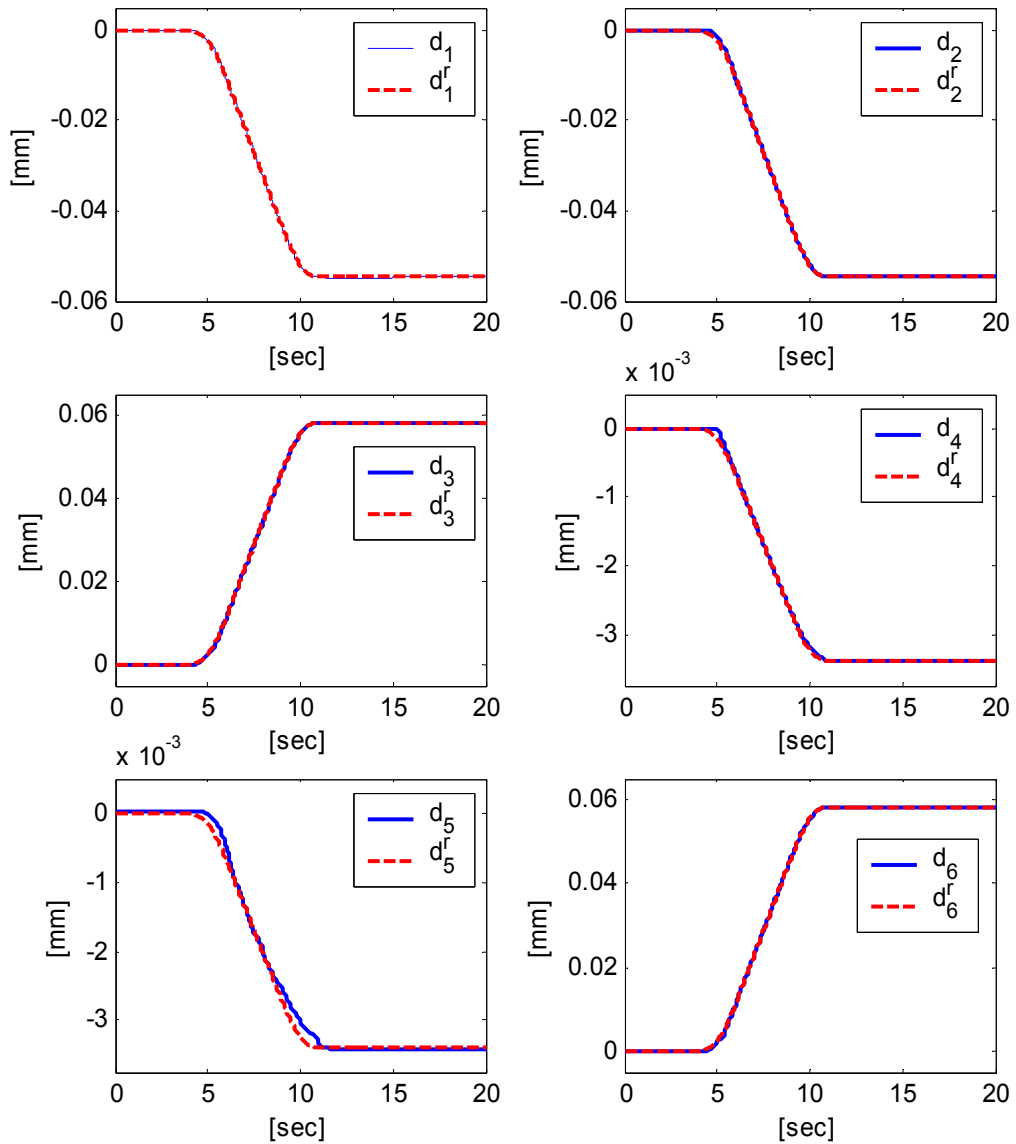


Figure 7.6. Reference limb trajectories for 0.2mm  $p_x$  trajectory

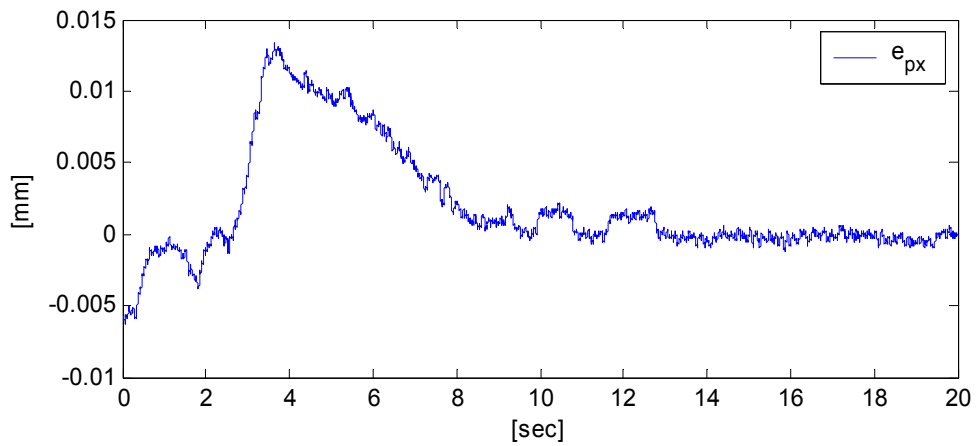
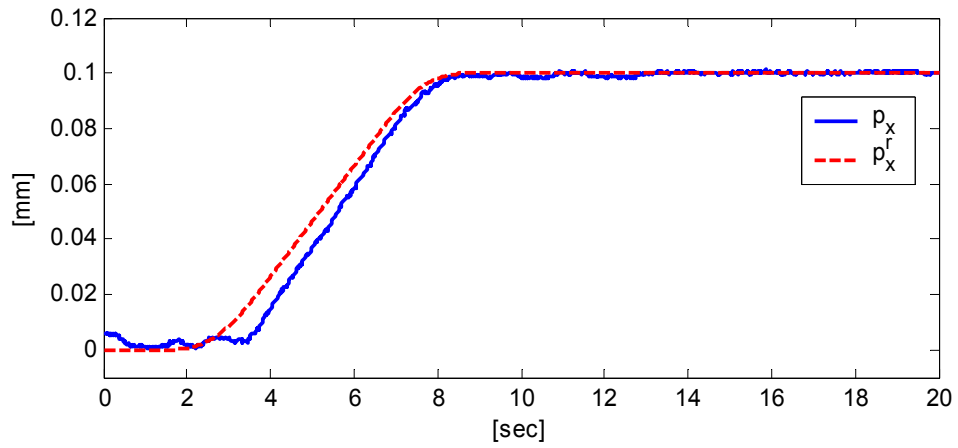


Figure 7.7. 0.1mm reference trajectory for  $p_x$  and measured motion

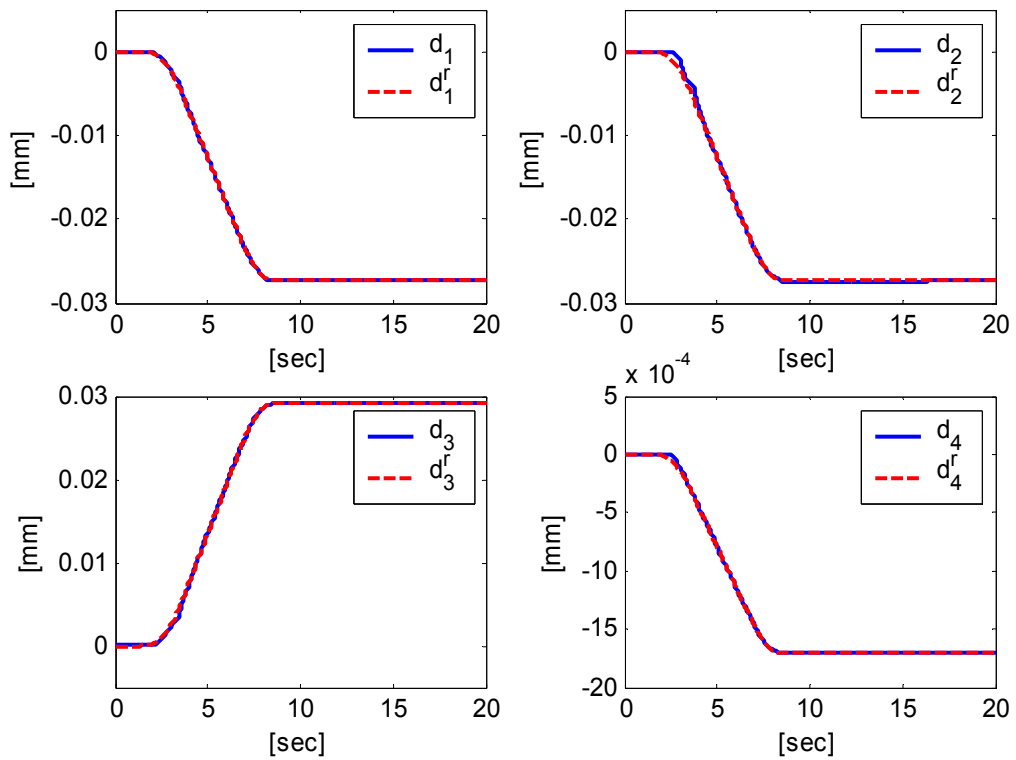


Figure 7.8. Reference limb trajectories for 0.1mm  $p_x$  trajectory

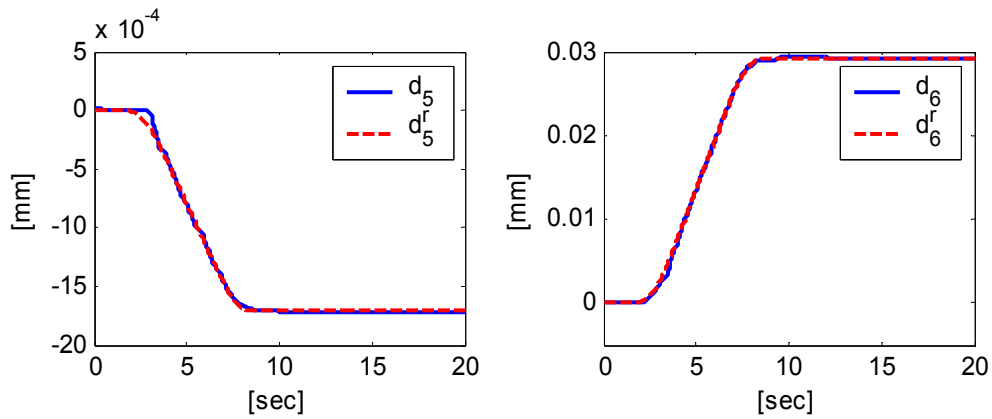


Figure 7.9. Reference limb trajectories for 0.1mm  $p_x$  trajectory (Contd.)

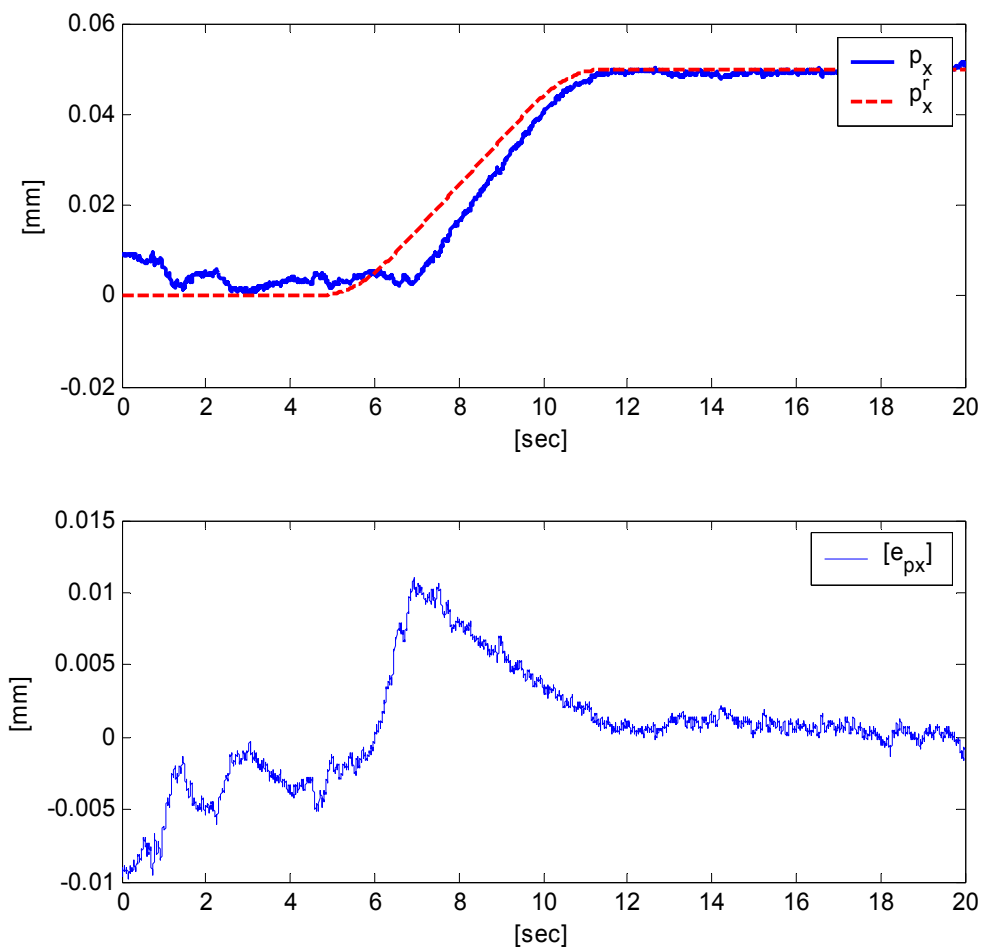


Figure 7.10. 50 $\mu$ m reference trajectory for  $p_x$  and measured motion

As it can be seen, the tracking deteriorates as the motion trajectory is made smaller. However, the limb trajectory tracking remains good even at these small displacements. Note that, the plate motion is not controlled but the limb elongations are, hence, backlash or other mechanical problems in the system would result in an overall discrepancy in the tracking.

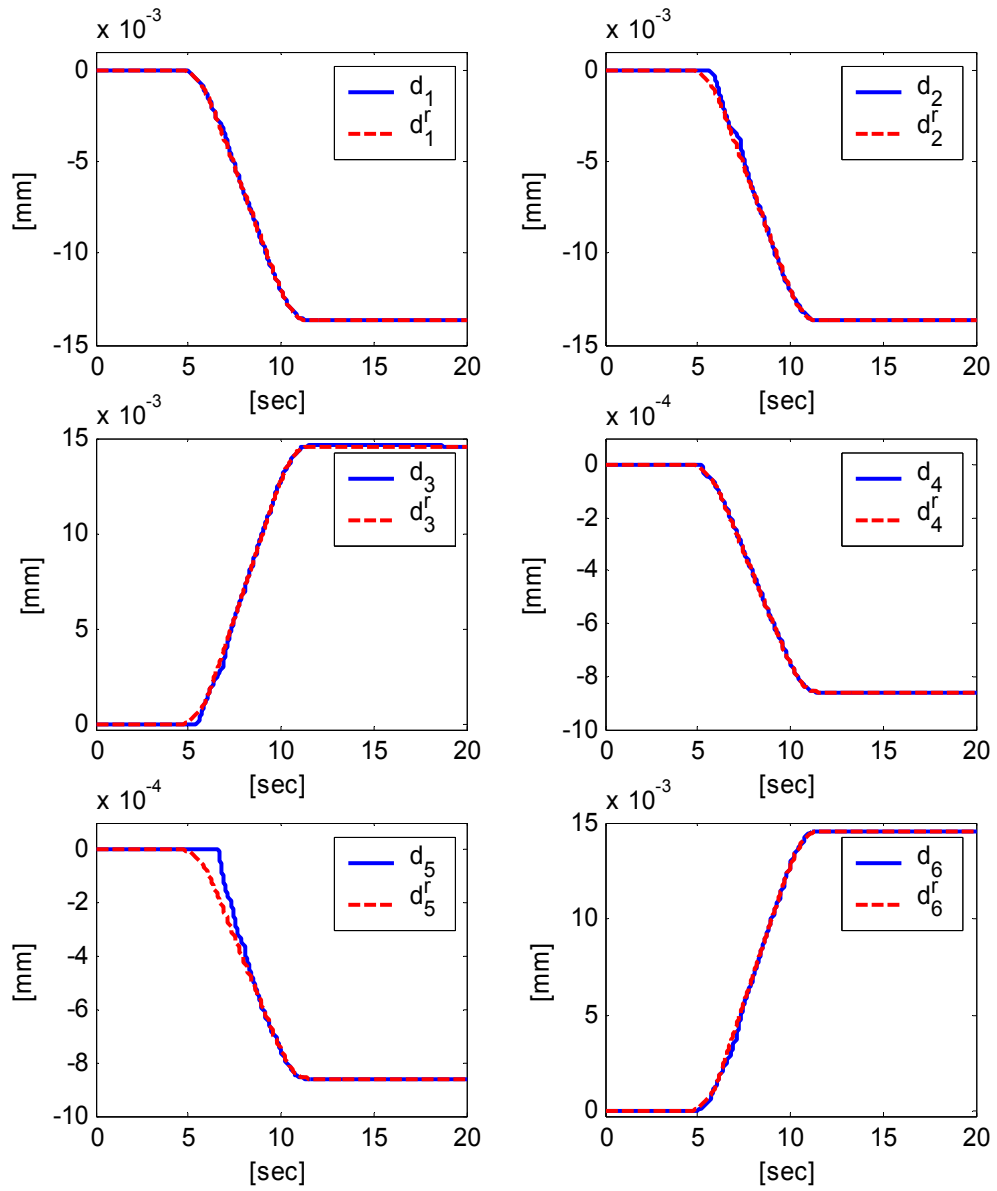


Figure 7.11. Reference limb trajectories for  $50\mu\text{m } p_x$  trajectory

## CONCLUSION

This thesis presents a control methodology that was successful in solving the problems involved in controlling systems with hysteresis and friction. By the proposed approach, the desired performance can be specified in terms of the sliding surface which is independent from the choice of the control, and a robust, accurate and chattering free controller can be obtained based on a second order nominal process model. It was also shown that the controllers were as easy to implement and design as well known controllers such as PD or PID and implementation did not require modeling or identification of either friction or hysteresis or the need for any on-line adaptive techniques. To show the strength of the technique, it was experimentally implemented on systems of varying complexities that contained either friction or hysteresis or both. Experimental results obtained show that, as simple as this technique is, it could produce better performance than the relatively more advanced control techniques available in the literature.

Although this thesis does not present any new theoretical concept, it does show that relatively complex control problems can be solved using existing technology. This work shows that the merging of two well established techniques, namely disturbance compensation based on disturbance observers and Sliding Mode control, in the literature can produce interesting effects. Disturbance compensation based on disturbance observers eliminated the need for modeling or identification of friction or hysteresis and thus simplified the implementation.

As a further extension of this work, it would be interesting to extend the control methodology to include resonance suppression in flexible systems such as belt-driven systems or flexible robotic manipulators. Also other disturbances such as backlash or disturbances that are not smooth or have unbounded derivatives could be investigated. Another interesting point that can be addressed is the analytical proof as to why the combination of both Sliding Mode control and disturbance compensation manages to achieve better experimental results than each technique used separately. This is

important since each technique has been proven theoretically to achieve high performance. As a final extension, it will also be interesting to eliminate the need for the hysteresis model in the estimation of the external force on the PZT and derive an observer based on the current and position measurement to calculate the external force. This is very useful since current measurement is easy to obtain as opposed to charge. Success in this could bring about interesting possibilities.

## REFERENCE

- [1] Michael Goldfarb, and Nikola Celanovic, "Modeling Piezoelectric Stack Actuators for Control of Micromanipulation," IEEE Contr. Sys. Mag., Vol. 17, pp. 69-79, 1997.
- [2] V. I. Utkin, "Sliding mode control in discrete-time and difference systems," Variable Structure and Lyapunov Control, Alan S.I. Zinober (Ed.) Springer-Verlag London Limited. 1994, pp. 87-107.
- [3] K.D. Young, V.I. Utkin, and U. Ozguner, "A control engineer's guide to sliding mode control," IEEE Transactions on Control Systems Technology, Vol. 7, Issue 3, 1999.
- [4] Yu-Feng Li, "High Precision Motion Control Based on a Discrete-time Sliding Mode Approach", Doctoral Thesis, Royal Institute of Technology, Sweden, Dec. 2001.
- [5] K. Erbatur, M. Okyay Kaynak, and Asif Sabanovic "A Study on the Robustness Property of Sliding-Mode Controllers: A Novel Design and Experimental Investigations", IEEE TRANSACTIONS ON INDUSTRIAL ELECTRONICS, Vol. 46, No. 5, October 1999.
- [6] Wu-Chung Su, Sergey V. Drakunov, and Umit Ozguner, "An  $O(T^2)$  Boundary Layer in Sliding Mode for Sampled-Data Systems", IEEE TRANSACTIONS ON AUTOMATIC CONTROL, Vol. 45, No. 3, March 2000.
- [7] Sergey V. Drakunov, Vadim Utkin, "A Semigroup Approach to Discrete-Time Sliding Modes", Proceedings of the American Control Conference, June 1995.
- [8] K. Ohnishi, Masaaki Shibata, and Toshiyuki Murakami, "Motion Control for Advanced Mechatronics," IEEE Transactions on Mechatronics, Vol. 1, No. 1, pp. 56-67, 1996.
- [9] R. Banning, W.L. de Koning and J. M. T. A. Adriaens, "Modeling Piezoelectric Actuators," IEEE/ASME Transactions on Mechatronics, Vol. 5, pp. 331-341, No. 4, 2000.
- [10] R. Banning, W.L. de Koning, J. M. T. A. Adriaens and K.R Koops, "State-space analysis and identification for a class of hysteretic systems," Automatica, 37(12), pp. 1883-1892, 2001.

- [11] Daowei Wu, Guoxiao Guo and T. C. Chong, "Adaptive Compensation of Microactuator Resonance in Hard Disk Drives," *IEEE Transactions on Magnetics*, Vol. 36, No. 5, pp. 2247-2250, 2000.
- [12] Hewong Jung, Jong Yuop Shim and DaeGab Gweon, "Tracking control of piezoelectric actuators," *Institute of Physics Publishing, Nano-technology*, Vol. 12, pp. 14-20, 2001.
- [13] Ben M. Chen, Tong H. Lee, Chang-Chieh Hang, Yi Guo and Siri Weerasooriya, "An  $H_{\infty}$  Almost Disturbance Decoupling Robust Controller Design for a Piezoelectric Bimorph Actuator with Hysteresis," *IEEE Transactions on Control Systems Technology*, Vol. 7, No. 2, pp. 160-174, 1999.
- [14] R. Ben Mrad and, H. Hu, "A Model for Voltage to Displacement Dynamics in Piezoceramic Actuators Subject to Dynamic-Voltage Excitations," *IEEE/ASME Transactions on Mechatronics*, Vol. 7, No. 4, pp. 479-489, 2002.
- [15] Seiichiro Katsura, Yuichi Matsumoto, and Kouhei Ohnishi, "Analysis and Experimental Validation of Force Bandwidth for Force Control," *International Conference on Industrial Technology, IEEE*, pp. 796-801, 2003.
- [16] Watura Iida, and Kouhei Ohnishi, "Sensorless Force Control with Force Error Observer," *International Conference on Industrial Technology, IEEE*, pp. 157-162, 2003.
- [17] Yuichi Matsumoto, Seiichiro Katsura, and K. Ohnishi, "An Analysis and Design of Bilateral Control Based on Disturbance Observer," *International Conference on Industrial Technology, IEEE*, pp. 802-807, 2003.
- [18] C. Canudas deWit, H. Olsson, K.J. Åström and P. Lischinsky, "A new model for control system with friction," *IEEE Transactions on Automatic Control*, vol. 40, pp. 419-425, 1995.
- [19] C. J. Kempf and S. Kobayashi, "Disturbance observer and feedforward design for a high-speed direct-drive positioning table," *IEEE Transactions on Control Systems Technology*, vol. 7, no.5, 1999.
- [20] Y-F. Li and J. Wikander, "Discrete-time sliding mode control for linear systems with nonlinear friction," *Proceedings of the 6th IEEE International Workshop on Variable Structure Systems. Gold Coast, Queensland, Australia, 7-9 December, 2000.*
- [21] K. Nagai, Y. Nakagawa, and S. Iwasa, Ohno, K., "Development of a redundant macro-micro manipulator and contour tasks utilizing its compliant motion," *Proceedings of the 1997 IEEE/RSJ International Conference on Intelligent Robots and Systems*, vol. 1, pp. 279-284, 7-11 September, 1997.
- [22] J.D. Gilsinn, B.N. Damazo, R. Silver, and H. Zhou, "A macro-micro motion system for a scanning tunneling microscope," *Proceedings of the 5th Biannual World Automation Congress*, vol. 14, pp. 280-289, 9-13 June, 2002.

- [23] Lung-Wen Tsai, Robot analysis: the mechanics of serial and parallel manipulators, John Wiley, New York, 1999.
- [24] V. I. Utkin, "Variable Structure Systems with Sliding-Modes," IEEE Transactions on Automatic Control, vol. 22, no. 2, pp. 212-222, 1977.
- [25] R.A. DeClarlo, S. H. Zak, and G. R. Mathews, "Variable structure control of nonlinear multivariable systems: A Tutorial," Proceedings of IEEE, vol. 76, no. 3, pp 212-232, 1988.
- [26] J. J. Slotine, and W. P. Li, Applied Nonlinear Control, Prentice-Hall, Inc., New Jersey, 1991.
- [27] J. Y. Hung, W. Gao, and J. C. Hung, "Variable structure control: A survey," IEEE Transaction on Industrial Electronics, vol. 40, no. 1, Feb., 1993.
- [28] A.S.I. Zinober, An Introduction to Sliding Mode Variable Structure Control, Variable Structure and Lyapunov Control, Alan S.I. Zinober (Ed.) Springer Verlag London Limited, 87-107, 1994.

## REFERENCE

- [1] Michael Goldfarb, and Nikola Celanovic, "Modeling Piezoelectric Stack Actuators for Control of Micromanipulation," IEEE Contr. Sys. Mag., Vol. 17, pp. 69-79, 1997.
- [2] V. I. Utkin, "Sliding mode control in discrete-time and difference systems," Variable Structure and Lyapunov Control, Alan S.I. Zinober (Ed.) Springer-Verlag London Limited. 1994, pp. 87-107.
- [3] K.D. Young, V.I. Utkin, and U. Ozguner, "A control engineer's guide to sliding mode control," IEEE Transactions on Control Systems Technology, Vol. 7, Issue 3, 1999.
- [4] Yu-Feng Li, "High Precision Motion Control Based on a Discrete-time Sliding Mode Approach", Doctoral Thesis, Royal Institute of Technology, Sweden, Dec. 2001.
- [5] K. Erbatur, M. Okyay Kaynak, and Asif Sabanovic "A Study on the Robustness Property of Sliding-Mode Controllers: A Novel Design and Experimental Investigations", IEEE TRANSACTIONS ON INDUSTRIAL ELECTRONICS, Vol. 46, No. 5, October 1999.
- [6] Wu-Chung Su, Sergey V. Drakunov, and Umit Ozguner, "An  $O(T^2)$  Boundary Layer in Sliding Mode for Sampled-Data Systems", IEEE TRANSACTIONS ON AUTOMATIC CONTROL, Vol. 45, No. 3, March 2000.
- [7] Sergey V. Drakunov, Vadim Utkin, "A Semigroup Approach to Discrete-Time Sliding Modes", Proceedings of the American Control Conference, June 1995.
- [8] K. Ohnishi, Masaaki Shibata, and Tushiyuki Murakami, "Motion Control for Advanced Mechatronics," IEEE Transactions on Mechatronics, Vol. 1, No. 1, pp. 56-67, 1996.
- [9] R. Banning, W.L. de Koning and J. M. T. A. Adriaens, "Modeling Piezoelectric Actuators," IEEE/ASME Transactions on Mechatronics, Vol. 5, pp. 331-341, No. 4, 2000.
- [10] R. Banning, W.L. de Koning, J. M. T. A. Adriaens and K.R Koops, "State-space analysis and identification for a class of hysteretic systems," Automatica, 37(12), pp. 1883-1892, 2001.

- [11] Daowei Wu, Guoxiao Guo and T. C. Chong, "Adaptive Compensation of Microactuator Resonance in Hard Disk Drives," *IEEE Transactions on Magnetics*, Vol. 36, No. 5, pp. 2247-2250, 2000.
- [12] Hewong Jung, Jong Yuop Shim and DaeGab Gweon, "Tracking control of piezoelectric actuators," *Institute of Physics Publishing, Nano-technology*, Vol. 12, pp. 14-20, 2001.
- [13] Ben M. Chen, Tong H. Lee, Chang-Chieh Hang, Yi Guo and Siri Weerasooriya, "An  $H_\infty$  Almost Disturbance Decoupling Robust Controller Design for a Piezoelectric Bimorph Actuator with Hysteresis," *IEEE Transactions on Control Systems Technology*, Vol. 7, No. 2, pp. 160-174, 1999.
- [14] R. Ben Mrad and, H. Hu, "A Model for Voltage to Displacement Dynamics in Piezoceramic Actuators Subject to Dynamic-Voltage Excitations," *IEEE/ASME Transactions on Mechatronics*, Vol. 7, No. 4, pp. 479-489, 2002.
- [15] Seiichiro Katsura, Yuichi Matsumoto, and Kouhei Ohnishi, "Analysis and Experimental Validation of Force Bandwidth for Force Control," *International Conference on Industrial Technology, IEEE*, pp. 796-801, 2003.
- [16] Watura Iida, and Kouhei Ohnishi, "Sensorless Force Control with Force Error Observer," *International Conference on Industrial Technology, IEEE*, pp. 157-162, 2003.
- [17] Yuichi Matsumoto, Seiichiro Katsura, and K. Ohnishi, "An Analysis and Design of Bilateral Control Based on Disturbance Observer," *International Conference on Industrial Technology, IEEE*, pp. 802-807, 2003.
- [18] C. Canudas deWit, H. Olsson, K.J. Åström and P. Lischinsky, "A new model for control system with friction," *IEEE Transactions on Automatic Control*, vol. 40, pp. 419-425, 1995.
- [19] C. J. Kempf and S. Kobayashi, "Disturbance observer and feedforward design for a high-speed direct-drive positioning table," *IEEE Transactions on Control Systems Technology*, vol. 7, no.5, 1999.
- [20] Y-F. Li and J. Wikander, "Discrete-time sliding mode control for linear systems with nonlinear friction," *Proceedings of the 6th IEEE International Workshop on Variable Structure Systems. Gold Coast, Queensland, Australia, 7-9 December, 2000.*
- [21] K. Nagai, Y. Nakagawa, and S. Iwasa, Ohno, K., "Development of a redundant macro-micro manipulator and contour tasks utilizing its compliant motion," *Proceedings of the 1997 IEEE/RSJ International Conference on Intelligent Robots and Systems*, vol. 1, pp. 279-284, 7-11 September, 1997.
- [22] J.D. Gilsinn, B.N. Damazo, R. Silver, and H. Zhou, "A macro-micro motion system for a scanning tunneling microscope," *Proceedings of the 5th Biannual World Automation Congress*, vol. 14, pp. 280-289, 9-13 June, 2002.

- [23] Lung-Wen Tsai, Robot analysis: the mechanics of serial and parallel manipulators, John Wiley, New York, 1999.
- [24] V. I. Utkin, "Variable Structure Systems with Sliding-Modes," IEEE Transactions on Automatic Control, vol. 22, no. 2, pp. 212-222, 1977.
- [25] R.A. DeCarlo, S. H. Zak, and G. R. Mathews, "Variable structure control of nonlinear multivariable systems: A Tutorial," Proceedings of IEEE, vol. 76, no. 3, pp 212-232, 1988.
- [26] J. J. Slotine, and W. P. Li, Applied Nonlinear Control, Prentice-Hall, Inc., New Jersey, 1991.
- [27] J. Y. Hung, W. Gao, and J. C. Hung, "Variable structure control: A survey," IEEE Transaction on Industrial Electronics, vol. 40, no. 1, Feb., 1993.
- [28] A.S.I. Zinober, An Introduction to Sliding Mode Variable Structure Control, Variable Structure and Lyapunov Control, Alan S.I. Zinober (Ed.) Springer Verlag London Limited, 87-107, 1994.